MONOLAYERS AND MULTILAYERS OF MESOGEN-SUBSTITUTED ACETYLENE MONOMERS AND POLYMERS

By

MARION JOSEPH ROBERTS

A DISSERTATION PRESENTED TO THE GRADUATE SCHOOL
OF THE UNIVERSITY OF FLORIDA IN PARTIAL FULFILLMENT
OF THE REQUIREMENTS FOR THE DEGREE OF
DOCTOR OF PHILOSOPHY

UNIVERSITY OF FLORIDA
1995

ACKNOWLEDGMENTS

Every scientific researcher owes a great debt to those who have preceded him and the author is no exception to this rule. The author wishes to personally acknowledge the support and opportunities provided by his research advisor, Dr. R. S. Duran. Also the encouragement and example of Dr. Karl Söderholm and Dr. Katherine Williams helped to provide the impetus toward the pursuit of an advanced degree.

Perhaps it is a little unorthodox to thank institutions or committees but the author must thank the Graduate selection committee for providing this chance to continue his education. Also the College Work Study Program allowed the author a chance to demonstrate his potential as a future scientist while still an undergraduate. The pooling of resources by Dr. George Butler, Dr. Ken Wagener, Dr. John Reynolds, and Dr. Randy Duran to create what is called the 'polymer group' has been a great help in that it not only provides access to equipment which might otherwise be unavailable but also brings about new interactions between researchers.

It is customary to acknowledge the contribution of ones coworkers. Here the author owes special gratitude to the postdoctoral researchers who have worked in Dr. Duran's

laboratory; namely, Dr. Huanchun Zhou, Dr. Willie Rettig, Dr. Mathias Naumann, Dr. Jörg Adams, and Dr. Thomas Servay. Each has provided invaluable advice and encouragement. During the four months while the author was working at the NASA Lewis Research Center, Dr. Mike Meador provided close advisement. Also, at the Lewis Research Center, Dr. Kathy Chuang, Dr. Jim Kinder, and Dan Schiemann were helpful. The advice and support of Dr. Radi Awartani of Farchan Labs is gratefully acknowledged. In an important way, Dr. Jacques Le Moigne's interpretation of the data changed the model developed in Chapter 3. Three undergraduate students, Ellis Teer, Joe Watson, and Wei Shen have worked with the author in the last two years. Their energy and willingness to learn (and sometimes teach) have been a great help. Among his fellow graduate students special acknowledgment is owed to now Dr. Angie Thibodeaux and Dr. Rigoberto 'Gobet' Advincula. Angie was always the expert on anything in the lab to which the author could turn for good advice. The author and now Dr. Advincula worked closely on much of the work reported in Chapter 2 of this dissertation.

Finally, it is important to acknowledge financial and material support from the NASA Lewis Research Center, KSV Instrument Company, NanoFilm Technologies Company, Visual Numerics Software Company, Oriel Instrument Company, and Farchan Laboratories. Without their support, the work reported in this dissertation would not have been possible.

TABLE OF CONTENTS

page

ACKNOWLEDGMENTS ii

LIST OF FIGURES vi

ABSTRACT xi

CHAPTERS

1 INTRODUCTION 1

Overview 1
Polyacetylene and NLO 2
Langmuir-Blodgett-Kuhn Technique 6
Polymers from Pre-oriented Monomers in Langmuir-Blodgett-Kuhn Films 15
Soluble Derivatives of Polyphenylene-ethynylene 17
Principal Objectives of this Dissertation . . . 18

2 LANGMUIR AND LANGMUIR-BLODGETT-KUHN FILMS OF MESOGEN SUBSTITUTED ACETYLENE MONOMERS 20

Introduction 20
Langmuir Technique 25
Polymerization of Langmuir-Blodgett-Kuhn Films 26
Experimental 27
Synthesis of 4-hydroxy biphenyl-4'(11-undecynoate), **III** 28
Synthesis of 4-(4'-ol-biphenyl-4-decanoxy)-phenylacetylene, **IV** 30
Synthesis of 2-(10-(4'-ol-biphenyl-4-oxy) dodecanoxymethyl)-anthryl)-trimethylsilylacetylene, **VII** 39
Langmuir-Blodgett-Kuhn Experiments 47
Results and Discussion 49
LBK Films of Mesogen-substituted Monoacetylene Monomers 49
LBK Films of Mesogen-substituted Phenylacetylene Monomers 61

Conclusion 69

3 PROPERTIES OF SOLUBLE DERIVATIVES OF POLYPHENYLENE-ETHYNYLENE IN LANGMUIR FILMS 73

Introduction 73
Theoretical Considerations 75
Monolayers of Rigid-Rod Polymers 75
Cellular Networks 76
Experimental Methods 85
Spectroscopy 85
Trough Setup 85
Formation of a Cellular Network 86
Brewster Angle Microscope 87
Epifluorescence Trough 87
Image Processing 88
Results and Discussion 89
Langmuir Film Properties of Poly(2-(11-hydroxyundecanoxy)-5-methoxyphenylene-ethynylene), PEHU 89
Langmuir Film Properties of Poly(2-(11-hydroxyundecanoxy)-5-methoxyphenylene-ethynylene-pyridine-ethynylene), PPEHU 95
Langmuir Film Behavior of Mixtures of PEHU and PPEHU 129
Langmuir Film Properties of Poly(2,5-di(11-hydroxyundecanoxy)phenylene-ethynylene-pyridinium bromide-ethynylene), PPYPYRI 134
Topology of the PPEHU Cellular Network . 141
Cellular Network Dynamics 145
Energetics of Cell Coalescence 150
Future Work 156

4 CONCLUSIONS 159

REFERENCE LIST 166

BIOGRAPHICAL SKETCH 175

LIST OF FIGURES

page

Figure 1-1. Polyacetylene consists of alternating carbon double and single bonds. 4

Figure 1-2. Langmuir film balance with an insoluble monolayer of molecules under compression. 8

Figure 1-3. Structures of X, Y, and Z-type LBK multilayers. 10

Figure 2-1. Mesogen-substituted amphiphilic compounds studied with the Langmuir-Blodgett technique. 21

Figure 2-2. Proton NMR of compound **III** in $CDCl_3$. . . . 29

Figure 2-3. Synthetic scheme used for mesogen-substituted phenylacetylene. 31

Figure 2-4. Proton NMR of **IV** in tetrahydrofuran-d_4. . . 38

Figure 2-5. Synthetic scheme for mesogen-substituted anthrylacetylene. 39

Figure 2-6. Proton NMR for **VII** in $CDCl_3$. 46

Figure 2-7. Isotherm for **I** at 6 °C. 51

Figure 2-8. Isotherm for the mixture of 95 mole % **I** and 5 % **II**. 54

Figure 2-9. UV spectrum for the **I+II** mixture in an LBK film on a hydrophobic quartz plate. . . 56

Figure 2-10. Isotherm for **III** at 27 °C. 60

Figure 2-11. Isotherms for **V** and **VI** at 25 °C. 62

Figure 2-12. Hysteresis exhibited by **V** during a compression and decompression cycle. . 64

Figure 2-13. Isotherm for **IV** at 23 °C. 66

Figure 2-14. Isotherm for **VII** at 25 °C. 68

Figure 3-1. Soluble derivatives of polyphenylene ethynylene. 74

Figure 3-2. Possible topological changes occuring during coarsening of a cellular network. Cell coalescence is a third such change. . . 83

Figure 3-3. UV absorbance of PEHU in THF solution. This spectra was obtained by Marc Moroni. 90

Figure 3-4. UV absorbance spectra of PEHU in a thin solid film cast on quartz. This spectra was obtained by Marc Moroni. 91

Figure 3-5. UV absorbance spectra of PEHU in a Langmuir film during compression between 0.2 and 0.45 nm^2/repeat unit. 92

Figure 3-6. Isotherm and surface potential for PEHU at 25°C. 92

Figure 3-7. Hysteresis of PEHU isotherm during six sweeps at 25°C. 93

Figure 3-8. PEHU's effective absorbance per repeat unit decreases with compression at 25°C. . 94

Figure 3-9. Isotherm of PPEHU at 25 °C. The phase coexistence region was observed at the specific areas between the dashed lines. The boxes, A and B, represent the observed morphology at the corresponding points on the isotherm during compression of the monolayer (white=MC phase, black=ME phase). The morphologies in C, D, and E are seen only on decompression of the monolayer. . 96

Figure 3-10. UV excitation spectra of a cast film of PPEHU on quartz (emission monitored at 500 nm). 98

Figure 3-11. UV excitation spectra of a chloroform solution of PPEHU (Emission monitored at 456 nm). 99

Figure 3-12. UV-Visible emission spectra of PPEHU in chloroform solution. 100

Figure 3-13. UV-Visible emission spectra of PPEHU in a cast film on quartz. 101

Figure 3-14. UV absorbance spectra of PPEHU in a Langmuir film during compression at 0.35 nm^2/repeat unit. 102

Figure 3-15. Temperature dependence of PPEHU isotherms. 103

Figure 3-16. Typical boundary of a liquid-expanded/liquid-condensed phase coexistence envelope seen for Langmuir films of long-chain fatty acids and alcohols. 104

Figure 3-17. Effective dipole moment for PPEHU at the air-water interface. 105

Figure 3-18. Lever rule plot for the phase coexistence region of PPEHU at 25 °C. 106

Figure 3-19. Idealized picture of the side-chain orientation of the PPEHU phases. . . 108

Figure 3-20. Hysteresis of PPEHU at 25 °C and a barrier speed of 2 mm/min (0.0084 nm^2/repeat unit/min). The plot shows the difference in surface pressure between the compression and decompression sweeps within the biphasic region. 113

Figure 3-21. Relative total reflectivity calculated from BAM images of PPEHU during one compression/decompression cycle. . . . 115

Figure 3-22. Domains of MC phase dispersed in the ME phase at 0.45 nm^2 and 25 °C. 118

Figure 3-23. Domains of the MC phase dispersed in the LC phase 30 minutes compressing and holding at 0.45 nm^2 and 25 °C. 119

Figure 3-24. Cellular network aged at 0.35 nm^2/repeat and 25°C. 120

Figure 3-25. Cellular network of PPEHU aged at 0.45 nm^2/repeat and 25°C. 120

Figure 3-26. Cellular network of PPEHU aged at 0.55 nm^2/repeat and 25°C. 121

Figure 3-28. Mosaic of BAM images of PPEHU after decompression to 0.62 nm^2 at 25°C. Each strip is 50 μm x 400 μm. 122

Figure 3-29. Metastable free-floating rings of PPEHU MC phase at 0.75 nm^2/repeat and 25°C. Image size is 1200 μm x 800 μm. 123

Figure 3-30. Dendrites formed during compression of PPEHU below 0.60 nm^2/repeat and 15°C (no analyzer in plane). Image size is 1200 µm x 800 µm. 124

Figure 3-31. Birefringent regions in PPEHU Langmuir film below 0.60 nm^2/repeat and 15°C (analyzer at 90° to usual polarization of the reflected beam). Image size is 1200 µm x 800 µm. 125

Figure 3-32. Epifluorescence microscope image of PPEHU at 0.60 nm^2/repeat and 25°C. 126

Figure 3-33. Isotherms for a 1:1 mixture of PEHU and PPEHU compared to the isotherm of each pure component at 23°C. 131

Figure 3-34. BAM image of a 1:1 molar mixture of PEHU and PPEHU at 5 mN/m and 23°C. Image size is 1200 µm x 800 µm. 132

Figure 3-35. BAM image of a 1:1 mixture of PEHU and PPEHU at 1 mN/m and 23 °C. Image size is 1200 µm x 800 µm. 132

Figure 3-36. Comparison of monolayer stability for a 1:1 mixture of PEHU and PPEHU, and each of the pure components 10 mN/m and 25 °C. 133

Figure 3-37. Isotherm and surface potential of PPYPYRI at 25°C. 134

Figure 3-38. BAM image of PPYPYRI as first spread at the air/water interface. Image size is 1200 µm x 800 µm. 135

Figure 3-39. BAM image of PPYPYRI during compression at 0.75 nm^2 and 25°C. Image size is 1200 µm x 800 µm. 136

Figure 3-40. BAM image of PPYPYRI under compression at 0.40 nm^2 and 25°C. Image size is 1200 µm x 800 µm. 136

Figure 3-41. BAM image of PYPYRI during decompression at 0.8 nm^2 and 25 °C. Image size is 1200 µm x 800 µm. 137

Figure 3-42. BAM image of PPYPYRI during decompression at 1.0 nm^2 and 25 °C. Image size is 1200 μm x 800 μm. 137

Figure 3-43. BAM image of PPYPYRI during decompression at 1.7 nm^2 and 25 °C. Image size is 1200 μm x 800 μm. 138

Figure 3-44. Lewis' law plot for PPEHU cellular network at 0.65 nm^2/repeat and 25°C. 142

Figure 3-45. Perimeter law plot for PPEHU cellular network at 0.65 nm^2/repeat and 25°C. . . 144

Figure 3-46. Von Neumann's Law plot. 146

Figure 3-47. Variation of cell growth exponent with relative phase fraction. 149

Figure 3-48. Section of a ruptured cell edge. 152

Abstract of Dissertation Presented to the Graduate School of the University of Florida in Partial Fulfillment of the Requirements for the Degree of Doctor of Philosophy

MONOLAYERS AND MULTILAYERS OF MESOGEN-SUBSTITUTED ACETYLENE MONOMERS AND POLYMERS

By

Marion Joseph Roberts

May 1995

Chairperson: Randolph S. Duran
Major Department: Chemistry

With a view toward improving knowledge of the properties of organic molecules in monomolecular films, the general class of mesogen-substituted acetylene compounds was chosen for study. Such compounds potentially find application as both nonlinear optical and electrically-conducting materials. Monolayer properties were discovered through surface analytical methods, such as, Brewster angle microscopy, epifluorescence microscopy, *in situ* ultraviolet spectroscopy, and surface potentiometry.

The Langmuir-Blodgett-Kuhn (LBK) technique was used to study the monolayer properties of a series of substituted acetylene monomers. Preliminary work with substituted liquid crystalline monoacetylenes and phenylacetylenes pointed the way toward possible improvements in the molecular design. Subsequently, synthesis of a new

phenylacetylene monomer, 4-(4'-ol-biphenyl-4-decanoxy)-phenylacetylene, with improved reactivity in thin solid films was achieved. In addition, a new substituted anthrylacetylene, 2-(10-(4'-ol-biphenyl-4-oxy) dodecanoxymethyl)-anthryl)-trimethylsilylacetylene, was synthesized.

LBK was also used to produce monomolecular films of phenylene acetylene rigid-rod polymers; poly(2-(11-hydroxyundecanoxy)-5-methoxyphenylene-ethynylene), poly(2-(11-hydroxyundecanoxy)-5-methoxyphenylene-ethynylene-pyridine-ethynylene), and poly(2,5-di(11-hydroxyundecanoxy) phenylene-ethynylene-pyridinium bromide-ethynylene). At the air-water interface, two of the polymers were observed to form microscopic network morphologies after treatment by a simple processing procedure. The properties of one polymer's network was studied in detail, including the network dynamics. A model for the nanoscale orientation of the polymer within its network is proposed. A new method for estimating the line tension between 2D phases based on the observation of cell coalescence is presented.

CHAPTER 1
INTRODUCTION

> . . . typical of class-one evolution are the two trends . . . - the *invisible* chemical, metallurgical, and electronic production of ever-more-efficient and satisfyingly effective performance with the investment of ever-less weight and volume of materials per unit function formed or performed - ie. *ephemeralization* - accomplished within ever-less increments of time - ie. *acceleration*.
>
> This overall and inexorable trending to do more with less is known sumtotally as "progressive ephemeralization". Ephemeralization trends toward an ultimate doing of *everything* with *nothing at all*, which is a trend of the *omniweighable physical* to be mastered by the *omniweightless metaphysics of intellect*.
>
> - R. Buckminster Fuller in *Critical Path*, 1981, page 73 [1]

Overview

As the world's population continues to increase, the consumption of available resources will also necessarily increase unless more efficient means are found and adopted. One of the more obvious successes is found in the construction of electronic and mechanical micro-devices from crystalline silicon. The limit of miniturization will soon be reached for electronic devices. Thus, there is growing interest in optical-based devices. Materials which alter the properties of propagating light are used in such

devices. In addition, techniques for shaping these new materials into working devices will be needed.

The invention of the laser has provided a source of high intensity, coherent, and directed light. Soon after came the discovery that materials can alter intense laser light by doubling or tripling the frequency of the light. These special materials are called nonlinear optical materials because of the way they alter the wavelength of intense light. It is important to note that the light must be intense in order for a nonlinear optical (NLO) material to double or triple the light frequency, otherwise the NLO material does not affect the exiting light frequency. Thus, it is not possible to induce NLO effects using normal light sources.

The first NLO effects were observed in inorganic materials such as quartz. In general, inorganic materials do not allow the researcher much flexibility for making new materials with desired properties. The discovery of NLO effects in organic materials opened the way to further improvements in the figures of merit for NLO materials. One organic material which has been found to have the best efficiency at tripling light frequency is polyacetylene.[2]

Polyacetylene and NLO

Polyacetylene (PA) consists of a chain of alternating double and single carbon-carbon bonds (Figure 1-1). In a

planar conformation, the PA chain is enshrouded in a delocalized cloud of π-electrons. When PA is exposed to an electric field, such as that in laser light, the electron density is displaced and the molecule becomes polarized along the main polymer chain. The polarization induced by the oscillating electric field of the laser light may be described by the equation,[3]

$$\mu = \mu_0 + \alpha E + \frac{\beta}{2}E^2 + \frac{\gamma}{6}E^3 + \ldots$$

where μ is the field-dependent dipole moment of the molecule in the field; μ_0 is the intrinsic dipole moment of the molecule; and the coefficients α, β, and γ are the linear polarizability, first hyperpolarizability, and second hyperpolarizability, respectively, for the molecule. Each of the three coefficients is a measure of how responsive the molecule is to the polarizing force of the electric field. In weak electric fields the displacement of the electron density is proportional to the electric field strength. A plot of dipole moment versus electric field strength gives a straight line with a slope of α. As the electric field strength increases to magnitudes which are only accessible with laser light, the nonlinear contributions such as β and γ become significant.

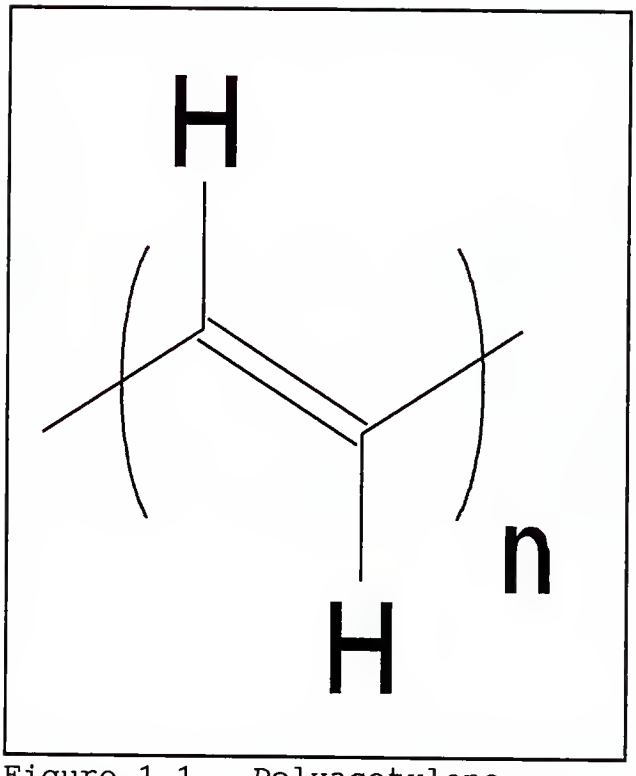

Figure 1-1. Polyacetylene consists of alternating carbon double and single bonds.

In substituted polyacetylenes, which have an electron accepting group at one end of the chain and an electron donating group at the opposite end, polarization occurs more in one direction along the chain than the other. The coefficient, β, is a measure of this polarization asymmetry and thus the molecule's potential ability to double the frequency of light passing through it. In polyacetylenes without the asymmetric substitution pattern, a small degree of polarization can make further polarization easier. The coefficient, γ, is a measure of how the polarizability is

changed by the molecule's polarization. This is important for such functions as optical switching, which is the use of one light beam to alter the path of a second beam by changing the refractive index of the material.[4] In addition to the optimization of NLO response at a molecular level, the researcher must also strive to arrange the molecules in the material so that the summed NLO response is maximized. Thus the macroscopic polarization, which is given by

$$P = \chi^{(1)}E + \chi^{(2)}E^2 + \chi^{(3)}E^3$$

becomes the quantity of interest. To a first approximation it is possible to infer the nonlinear optical properties of the bulk medium from those of the individual molecules. Thus, the molecules' β influences the ultimate $\chi^{(2)}$ of the material and likewise, γ affects $\chi^{(3)}$. For example, with polyacetylene it has been shown that the third order NLO response is increased by ordering the polymer chains such that the planarity of each main chain is maintained. Furthermore, interchain alignment of the polymer also affects the nonlinear response of the material. In Langmuir-Blodgett films, the third order hyperpolarizability can be written[5] as

$$\chi^{(3)} = O_p N \gamma$$

where O_P incorporates the local field correction factor and a factor taking into account the chain alignment and N is

the number of molecules per unit volume. The effect of the side chains on the main chain conformation can vary depending on their bulkiness or the presence of inter-side chain interactions.[6,7]

Langmuir-Blodgett-Kuhn Technique

The Langmuir-Blodgett-Kuhn technique is one method by which organic materials may be processed to achieve such ordering of molecules. LBK utilizes the orienting properties of an interface between two phases. Typically, the two phases are air and water but other systems have been exploited such as air-mercury. Desirable properties for the system include high interfacial tension, inertness, and that the materials to be processed at the interface should be insoluble in the subphase. A commonly studied material is stearic acid. Stearic acid is an amphiphilic molecule, that is, it has a hydrophilic headgroup (-COOH) and a hydrophobic tail ($-C_{17}H_{35}$). Thus, in a monolayer, stearic acid is on average oriented with its headgroup immersed in the water and its tailgroup outside the water.

The apparatus used to perform the LBK technique is the Langmuir film balance (Figure 1-2). The experimental quantities which are readily accessible with the Langmuir film balance include the surface concentration (usually expressed as its inverse or mean molecular area) and the surface pressure. The surface pressure is defined as the

difference between the surface tension of the pure solvent and that of the film-covered surface.[8] Surface tension is defined as surface free energy per unit area of the boundary between the solvent and the air above it. Surface tension has units of energy per area or force per length. Boundaries between two dimensional phases within Langmuir monolayers lead to line tension which is a one dimensional analog of the surface tension. Line energy is defined as the line free energy per unit length of the boundary between domains of two dimensional phases. Line tension has units of energy per length or force.

The first experiment performed with the Langmuir film technique is usually the isothermal surface pressure versus area diagram (isotherm). Molecules are spread on the water surface and laterally compressed with the mechanical barriers while the surface pressure and area are recorded. The isotherm can give important information such as the compressibility of the monolayer and also the cross sectional area of the molecules within the close-packed monolayer. This method was actually used to determine the diameter of buckminsterfullerene a few years ago. A second experiment usually performed is the hysteresis experiment, in which the monolayer is subjected to repeated compression and decompression cycles while the surface pressure is recorded. Among other things, the hysteresis experiment is useful to determine the elasticity of the monolayer. A

third type of experiment is the monolayer stability or isobaric creep experiment. The monolayer stability is determined by maintaining a constant surface pressure while recording the change in area over time.

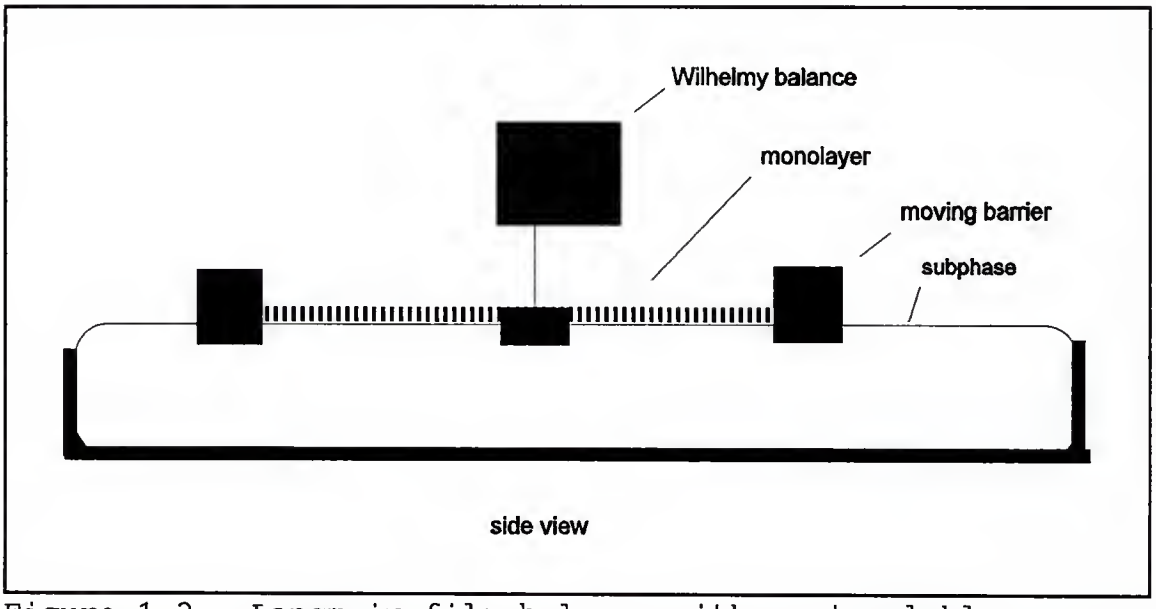

Figure 1-2. Langmuir film balance with an insoluble monolayer of molecules under compression.

LBK films are the result of sequentially depositing monolayers on a solid supporting surface such as a glass slide.[9] To clarify the definition of the terms introduced here, a Langmuir film refers to an insoluble monolayer at the air-water interface. An LBK film is supported on a solid substrate. With LBK technique, a suitable substrate is repeatively passed through the material at the interface. The substrate may be hydrophilic (such as a glass slide) or hydrophobic (such as a glass slide which has been

silylated). During the experiment, an indication of the quality of the deposition is given by the transfer ratio. The transfer ratio is defined as the area of monolayer removed from the water surface divided by the area of substrate coated by the monolayer. In this way, a multilayered thin film is created one layer at a time on the supporting substrate. Layers may be all of one material or any combination of materials which are amenable to transfer to the growing film. If the layers are laid down each time the substrate moves across the phase boundary, then the deposition is of the Y-type (Figure 1-3). It is also possible to have deposition occur only when the substrate enters the subphase (X-type) or leaves it (Z-type), depending on the monolayer material, substrate, subphase, and the surface pressure.[10] When the desired film thickness is achieved, the film on its supporting substrate may be subjected to further processing by other techniques and/or evaluated by the wide variety of analytical methods available for thin films.[11,12]

Oftentimes, the uniformity and fluidity of the Langmuir film gives a good indication of the quality of the resulting LBK technique. For this reason, among others, many researchers have worked to find ways to image Langmuir films.

One of the new imaging techniques that has been developed in the last two decades is the epifluorescensce

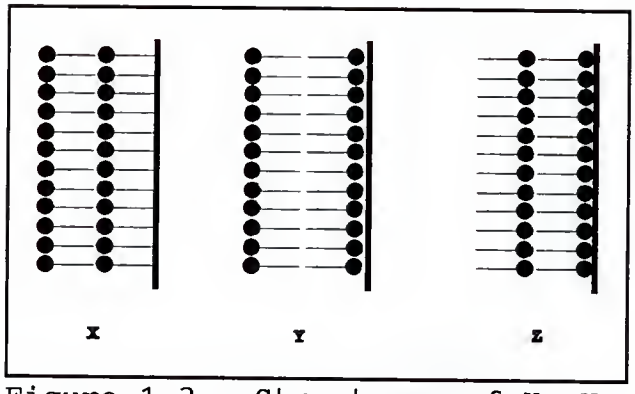

Figure 1-3. Structures of X, Y, and Z-type LBK multilayers.

microscopy technique.[13,14,15,16,17] This technique allowed for the first time the study of morphological changes in the material adsorbed at the interface in real time. The technique suffers somewhat if the material of interest is not fluorescent because the introduction of a probe material with suitable compatibility is then necessary.

A second more recently developed imaging technique is Brewster angle microscopy, BAM.[18,19,20] It is an improvement over epifluorescensce microscopy to the extent that probe molecules are not necessary. On the other hand, early BAM systems suffer from lower resolution (4 μm^2) and image quality. Image quality is lost through the ever-present interference fringes which are the result of using coherent light to illuminate the interface. Nevertheless, the information gained is useful for finding the best conditions for transfer or basic studies of the changing morphology of the material at the interface.

Of course, many other surface analytical techniques besides microscopy have been exploited to learn more about the behavior of molecules at the air/water interface. For example, monitoring surface potential changes during Langmuir film compression can give a clue as to the orientation of dipoles at the interface. The method for measuring the surface potential values reported in this dissertation was the vibrating electrode method. In this method, there is one electrode beneath the water surface and the other electrode in the air above the water surface. The upper electrode is moved with respect to the water surface and the resulting change of the capacitance of the air gap leads to current flow in an external circuit. The magnitude of the current is proportional to the potential difference across the gap. A potentiometer in the circuit is used to find the voltages necessary to prevent the current flow. In an actual measurement, the potential of the clean water surface is set to zero and the change in the surface potential caused by the molecules introduced to the interface is recorded.[8] The effective dipole of the molecules in the Langmuir film may be estimated using the equation,

$$\Delta V = \frac{4\pi\mu_{\perp}}{\langle A_{molecular} \rangle}$$

where $\mu_{\perp}$ is the effective dipole of the film, ΔV is the measured surface potential, and $\langle A_{molecular} \rangle$ is the mean molecular area. The molecules of water are preferentially oriented at the water surface and the introduction of the film-forming molecules alters that structure. Rearrangement of this structure in the water surface changes its contribution to the surface potential to an unknown degree. Thus care must be taken in the interpretation of surface potential data.[21]

Another surface analytical technique is *in situ* UV spectroscopy of the Langmuir film. The apparatus consists of a xenon arc lamp source with a quartz fiber optic cable piping the light through the water surface. The light is collected by a mirror resting on the bottom of the trough and focussed onto the end of a second quartz fiber optic cable suspended above the water surface. This second fiber optic cable carries the light to a diffraction grating which is precisely aligned so that each wavelength strikes a separate diode in a diode array. The discrete voltages generated by each diode are processed to give a reading corresponding to the intensity of each wavelength. In an actual experiment, the range of intensities from the clean water surface are subtracted from the intensities with the monolayer present. In this way an absorbance spectrum is obtained in a range of wavelengths determined by the choice of diffraction grating.

Scientific interest in LBK films arises from the possibility of constructing designed molecular architectures which allow the study of physical phemomena on a molecular level. Practical interest arises from the continuous trend of size reduction of electronic devices, which calls for new materials and processing techniques.

Macroscopic properties of organic solids are closely related to their microstructure. LBK films often possess a highly crystalline lamellar structure with domains of diameter between 0.1 and 10 micrometers. Shear forces occuring during the monolayer deposition can deform the domains and induce a highly anisotropic morphology.[22]

In principle all substances which form stable monolayers and contain isolated or conjugated double or triple bonds or epoxide moieties can be polymerized in LBK films upon high energy radiation. However, monomers containing vinyl groups were found to be less suited than monomers containing the larger butadiene or diacetylene group, because during polymerization a mismatch arises between the packing of the hydrocarbon chains and the polymer chain containing the rather short vinyl repeat unit formed *in situ*.[23] Thus, phase transitions are induced which are often accompanied by incomplete conversion and a disordering of the layer structure. The reported electrical conductivities of LBK films have been lower than the corresponding values of single crystalline materials. This

is probably due to relatively poor contacts between individual domains.[24]

Further research on LBK films has to be directed towards better morphological control and improved thermal and mechanical stability. One approach is to change molecular architecture. Results with polymeric LB films based on polyimides,[25] maleic anhydride copolymers,[26] polyglutamates in the α-helix form,[29] or polyphthalocyaninatosiloxanes[27] are quite promising. Molecules which are amphiphilic are usually but not always best suited for processing by the LBK technique. Besides the usual amphiphiles, molecules of completely different structures such as porphyrins, phthalocyanines, oligothiophenes, polycyclic aromatic quinones, and a variety of polymers form stable monolayers and LBK films.[9]

A second tactic has been to improve processing experimental conditions. A more suitable shaping of LBK troughs might also help to improve morphological quality.[9] Also, various annealing, thermal treatments, and compression schemes have been discussed.[28] Unfortunately, at present, there is no tool for organizing microstructures within the layer plane and a specific interlayer alignment of molecular domains is not possible yet either.[29] The incorporation of liquid crystalline order into LBK films is one possible strategy to increase the size of these domains. For example, after the usual LBK processing to generate a

multilayer film with each layer having multiple domains, the film could be heated up to the transition temperature between the crystalline and liquid crystalline (LC) state. In the liquid crystalline state the molecules are less ordered but are still quite highly aligned. Also while in the LC state, the domains in each layer may increase in size through normal coarsening processes or the direction of alignment may be changed using electric or magnetic fields. Now when the film is cooled back to the crystalline state, each layer can have fewer but larger domains. This type of processing of LBK films has been demonstrated using preformed LC side chain polymers.[30]

Several excellent reviews of the diverse materials that have been studied with LBK may be found.[9,31,32] The use of preformed polymers for the preparation of LBK films has been discussed along with recent developments in the different classes of polymers for LBK multilayers and their outstanding properties highlighted.[33]

Polymers from Pre-oriented Monomers in Langmuir-Blodgett-Kuhn Films

Highly ordered crystals of macromolecules can be obtained using solid-state polymerization of LBK films. The initiation of the polymerization is typically stimulated by thermal,[34] radiative,[35] or chemical methods.[36] There are a number of fundamental questions associated with initiation,

propagation, and termination processes in an LBK film. A central problem in solid-state polymerization is associated with chain propagation in which the hybridization of the atoms involved changes during the reaction, for example, sp to sp^2 in acetylene polymerization.[34] In such reactions, the van der Waals contact distances change to covalent bond distances. Thus there is necessarily a change in lattice distances during the polymerization; nevertheless, fully crystalline polydiacetylene has been obtained in a solid state reaction. Highly ordered films of polydiacetylene are obtained either on the air/water interface or on solid supports.[37,38]

Chemically adsorbed monolayers of substituted monoacetylenes have been polymerized using catalysts or high energy electron beam irradiation.[39] Monoacetylenes have also been polymerized in solid crystals. For example, crystalline metal propiolates are converted by gamma irradiation to amorphous metal polypropiolates.[40] Propargylamine in a tetrachlorocadmate layer complex was polymerized by gamma irradiation.[41] Some questions that have not been answered by these studies remain. The polymer repeat structure could be critically dependent on the substituent of the terminal acetylene and the details of the monomer orientation. Still, short crystallographic contacts between potentially reactive acetylenic carbons are not sufficient to guarantee reactivity, and mechanistic issues

associated with initiation and propagation, which are unknown at present, are important[42]. One of the questions explored in this thesis is the effect of substituent on the terminal acetylene by studying LB films of alkylactylenes and arylacetylenes.

Soluble Derivatives of Polyphenylene-ethynylene

Rigid rod polymers with a linear conjugated backbone built up by para-linked arylene units are interesting compounds due to their unique properties concerning heat stability and photoconductivity. Rod-like polymers can be organized in the form of LB films for reasons related to the stiffness of their backbone. Stable monolayers are formed by polymers which exhibit groups with few or very small polar functional groups. Generally, the transfer of these materials is poor[43] and therefore these materials were not considered to be suited for formation of multilayers. To overcome this problem, rod-like polymers surrounded by conformationally mobile side chains to prevent crystallization were developed.[44] On a 2D plane, the shape of objects governs to a great extent the efficiency of packing as the objects are forced together by pressure. For example, when equal-sized disks pack together in a plane, the maximum coverage of the surface is only 0.9069. An elliptical shape will cover greater and greater fractions of the surface as the aspect ratio (length to width) is

increased. Extreme aspect ratios seen in rigid rods or hard needles are predicted to lead to the most efficient packing and also anisotropy within the plane.[45]

Thus, soluble polyphenylene-ethynylenes offer the potential to obtain well defined layered structures in LBK films.[46]

Principal Objectives of this Dissertation

The overall objective of this dissertation is the description of the behavior of mesogen substituted acetylene monomers and polymers in monolayer films at the air/water interface and as multilayer films including the formation of such films. Fundamental knowledge to be gained would include the effect of balancing hydrophilic and hydrophobic tendencies in a molecule more complex than the classical fatty acids or lipids. The effect of molecular shape on the packing and thus the ultimate stability of monolayers formed from these new molecules was explored. In Chapter 2, the work takes on the challenge of preorienting monomers in well-ordered arrays prior to attempting polymerization with the hope that order would be preserved in any resulting polymer. New knowledge gained with regard to the acetylenic monomers includes processing of the acetylene monomer into multilayer films, followed by the design and synthesis of a second generation of improved monomer structure for superior LBK film transfer properties. A third generation of

acetylenic monomer was synthesized which approaches more closely the goal of solid state polymerization of these materials.

The work reported in Chapter 3 takes a different approach. The materials are pre-formed poly(phenylene-acetylene) polymers so questions about reactivity are mute. The materials are a variation on the well-known hairy-rod polymers with regard to their Langmuir film-forming properties. The shape of these rigid-rod molecules leads to comparisons with theoretical models of needles on a 2D plane. These polymers differ from previously studied rigid-rod polymers in that the alkyl side chains which give these polymers their solubility are terminated with a hydroxy group. Thus the Langmuir films gain stability not only from the packing of the polymers but also through strong adsorption to the water surface. This difference leads to non-classical 2D phase behavior. New knowledge gained with regard to the poly(phenylene-acetylene)s includes detailed description of the two-dimensional phase behavior of these materials. This description includes not only the microscale morphology of 2D phase separation but also a description of the nanoscale intra- and intermolecular arrangement.

CHAPTER 2
LANGMUIR AND LANGMUIR-BLODGETT FILMS OF MESOGEN SUBSTITUTED ACETYLENE MONOMERS

Introduction

Toward the ultimate goal of developing polymeric materials with high electrical conductivity and high third order nonlinear optical properties, this work focussed primarily on a class of substituted acetylenes which might exhibit liquid crystalline behavior while at the same time possessing amphiphilic character (Figure 2-1). It is known that both the conductivity and nonlinear optical properties are improved when the polyacetylene is highly ordered.[47]

Since the discovery of electrical conductivity in polyacetylene, this class of compounds has become the subject of intense research activity.[48] The subsequent discovery of the nonlinear optical properties[49] of acetylenes has created additional interest. Polyacetylenes are characterized by large molecular hyperpolarizability as a consequence of having highly displacable electron clouds, e.g. in extended π - electron systems.[50] High nonlinear properties are dependent on not only the extended π-electron system but also on the overall order of the molecules. The ultimate goal of this research is the

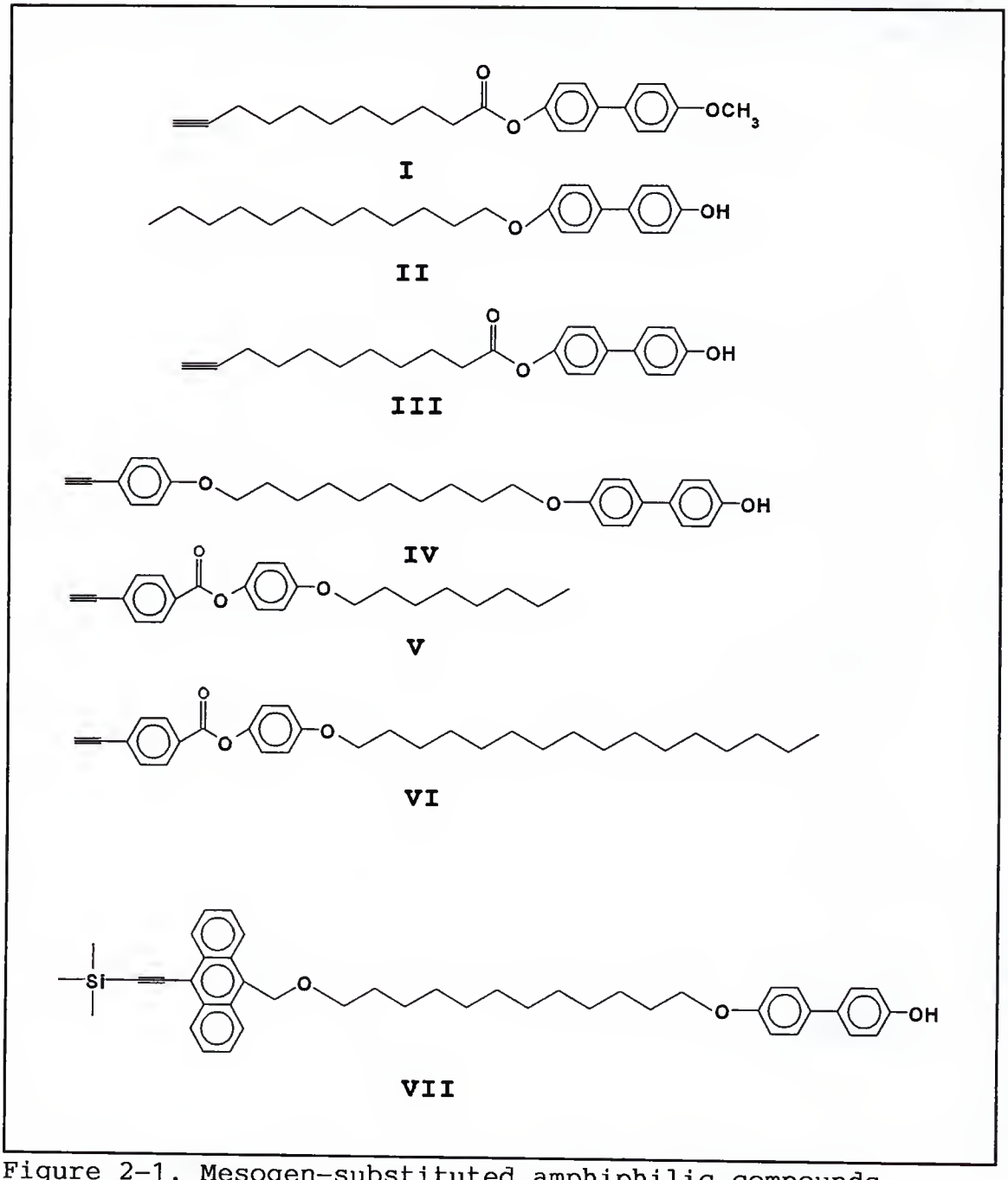

Figure 2-1. Mesogen-substituted amphiphilic compounds studied with the Langmuir-Blodgett-Kuhn technique.

polymerization of these LC-substituted acetylenes. As a first step toward that goal the production of LBK films of these materials has been achieved.

Liquid crystals are used as display devices in which the function comes from the ability of the liquid crystalline molecules to self organize.[51] The use of liquid crystals in making Langmuir-Blodgett-Kuhn films is a step towards better morphological control.[52] The Langmuir-Blodgett-Kuhn technique offers potentially greater control over molecular orientation and inter-molecular packing which could lead to the creation of new types of thin-film devices.[53] Previous attempts at polymerization of alkyl substituted monoacetylenes by catalysts in solution have been mostly unsuccessful.[54,55] On the other hand, solid state polymerization of monoacetylenes has been achieved by gamma irradiation in some cases[56,57] but failed in another.[58] Yet, in general, a successful solid state polymerization can lead to highly ordered polymer.[59] In this work, an approach to solid state polymerization, utilizing amphiphilic mesogen-substituted acetylenes, was tried. Such compounds are amenable to manipulation using the Langmuir-Blodgett-Kuhn technique into a two-dimensional monolayer.[60,61] The ideal monomer, incorporated in the monolayer, would polymerize to yield high molecular weight, highly ordered substituted polyacetylenes.

It has been shown that conductivity in polyacetylene is a function of the conjugation length and degree of long range order present in the material.[62] This work was based on a two-pronged strategy to increase inherent order of the

monomers prior to polymerization (the polymerization, in essence, "locking-in" the predetermined geometry of the monomers). First, the liquid crystallinity of the monomer should be such that the acetylene group present on each molecule would be positioned as near to the ideal for polymerization as possible. Second, the amphiphilic character of the monomer is exploited to create two-dimensional films using the Langmuir-Blodgett-Kuhn technique. In other words, the liquid crystallinity influences the orientation of the monomers normal to the plane of the monolayer while the Langmuir-Blodgett-Kuhn technique determines the orientation of the monomers within the plane. The repeat unit length of two acetylene units joined in cisoid conformation is in the range of 4 to 4.5 Å.[63] This distance between acetylene groups would be optimal for the polymerization. For a usual head to tail polymerization the acetylene groups should be at a 120° angle with the α carbon of each acetylene within 4 to 4.5 Å of the β carbon of its neighbor. This is a reasonable geometry to expect from Y-type LBK deposition because the tilt angle of monomers is often in the range of 30° from the normal.

Previous work with liquid crystalline substituted monoacetylenes has been largely done by three other research groups. Sandman et al. have worked with liquid crystalline acetylenes for many years and published a review article.[64]

Le Moigne and coworkers have synthesized a number of liquid crystalline substituted monoacetylenes and polymerized a few of these acetylenes in solution using Ziegler-Natta catalysts (albeit to low yield).[65] X. Zhang of the Blumstein research group has synthesized several liquid crystalline substituted monoacetylenes (for example, compound **I**), but also had little success with polymerization[66] by conventional techniques.

The compounds listed in Figure 2-1 represent variations of the basic theme. Preliminary work showed that **I** when mixed with **II** led to processible Langmuir films. Compound **III** has the desirable properties of **I** and **II** in one molecule. Compound **IV** is a variation on compound **III**. A phenyl ring is introduced next to the acetylene group for two reasons. First, conjugation between the phenyl ring and the acetylene group will increase the wavelength of peak absorbance. Thus it may be possible to initiate radical polymerization using UV irradiation or by heating instead of the more drastic gamma irradiation. Secondly, the phenyl group was introduced at this position so that the phenyl group would serve to limit the distance of interdigitation between LB layers (assuming Y-type deposition). Compounds **V**, and **VI** are also phenylacetylenes like **IV** but they have the mesogen located close to the polymerizable group. It is well known that side chain liquid crystalline polymers with the mesogen close to the main chain can form ribbon-like

conformations of the main chain whereas the presence of a spacer between the main chain and the mesogen favor helical conformations.[67] The series, **V** and **VI**, also differ from the other compounds in this study, in that the most hydrophilic part of the molecule includes the acetylene group (which has a significant dipole). Within the series, **V** and **VI**, the length of the hydrophobic tail was varied to study its effect on film properties. Compound **VII** is an extention of the strategy that led to **IV**. The anthracene moves the maximum absorbance peak to still longer wavelengths, indeed, unsubstituted 9-ethynylanthracene has been reported to "spontaneously" polymerize.[68] The substitution pattern on the anthracene ring allows it to strongly affect the conformation of the polymer main chain possibly leading to ribbon-like conformation. Anthracene is also stable while carrying a -2 charge.[69] Thus polyethynylanthracene would be an interesting polymer with regard to its ability to maintain charge separations. Such charge separations are a key element of photorefractive nonlinear optical materials.

Langmuir Technique

One goal of this work has been to explore the possibility of polymerizing arylacetylene compounds through the irradiation with UV light of monomer arranged in a monolayer at the air-water interface. It is anticipated that the resulting polymer film will have fewer defects

caused by polymerization shrinkage because the computer controlled apparatus can maintain a constant lateral pressure on the monolayer to compensate for this shrinkage. These experiments required apparatus for purging the atmosphere around the trough with an inert gas, such as Ar to eliminate the problems of free-radical scavenging by O_2 and O_3 attack on any polymerizing acetylene. The fact that the monomers are pre-oriented prior to polymerization may lead to a more ordered polymer configuration. This has been observed, for instance, in the case of the 3-alkyl pyrroles, where a very high degree of 2,5 substitution is observed by Langmuir film polymerization.[70] The polymer film may then be transferred to a solid support or a solution for further characterization.

Polymerization of Langmuir-Blodgett-Kuhn Films

Monolayers of the monomers were transferred to a solid substrate, for example, a quartz plate to produce Langmuir-Blodgett-Kuhn films. The computer controlled system has the capability of dipping a quartz plate through the monolayer while at the same time maintaining the same amount of lateral compression of the monolayer by moving the barrier. Any number of monolayers may be built up on the quartz plate in this way. Attempts were made to polymerize the deposited multilayers by gamma and UV irradiation. Preliminary work

with the compounds has suggested that it is possible to polymerize this class of compounds with gamma irradiation.[55]

Using the Langmuir-Blodgett-Kuhn technique, two-dimensional monolayers of these compounds may be made. Monolayer by monolayer, the acetylene monomer can be built up on a solid substrate into a multilayer microstructure. In order for solid state polymerization to be possible, the intermolecular geometry of the acetylene functional groups must fall within precise constraints. Thus, realistically, it is necessary to first show that such compounds can indeed be processed into LBK multilayers. Once LBK multilayers are made, then "fine-tuning" of the molecular structure can be undertaken to achieve the required intermolecular geometry. However, correct geometry between the acetylene functional groups does not guarantee that polymerization will take place.[64]

Experimental

Compound **I** was synthesized by X. Zhang of the Blumstein group at the University of Lowell, Massachusetts.[55] Compound **II** was synthesized by A. Shüster of the Ringsdorf group at the University of Mainz, Germany. Compounds **V** and **VI** were synthesized by R. C. Advincula of the Duran group at the University of Florida.[71] All the other monomers were synthesized as described below.

The proton and carbon-13 nuclear magnetic resonance spectroscopy was performed using a General Electric QE-300 300 Mhz NMR. The Fourier transform infrared spectra were obtained using a Biolab FTIR fitted with the diffuse reflectance attachment. Mass spectroscopy were performed by Maria Ospina in the lab of Dr. David Powell at the University of Florida. Melting points were obtained using a oil bath melting point apparatus.

Synthesis of 4-hydroxy biphenyl-4'-(11-undecynoate), **III**

The 4-hydroxy biphenyl-4'-(11-undecynoate), **III**, was synthesized using the following procedure. A solution of 10 mmol 10-undecynoic acid (Farchan), 10 mmol biphenol (Aldrich), and 0.5 mmol p-toluene sulfonic acid was made in a minimum (10 ml) of dry pyridine and placed in a 100 ml round bottom two neck flask under dry N_2 purge. Stirring continuously, a solution of 15 mmol 1,3-dicyclohexylcarbodiimide (DCC, Aldrich) in 5 ml dry pyridine was added dropwise over a 5 minute period. After all the DCC solution was added, the reaction solution remained clear yellow-orange in color. Three minutes after the DCC was added, white crystals of the urea began to precipitate. After 6 days, the urea crystals were filtered and washed with cold pyridine. The filtrate was collected. Chloroform (0°C, 50 ml) was added to the filtrate. The pyridine was removed from the filtrate by reaction with 5M HCl leaving

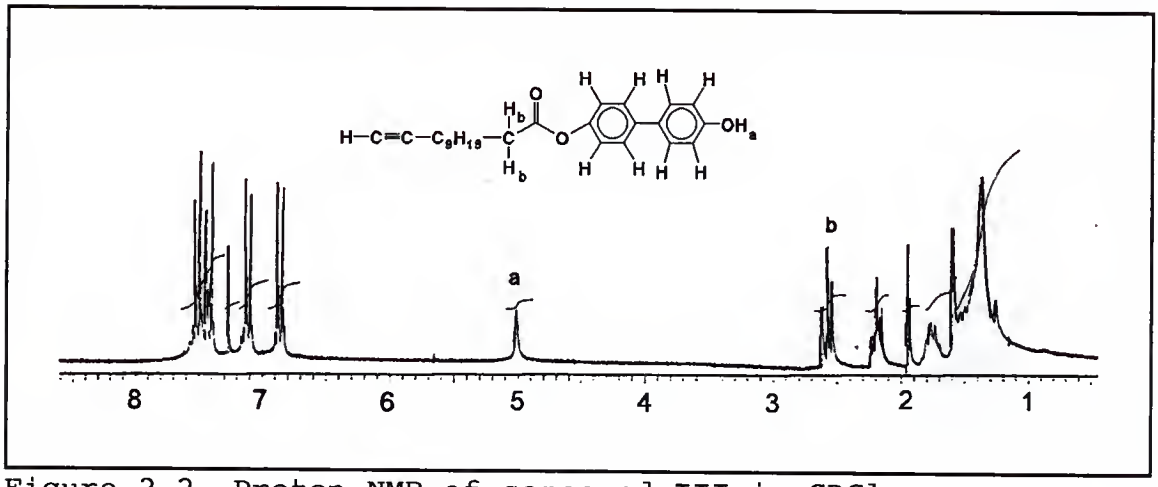

Figure 2-2. Proton NMR of compound **III** in $CDCl_3$.

the product mixture in the chloroform phase. Enough 5M HCl was added to give an acidic reading on the pH paper. The phases were separated and another 50 ml of 5M HCl was added to the chloroform phase. The chloroform phase was washed twice more with 50 ml portions of 5M HCl followed by two washings with 50 ml of deionized water and then two washings with 50 ml portions of saturated $NaHCO_3$. The chloroform phase was left overnight to dry over anhydrous Na_2SO_4. The chloroform solution was filtered again and then rotavapped to give off-white crystals. Thin layer chromatography was used to determine that the best solvent system for separation of the product mixture was $CHCl_3$:ethyl acetate; 4:1. TLC of the product mixture showed four spots. The spots with the two lowest R_f values corresponded to the unreacted biphenol and undecynoic acid. The spot with the highest R_f corresponded to the diester product and the second highest R_f spot was the desired product. The product

mixture was dissolved again in a minimum of the $CHCl_3$:EtAc for separation on a silica gel (100-200 mesh) chromatography column. ^1H NMR in $CDCl_3$ of the purified product (Figure 2-2) gave δ = 1.4 m, 1.8 m, 1.9 t, 2.2 m, 2.6 t, 5.0 s, 6.8 d, 7.1 d, 7.3 s, 7.4 d, and 7.5 d. The peaks from 6.8 to 7.6 ppm are the aromatic protons of the biphenyl moiety. The peak at 7.26 is the chloroform peak.

Synthesis of 4-(4'-ol-biphenyl-4-decanoxy)-phenylacetylene, **IV**

The overall synthetic scheme for the synthesis of this mesogen-substituted phenylacetylene is shown in Figure 2-3.

Synthesis of 4-(10-hydroxyldecanoxy)-iodobenzene, **IX**

The reaction was set up by transferring 54 ml of 1 N KOH and 100 ml of toluene to a 500 ml 3-neck roundbottom flask fitted with a reflux condenser under N_2. The next reagents added were 7.3 g of tetra(n-butyl)ammonium bromide followed by 10 g of iodophenol. At this point, the organic phase had a light hint of purple color while the aqueous phase was clear. The final reactant added to the reaction flask was 5 ml of 10-chlorodecanol. After 12 hours of reflux, the final 5.1 ml portion of 10-chlorodecanol was added using a transfer pipette. The yield of desired product was found to increase with the number of days the reaction mixture was allowed to reflux. After 7 days of

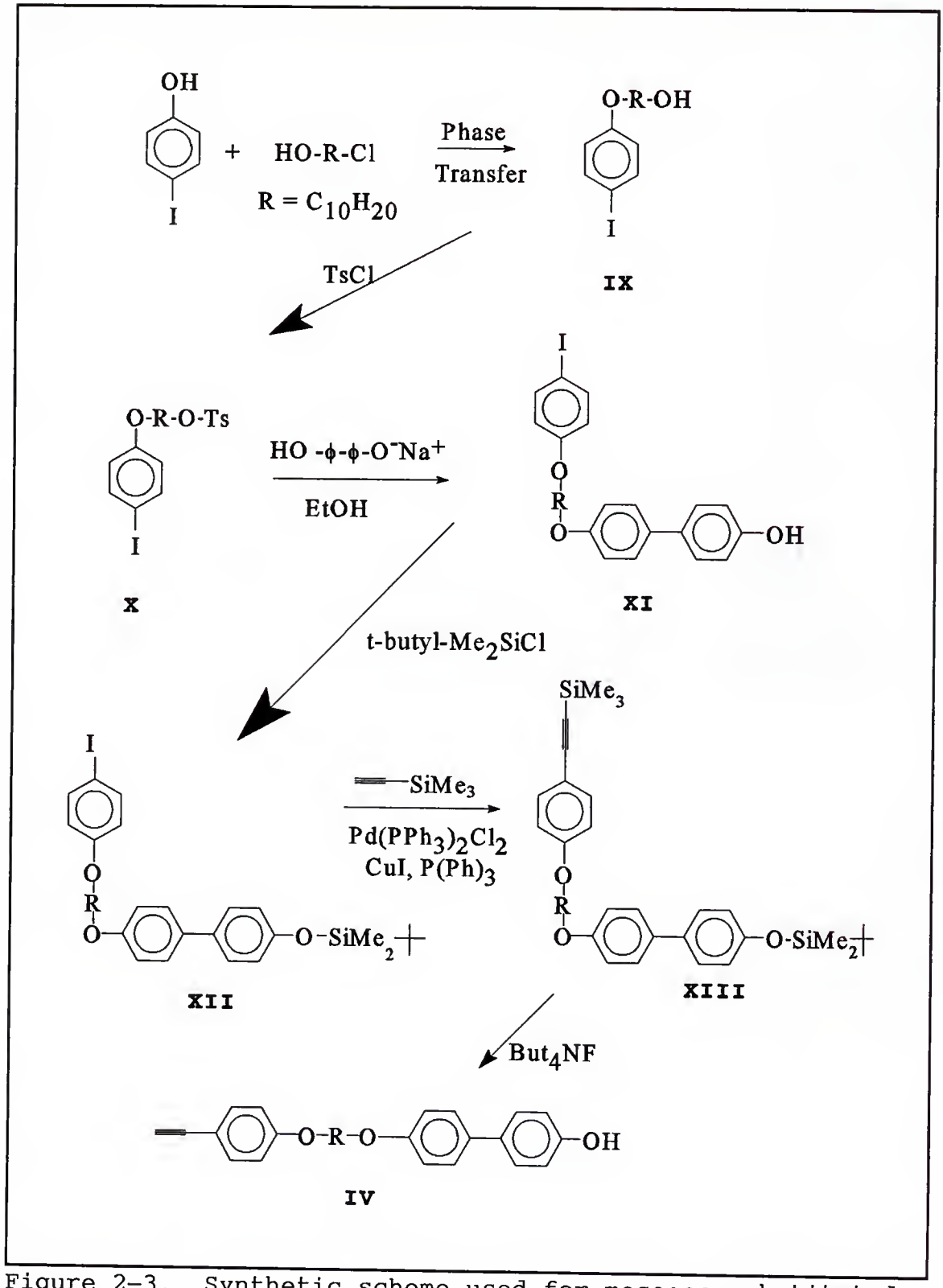

Figure 2-3. Synthetic scheme used for mesogen-substituted phenylacetylene.

reflux, the organic phase is clear golden yellow. The reaction was stopped by turning off the heat and transferring the reaction solution to a separatory funnel with 250 ml of chloroform. The organic phase was washed with two 250 ml portions of deionized water, two 100 ml portions of 5% by weight KOH solution, two 100 ml portions of saturated NH_4Cl solution, and finally with 100 ml of deionized water. The organic phase was dried over $MgSO_4$ and filtered. The solvent was removed under reduced pressure with a rotary evaporator. The clear yellow oil so obtained slowly solidifies to a white waxy solid. Yield was 16.1 g of **IX** or 95%. Elemental analysis found 32.4% iodine (calculated 33.7%), 52.2% carbon (51.2%), and 7.0% hydrogen (6.7%). Proton NMR in $CDCl_3$ of the product shows δ = 1.3 (m, alkyl); 1.8 (m, alkyl); 3.6 (s, 1H, alcohol proton); 3.7 (t, 2H, methylene protons α to the OH); 3.9 (t, 2H, methylene protons α to the arylether); 6.6 (d, 2H, aromatic); and 7.5 (d, 2H, aromatic).

Synthesis of the Tosylate of 4-(10-hydroxyldecanoxy)-iodobenzene, **X**

Three grams of 4-(10-hydroxyldecanoxy)-iodobenzene, **IX**, were dissolved in 50 ml of dry pyridine and cooled to 0°C in a stoppered 125 ml Erlenmeyer flask held in an ice water bath. Two equivalents (5.2 g) of toluene sulfonyl chloride were added and dissolved. The top of the stoppered flask

was wrapped with parafilm and the flask was kept in a refrigerator (< 5°C) for 24 hours. The reaction mixture was initially clear yellow but became darker in color (sometimes becoming clear red) over time with the precipitation of clear long needle-like crystals. The reaction mixture was poured into a 600 ml beaker filled with 400 g of ice water while stirring with a magnetic stir bar. The reaction mixture was milky white in the ice water. Sometimes the white crystals of the tosylate would precipitate at this point and the crystals were then filtered and dried in a dessicator. Other times the crystals did not precipitate at this point so the reaction mixture was extracted twice with diethyl ether. The ether solution was extracted twice with 1:1 $HCl:H_2O$ to remove the pyridine, then washed with deionized water and dried with anhydrous Mg_2SO_4. The ether was then removed using a rotary evaporator at room temperature. It is important to keep the tosylate at or below room temperature until ready for use. This procedure yields 2.3 g of pure white crystals of the tosylate, **X**. Proton NMR in $CDCl_3$ shows all of the peaks of the starting material (except the alcoholic proton), plus the characteristic methyl peak at 2.4 ppm of the tosylate. The FTIR also shows a band at 1355 cm^{-1} due to the asymetric $S(=O)_2$ stretch and a band at 1177 cm^{-1} due to the symmetric $S(=O)_2$ stretch also characteristic of a tosylate.[72]

Synthesis of 4-(10-(4-Iodophenoxy)decanoxy) biphenyl-4'-ol, **XI**

This reaction was set up by dissolving 0.2 g (1 equivalent) of NaOH with 50 ml of pure ethanol in a 250 ml three-neck round-bottom flask fitted with a reflux condenser under a slight positive pressure of dry N_2 gas. After the NaOH dissolved, 0.9 g of 4,4'-biphenol was added and the reaction mixture was heated to a light reflux. The reaction mixture had a clear lime green color due to the biphenolate anion. After 30 minutes, 2.3 grams of **X** was added. As the reaction proceeds, white solids precipitate and the green tint of the solution becomes colorless. After 4 to 8 hours reaction time, the heat was removed and the reaction mixture was allowed to slowly cool to room temperature. The white solids formed were filtered and recrystallized with ethyl acetate. The product yield is 0.7 grams of small pure-white crystals of **XI**. The melting point was 154-156 °C. The 2 °C range of melting is an indication of the product purity. The product was soluble in tetrahydrofuran or pyridine. The proton NMR in pyridine-d_5 of the product shows peaks δ = 1.5 (m, alkyl); 3.9 (t, methylene protons α to arylether linkage); 4.1 (t, methylene protons α to the other arylether linkage); 5.3 (s, aryl OH proton); 6.7 (d, aromatic); 6.9 (d, aromatic); 7.4 (m, aromatic). Elemental analysis results were 21.9% iodine (calculated 23.3%), 62.6% carbon (61.8%), and 6.2% hydrogen (6.1%).

Synthesis of 4-(10-(4-Iodophenoxy) decanoxy)biphenyl-4'-(t-butyldimethylsilanol), **XII**

This reaction was set up by dissolving 3.4 g of 4-(10-(4-Iodophenoxy) decanoxy)biphenyl-4'-ol, **XI** in 200 ml of dry tetrahydrofuran in a 250 ml round bottom flask under a positive pressure of dry N_2 gas. Next, 0.9 g (2 equivalents) of imidazole was added to the reaction flask followed by 1.1 g (1.2 equivalents) of t-butyldimethylsilylchloride. The reaction mixture was stirred with a magnetic stirrer at room temperature for 12 hours. Progress of the reaction is indicated by the precipitation of the fine white crystals of imidazole·HCl. The product is obtained by filtering off the imidazole·HCl crystals and removing the solvent using a rotary evaporator. This procedure yielded 3.6 g of product. The presence of the protecting group is seen in the proton nmr in $CDCl_3$ by the strong peaks at 0.1 ppm due to the presence of the silyl protecting group (Note: The starting material is sparingly soluble in $CDCl_3$ but the protected material is moderately soluble and allows a good nmr to be obtained).

Synthesis of 4-(4'-ol-biphenyl-4-decanoxy)-phenylacetylene, **IV**

This reaction was started by dissolving 0.1 g of **XII** with 20 ml of triethylamine from a freshly opened bottle and 10 ml of dry THF in a 100 ml 3-neck round bottom flask

fitted with a dry ice condenser and magnetic stir bar. The reaction was run under a slight positive pressure of dry N_2. The catalyst, di(triphenylphosphine)palladium dichloride and cocatalysts, CuI and triphenylphosphine were transferred in the amount of 6.9 mg catalyst (nominal would be 0.02 equivalents to **XII**) and 1.3 mg of CuI (nominal would be 0.02 equivalents to **XII**) and 4.9 mg PPh_3 (nominal would be 0.08 equivalents to **XII**) with a minimum of dry THF to the reaction flask. Next, 0.1 ml of trimethylsilylacetylene (nominal would be 1.1 equivalents to **XII**) was transferred using a syringe through a septum from the stock bottle and then through a septum into the reaction flask. The reaction mixture was allowed to stir at room temperature for 10 minutes before a heating mantle controlled by a Variac was used to heat the reaction mixture to a gentle reflux. The reaction mixture slowly turned from clear through clear yellow with suspended white solids to clear yellow with suspended black solids during the 24 hour reaction time. After 24 hour, the reaction flask was removed from the heating mantle and allowed to cool to room temperature. The solvent was removed with a rotary evaporator. The solids were resuspended in a minimum of chloroform and filtered through a silica gel plug to remove the black precipitated amine salts, triphenylphosphine, CuI, and catalyst. An additional 300 ml of chloroform were passed through the silica plug. Thin layer chromatography showed four spots

when developed with chloroform. The desired protected product, **XIII** was obtained by chromatography through silica gel eluted with chloroform, R_f=0.5, as a off-white solid (43 mg). Proton NMR in $CDCl_3$ of the product **XIII** shows peaks δ = 0.05 (t, methylsilyl); 0.1 (t, methylsilyl); 0.15 (t, methyl silyl); 1.5 (m, alkyl); 3.9 (t, methylene aryl ether); 4.1 (t, methylene aryl ether); 5.3 (s, phenolic OH); 6.7 (d, aromatic); 6.9 (d, aromatic); 7.4 (m, aromatic). Carbon-13 NMR of **XIII** in $CDCl_3$ shows peaks δ= -1.5 (silyl C); -0.9 (silyl C); 0.0 (silyl C); 24.7 (alkyl); 25.0 (alkyl); 28.1 (alkyl); 28.3 (alkyl); 28.5 (alkyl); 52.4, 67.1, 75.6 ($CDCl_3$); 76.0 ($CDCl_3$); 76.4 ($CDCl_3$); 84.9, 92.0, 104.5, 113.4, 113.8, 114.6, 119.3, 126.6, 126.8, 132.4 and 158.0.

To remove the silyl protecting groups, 0.9 g of **XIII** was dissolved in 20 ml of THF in a 100 ml round bottom flask. Next, 8 ml of 1 M tetra(n-butyl)ammonium fluoride (3 equivalents) were added to the reaction mixture and the flask was stoppered. The reaction was allowed to proceed at room temperature for 50 minutes with occasional swirling. The solvent was removed using a rotary evaporator. Next, 50 ml of deionized water were added, resulting in the precipitation of an off-white solid. The solid was filtered with a Buchner funnel, then put in a dessicator to dry overnight. Thin layer chromatography using a 7:3

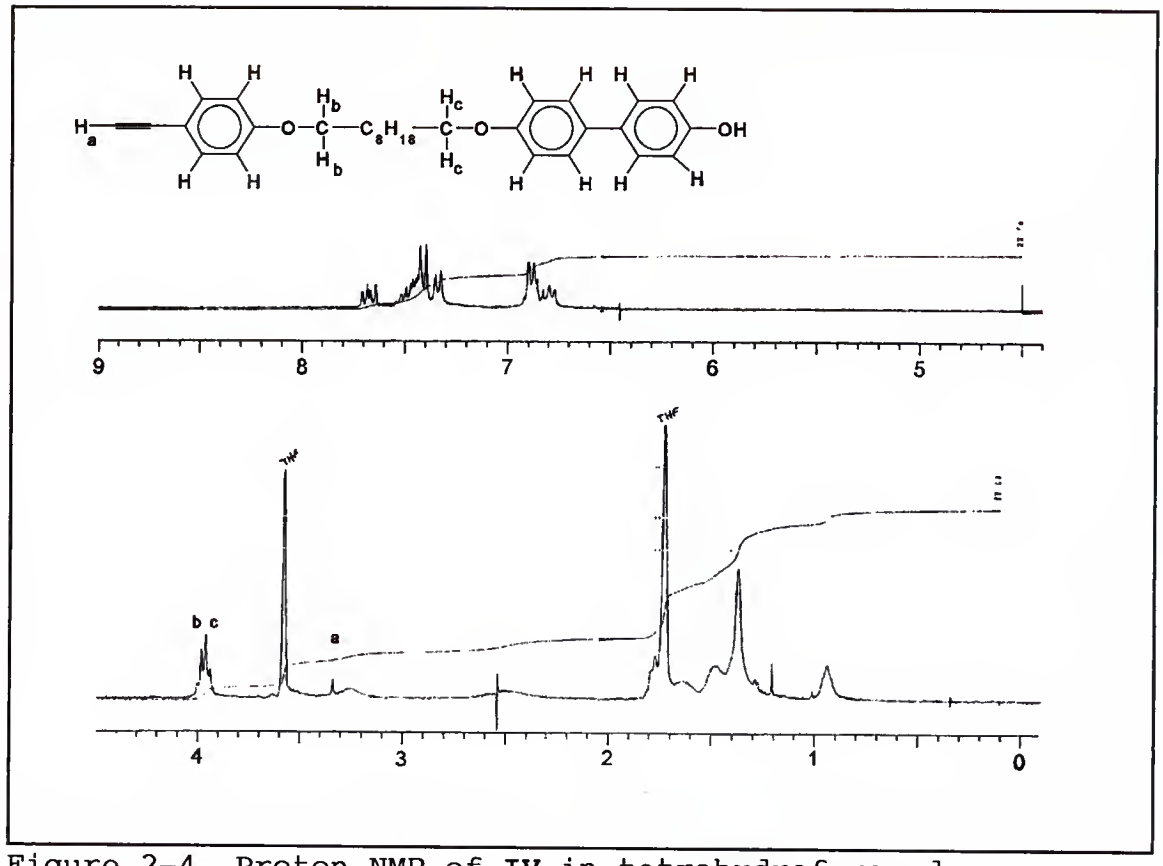
H
H
H

triple bond. The product, **IV** slowly decomposes over a few days so material used for LBK experiments must be freshly purified.

Synthesis of 2-(10-(4'-ol-biphenyl-4-oxy) dodecanoxymethyl)-anthryl)-trimethylsilylacetylene, VII

The overall synthetic scheme for the synthesis of this mesogen-substituted anthrylacetylene is shown in Figure 2-5.

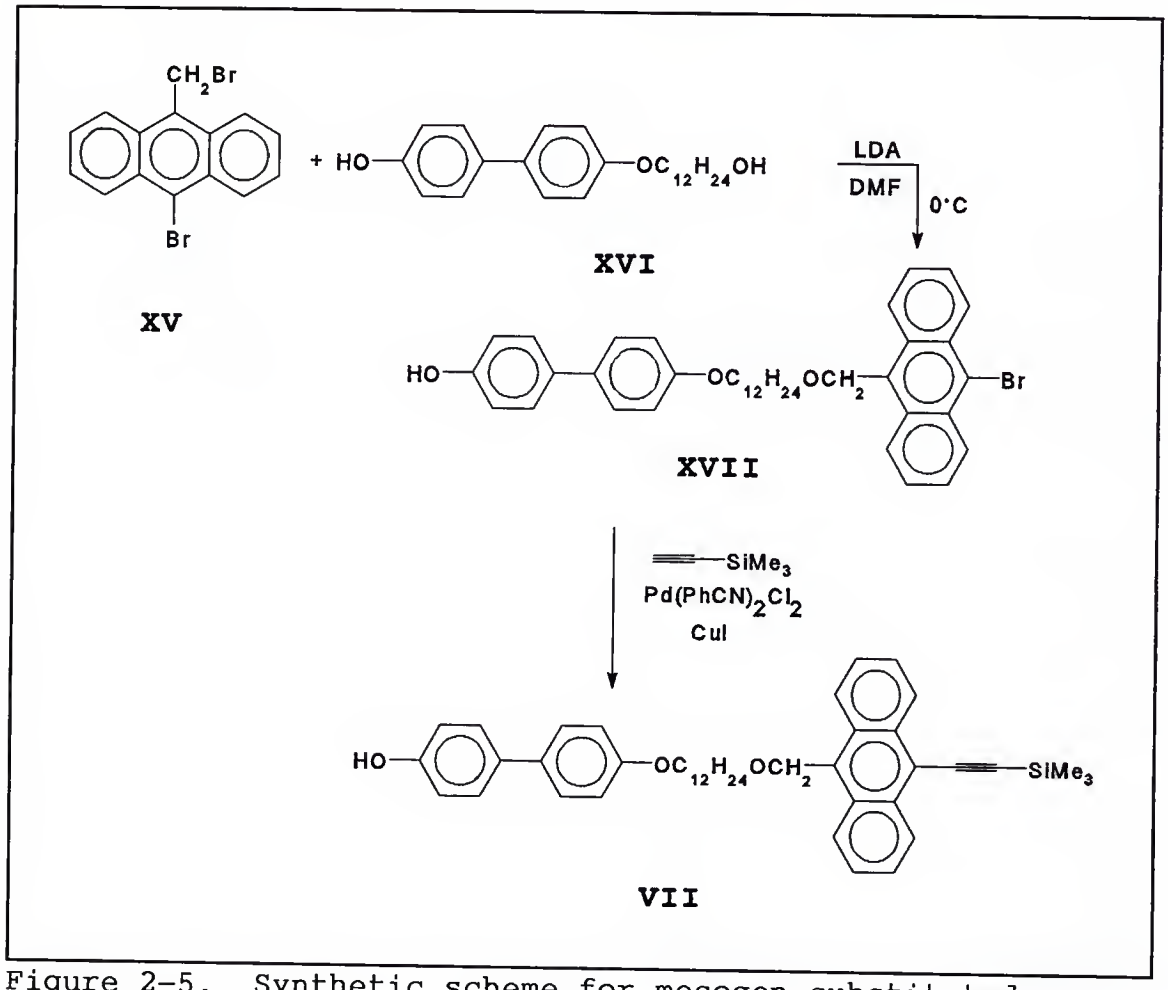

Figure 2-5. Synthetic scheme for mesogen-substituted anthrylacetylene.

Synthesis of 9-bromo, 10-(12-(4'-ol-biphenyl-4-oxy)dodecanoxymethyl)anthracene

The dibromomethylanthracene and the 4-(12-bromododecanoxy)-biphenyl-4'-ol used in this reaction were provided by Mr. Wei Shen and Dr. Thomas Servay. This reaction requires that special care be taken to minimize the amount of water in the reaction flask. All glassware was dried at least overnight in an oven. To determine the best reaction conditions, two series of screening reactions were performed. These screening reactions were carried out in 5 ml test tubes covered with rubber septa. The solid reactants were weighed directly into the test tubes and dissolved in 1 ml of solvent before the tube was flushed with dry N_2 and sealed with the septa. For the reactions which used NaH (a solid) as the base, the NaH was transferred to the reaction test tube with the solvent before sealing the tube with a septum. In the first series, the conditions were varied to find out the best base and solvent to use for the reaction. The reactions were followed by thin layer chromotography (TLC) developed with 1:9 toluene:acetone. TLC were graded on the basis of disappearance of the spot for the dibromomethylanthracene (DBMA) and the presence of side products. The reaction conditions used and the results obtained are listed in Table 2-1.

Table 2-1. Screening reaction results for determination of base and solvent (LDA is Lithium diisopropyl amide; tbL is t-butyl Lithium).

	solvent	DBMA µmol (mg)	**XVI** µmol(mg)	mole ratio (**XVI**/ DBMA)	Base, equiv	Time to completion, time to side products, min
1	DMF	3.1 (1.1)	2.4 (0.9)	0.8	NaH 2.1	30 @ 25°C 25 @ 80°C
2	DMF	3.1 (1.1)	2.7 (1.0)	0.9	LDA 2.0	<5 @ 25°C 30 @ 45°C
3	THF	5.4 (1.9)	6.2 (2.3)	1.1	LDA 2.0	>25 @ 80°C 30 @ 45°C
4	THF	5.4 (1.9)	5.7 (2.1)	1.0	tbL 2.0	>25 @ 80°C 30 @ 45°C
5	CH_3CN	2.6 (0.9)	2.2 (0.8)	0.9	LDA 2.0	>25 @ 80°C 30 @ 45°C

Table 2-2. Screening reactions to determine the optimum reaction temperature.

	DBMA µmol (mg)	**XVI** µmol(mg)	mole ratio (**XVI**/ DBMA)	LDA, equiv	Time to completion, min
6	8.2 (2.9)	9.2 (3.4)	1.1	2.0	>30 @ -30°C
7	5.7 (2.0)	5.2 (1.9)	0.9	2.3	>30 @ -30°C
8	6.9 (2.4)	8.1 (3.0)	1.2	1.8	<30 @ -30°C
9	2.5 (0.9)	2.2 (0.8)	0.9	2.0	45 @ 0°C

The results from the first series of screening reactions pointed to LDA as the best base and DMF as the best solvent. The second series of reactions were set up to

find the best temperature for the reaction and the optimum number of equivalents of LDA (Table 2-2). Based on the results from Table 2-2, the optimum temperature chosen was -30°C mainly because side products began to show up in the 0°C reaction after 75 minutes.

The reaction was set up by dissolving 1.0 g of **XVI** in 50 ml of dimethylformamide from a freshly opened bottle in a 100 ml 2-neck flask fitted with a dropping funnel, septum, and magnetic stirrer. A positive pressure of dry N_2 was maintained throughout the reaction. The reaction flask was cooled to -40 °C by lowering into a shallow Dewar flask containing isopropanol and dry ice. Next, 3.6 ml of LDA was added with a syringe through the septum. The reaction mixture turned to light yellow-lime green in color after 5 minutes stirring. Next, 0.95 g of DBMA was dissolved in 50 ml DMF using mild heating to facilitate the dissolution. The DBMA solution was added to the reaction flask through the dropping funnel over a 5 minute period. The reaction mixture temperature was maintained below -30 °C throughout the reaction. After all the DBMA was added, the progress of the reaction was followed with TLC (1:9 acetone:toluene). After 15 minutes the reaction mixture was red-orange in color. Though TLC showed that not all of the DBMA was consumed, the reaction was stopped at 60 minutes reaction time due to concern that side products might begin to form. The reaction was stopped by pouring the reaction mixture

into 150 ml of ice water and allowed it to stand for 30 minutes in a freezer followed by filtration through a buchner funnel. The yellow solid was placed in a dessicator to dry overnight. Later runs of this reaction showed slightly improved yields by increasing the amount of DMF and running the reaction at 0 °C. No solvent system was found that could separate out the product from the other material, so a two step procedure was used. In the first step of the purification, a 'plug column' was used with chloroform as the eluting solvent. This plug column was a 350 ml fritted glass filter which was extended in height by 6 inches by Rudy Strohschein at the glass shop. As the product mixture is eluted through the silica gel column, initially, a broad band of yellow material is eluted. The desired material is nearly colorless on the column unless illuminated by a black lamp. The use of the black lamp was minimized when it caused a change in coloration of the material in the column. The desired product moves just in front of a narrow slow moving yellow band. As the narrow yellow band approaches to within 2 inches of the bottom of the column, no more chloroform was added at the top of the column and the column was allowed to run until no more solvent came out the bottom even with light pressing on the filter paper at the top of the column with a spatula. This insured that the silica gel packing was rigid enough to be scooped out without flowing. The column was kept in a vertical orientation while the

bands were scooped out. The band of silica gel containing the desired product was scooped out and washed with THF through a 350 ml fritted glass filter. The resulting THF solution was filtered by gravity through a fine filter paper to remove any fine silica gel particles that escaped through the fritted glass. The THF was removed with a rotary evaporator to yield a light yellow solid. This solid was washed with acetonitrile. The 30 mg of yellow solid, insoluble in acetonitrile is the desired product, **XVII**. The proton NMR in tetrahydrofuran-d_4 of the product shows peaks δ = 1.4 (m,alkyl); 3.6 (t, 2H, methylene ether); 4.0 (t, 2H, methylene arylether); 6.1 (s, 2H, methylene protons between the ether linkage and anthracene rings); 6.8 (d, aromatic); 7.2 (d, aromatic); 7.6 (m, aromatic); 8.3 (d, 2H, anthryl protons); 8.5 (d, 2H, anthryl protons); 10.7 (s, 1H, OH). Mass spectroscopy showed the presence of material with a molecular weight of 640 g/mol (calculated 640 g/mol). The peak on the mass spectrum was a doublet corresponding to 638 g/mol (intensity=76428) and 640 g/ml (intensity=93000) which indicates that the material contains a bromine atom (two isotopes of bromine are separated by 2 amu).

Synthesis of 2-(10-(4-(4'-ol-biphenyl-4-dodecanoxymethyl)-anthryl)-trimethylsilylacetylene, **VII**

This reaction requires that special care be taken to minimize the amount of water in the reaction flask. All

glassware was dried at least overnight in an oven. The triethylamine solvent was held over CaH_2 for 4 days and freshly distilled just prior to use. Next, 0.1 g of **XVII** was placed in a 200 ml 3-neck round bottom flask with 25 ml of dry triethylamine which was fitted with a dry ice condenser, magnetic stir bar, and a rubber septum. Next, 4.8 mg (0.04 equivalents to **XVII**) of di(triphenylphosphine) palladium dichloride, 1.9 mg of CuI (0.04 equivalents), and 6.6 mg triphenylphosphine (0.16 equivalents) were transferred with a minimum of dry triethylamine to the reaction flask. Finally, 24 µl of trimethylsilylacetylene was added with a syringe through the septum. The reaction mixture was allowed to stir at room temperature for a few minutes while the dry ice condenser was filled. The **XVII** does not completely dissolve until the solvent is heated. The reaction mixture was heated with a heating mantle controlled by a variac to a gentle reflux. The reaction mixture is a clear light yellow. The progress of the reaction is followed by TLC on silica gel plates using chloroform as the developing solvent. After two hours heating, the reaction mixture was clear reddish-orange with white suspended solids. Another 2 mg of the palladium catalyst was added at the three hour mark. The reaction mixture was clear reddish-orange with white suspended solids until the reaction was stopped after 18 hours heating. The solvent was removed using a rotary evaporator. The solid

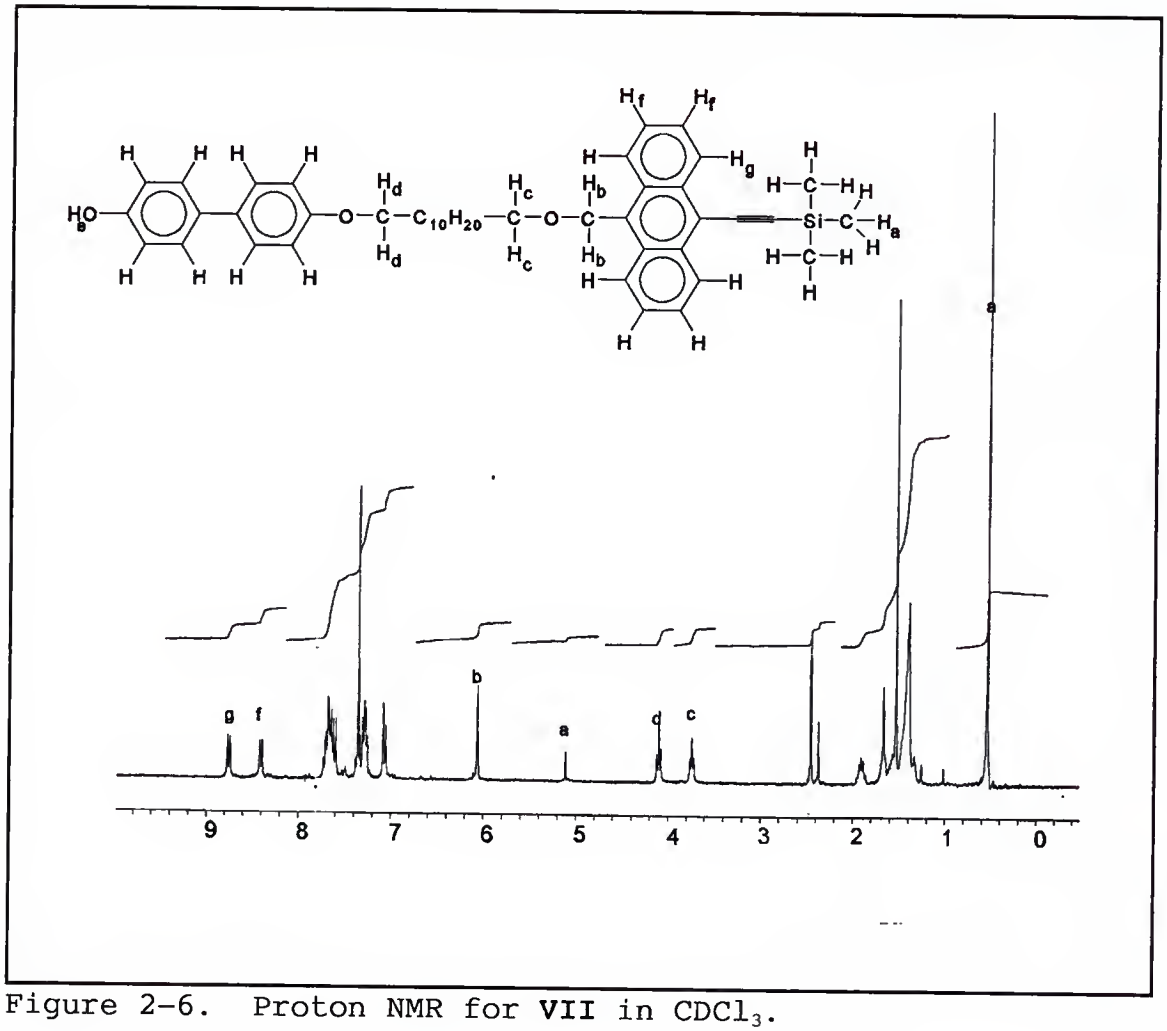

Figure 2-6. Proton NMR for **VII** in $CDCl_3$.

was taken up in THF and gravity filtered through medium porosity filter paper to remove the precipitated amine salts. The THF was removed with the rotary evaporator to get a red-orange solid. The solid was stored in the freezer wrapped in foil until purification. The desired product, **VII**, was obtained by silica gel chromatography using 9:1 toluene:THF as the eluting solvent. The proton NMR (Figure 2-6) in $CDCl_3$ of the product shows peaks δ = 0.4 (s, 9H, silylmethyl); 1.4-2.0 (m, alkyl); 3.6 (t, 2H, methylene

ether); 4.0 (t, 2H, methylene arylether); 5.1 (s, 1H, OH); 6.1 (s, 2H, anthryl methylene ether); 6.8 d (aromatic); 7.2 (d, aromatic); 7.6 (m, aromatic); 8.3 (d, 2H, anthryl); 8.5 (d, 2H, anthryl). FTIR shows a sharp medium intensity absorption at 2139 cm^{-1} due the carbon-carbon triple bond.

Langmuir-Blodgett-Kuhn Experiments

A solution of each compound, ca. 0.5 mg/ml in spectro-grade chloroform (Kodak), was prepared. The behavior of the monolayers was investigated using a KSV 5000 Langmuir-Blodgett System (KSV Instruments) under a HEPA filter hood (Baker Company). Surface pressure was measured using a modified Wilhelmy balance. The teflon LBK trough was 45.5 cm long by 14.8 cm wide. Teflon (hydrophobic) or Nylon (hydrophilic) barriers were used to compress the monolayers symmetrically at a typical barrier speed of 20 mm/min. Water for the subphase was purified to 18 MΩ resistivity using a Milli-Q water system (Millipore). The temperature of the subphase was controlled by circulating ethylene glycol/water from a constant temperature bath (Neslab) through channels cut in the trough base. UV spectra of deposited films were obtained using a Perkin-Elmer UV/VIS/NIR Lambda 9 spectrophotometer. UV spectra of the deposited monolayers were obtained by placing the quartz plate in a specially constructed sample holder.

Langmuir-Blodgett-Kuhn films were deposited on specially prepared quartz plates. The quartz plates were cleaned using the following procedure: the plates were immersed in a detergent solution and sonicated for 10 minutes and then placed in a solution consisting of a 1:1:3 mixture containing NH_4OH, H_2O_2, and Milli-Q water respectively. The plates in the solution were then heated for 30 minutes at 80 °C, followed by sonication for 10 minutes, sequentially, in each of the following solvents: $CHCl_3$, $CHCl_3$ / CH_3OH, CH_3OH. Hydrophobic quartz plates were prepared by placing a clean quartz plate in a mixture of 70 ml pure decalin, 10 ml chloroform, 20 ml carbon tetrachloride, and 2 vol % octadecyltrichlorosilane and sonicating for 2 hours.

For dipping, the applied surface pressure could be maintained by the computer controlled film balance at any possible value. The automated dipping speed could be varied in both directions. The dipping motion could be delayed at the top of its travel to allow time for the previously deposited layers to dry in the air. The transfer ratio and surface pressure were monitored and recorded during the dipping process.

Irradiation of the LBK films with γ-ray was performed by placing the fused-silica quartz slide supporting the deposited films approximately 2 cm away from the ^{60}Co source so that the rays penetrated the sample normal to the plane

of the slide. Depending on the dose rate of the source, the sample was left for several days until at least a 160 Mrad dose had been passed through the sample. The slide was kept in a bottle with a bakelite lid and purged with nitrogen gas before sealing the bottle with teflon tape.

Irradiation of the LBK films with UV light was performed by placing the slide in a glass jar wrapped with aluminum foil and purged with argon gas. A 75 W mercury pen lamp was supported within the jar with a clamp. The lamp was held approximately 1 cm from the surface of the quartz slide. The slide was irradiated for 30 minutes.

Gel permeation chromatography (GPC) data were obtained using a Waters Associates GPC System with an LC-75 Perkin Elmer Spectophotometric Detector. The GPC was fitted with two Phenomenex 300 mm x 7.8 mm GPC columns in series prepacked with Phenogel 5 which has a 500 Å pore size. Polystyrene was used as a calibration standard. Tetrahydrofuran was used as the eluting solvent at a flow rate of 1 ml/min. The samples were prepared for the GPC by washing the LB layers from the substrate with a minimum amount of THF.

Results and Discussion

LBK Films of Mesogen-substituted Monoacetylene Monomers

LBK Film-forming Properties of 4-methoxy biphenyl-4'(11-undecynoate), I

The pure compound, **I**, formed unstable monolayers at the air/water interface. However, the monolayer stability of **I** was improved by blending the compound of interest with another liquid crystalline amphiphile, **II**, which was known to produce stable monolayers. Monolayers of the blends were successfully deposited on hydrophobic and hydrophilic quartz substrates.

Comparisons were made of the stability of the monolayers over time with stearic acid used as a standard for stability. First, the monolayer was compressed until it reached a given surface pressure and the barrier was stopped. The surface pressure changes were then monitored as a function of time and the slopes were compared with those of stearic acid. An alternate procedure for determining the monolayer stability was also used. In this second method, the mean molecular area of the compound or blend was monitored as a function of time while keeping the applied surface pressure constant.

Plots of surface pressure versus mean molecular area were done for all the compounds under study. For compound **I** at ambient temperature, the surface pressure onset occured at mean molecular areas (Mma) of 10 $Å^2$ and the apparent collapse pressure was very low for the compound **I**. Even though the isotherms were reproducible, consideration of the chemical structure of the monomer suggests that this onset

is too small to correspond to the formation of a true two-dimensional monolayer. Figure 2-7 shows the isotherm for **I** recorded at a temperature of 6°C. It is apparent that at lower temperatures greater onset Mma (higher than 20 $Å^2$) values are obtained and the collapse pressure increased substantially. These onset Mma values are more reasonable in view of the chemical structure of the monomers.

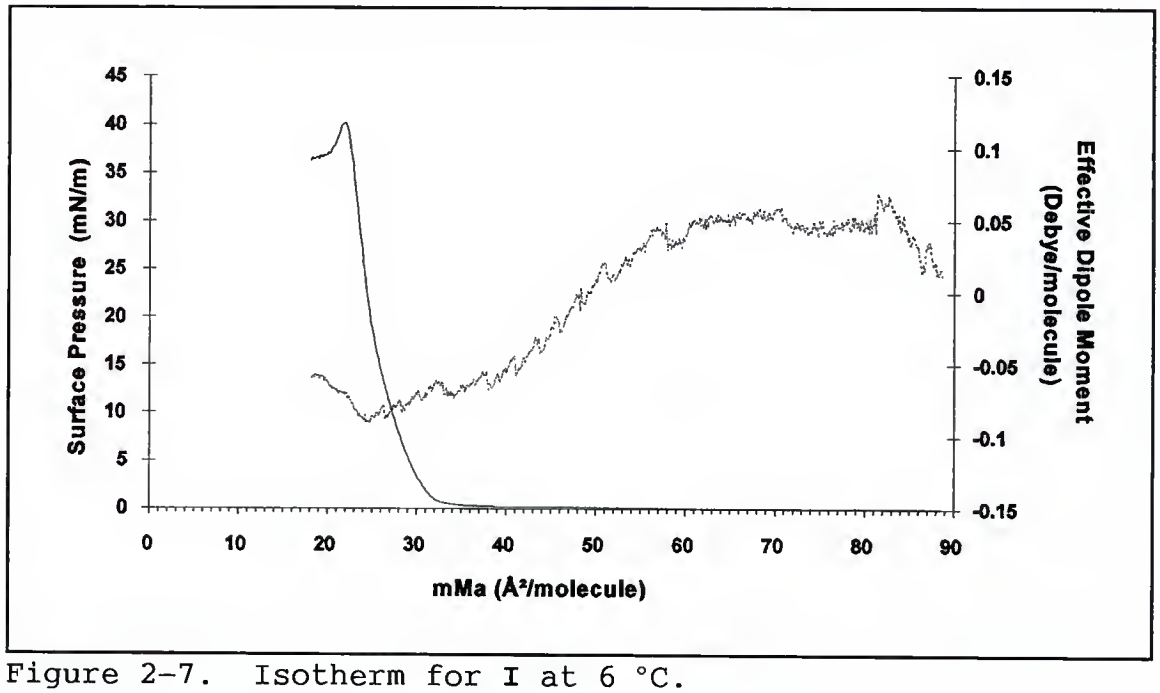

Figure 2-7. Isotherm for **I** at 6 °C.

As the film was compressed, the plot of the effective dipole moment indicates that the molecules are beginning to orient closer to the normal with the interface beginning at approximately 60 $Å^2$/molecule. The effective dipole becomes

more negative as the molecules become closely packed. The effective dipole becomes negative rather than positive because the acetylene group has a considerable dipole moment opposing the dipole of the methoxy group and also the carbonyl in the ester linkage must contribute to the negative value as the molecule orients perpendicular to the water surface.

For good deposition of the liquid crystal on a substrate, the formation of a stable monolayer is essential. A monolayer is considered stable when it displays a steady Mma at constant surface pressure over several minutes. Stability studies versus time showed that the films of compound **I** are not stable over long periods of time (>30% loss in 10 minutes) at low temperatures although they show better hysteresis as compared to higher temperatures. In general, the lower temperature runs were characterized by more reasonable Mma values in the condensed phase region and more stable monolayers, but not stable enough for multilayer depositions.

In order to improve the monolayer stability of compound **I** the effect of mixing other compounds which could act as "stabilizers" was explored.

Several experiments were performed on mixtures of the compound. Mixing the monomer with compound **II** often increased the stability of the resulting monolayer film. However, since polymerization of the acetylenic compounds is

desired, the amount of the "monolayer stabilizer" has to be minimized. Isotherms of blends of compound **I** with 5 mol % of compound **II** are shown in Figure 2-8. Concentrations of stabilizing compound **II** as low as 5 mol % were adequate to stabilize monolayers containing **I**. This behavior might be due to a greater degree of intermolecular π – orbital overlap between the aromatic rings of the mesogenic groups. In general, much higher Mma values were obtained for the condensed phases of compound **I** in blends with compound **II**. The monolayer stability of compound **I** with compound **II** at constant Mma was greater than that found for pure **I**. The slope of the curve for the blend lies intermediate between the values for compounds **I** and **II**, with the latter being the more stable monolayer because of its terminal hydroxyl group[73]. In general, by varying the mole ratio of the mixtures and careful choice of "interactant" one can improve the monolayer stability. The interactant increases the stability of the monolayer because it packs well laterally with the other molecule and its strong hydrophilic group keeps it 'pinned' to the water surface.

Multilayers were deposited on 25 mm x 75 mm hydrophilic quartz plates. For dipping the **I+II** blend, the subphase temperature was controlled at ca. 15°C with an applied surface pressure of 7 mN/m. The automated dipping speed was maintained at 1.0 mm/min in both directions. The dipping motion was delayed at the top of its travel for up

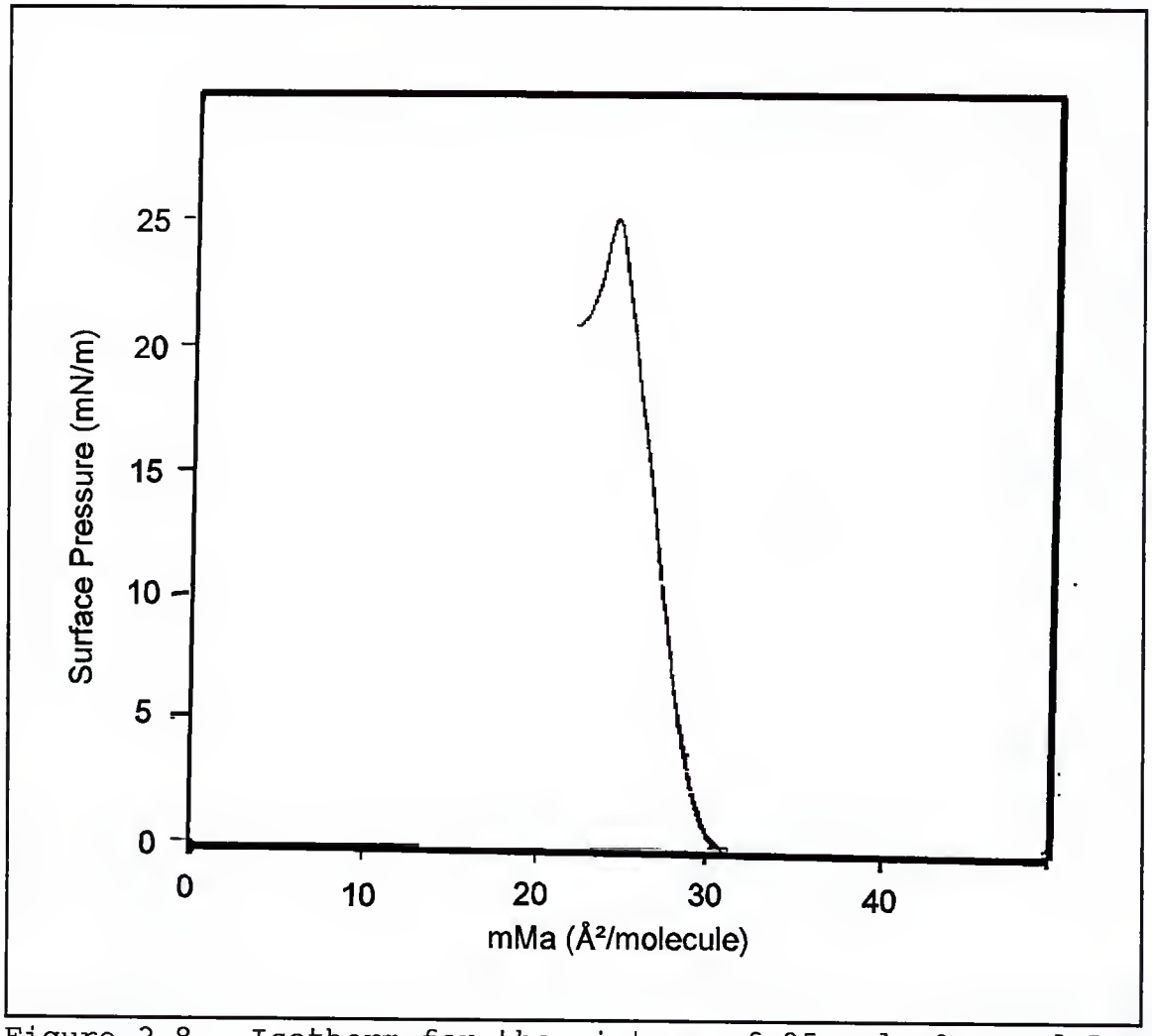

Figure 2-8. Isotherm for the mixture of 95 mole % **I** and 5 % **II**.

to 10 minutes to allow time for the previously deposited layer to dry in the air. The transfer ratio and surface pressure were monitored and recorded during the dipping process.

UV spectra of the deposited **I+II** blend monolayers were obtained by removing the plate from the dipping attachment,

placing the quartz plate in a specially constructed sample holder, running the scan, and then returning the plate to the dipping attachment. Cast films of each blend were made for comparison.

Multilayers of the stable blends were successfully deposited on quartz substrates. Blends with compounds **I+II** were deposited at 7 mN/m because the film is not adequately stable at higher surface pressures. During the depositions, the transfer ratio was recorded. The transfer ratio (TR) gives an indication of the quality of the dipping process and ideally should be unity. The **I+II** monolayer was transferred to the substrate very well (TR near unity) while the substrate was moving up, but a fraction of the deposited monolayer was removed (TR approaching -0.2) when the substrate was moving down into the subphase. It is found that Z-type films were formed for the blend using both hydrophilic and hydrophobic quartz substrates. Z-type films are defined as those resulting from good transfer on the upstroke but poor or little transfer on the downstroke. A total of 7 layers were deposited for the **I+II** blend. The blend **I+II** tends towards Z-type deposition after the first three layers on a hydrophobic substrate.

The absorption (Figure 2-9) observed between 220 and 230 nm are the bathochromic shifted E bands of the substituted benzene rings and the absorption between 260 to 290 nm are for the K bands of the biphenyl in the

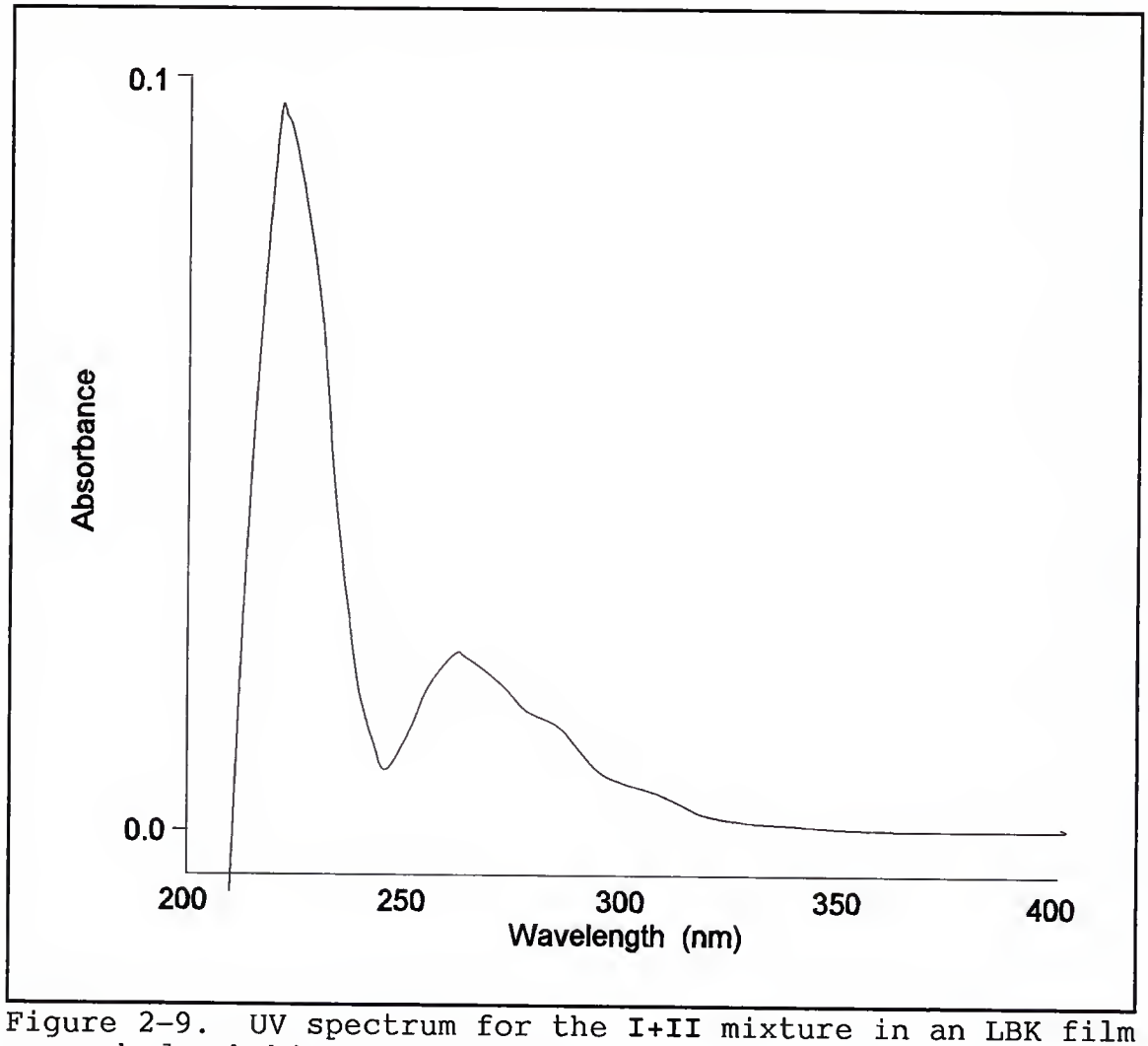

Figure 2-9. UV spectrum for the **I+II** mixture in an LBK film on a hydrophobic quartz plate.

substituted mesogenic group.[73] The $\pi - \pi^*$ transition for the acetylenic group at 173 nm and the allowed transition (E bands) of the benzene ring at the 184 to 200 nm region were not observed in the spectra due to the limitations of the instrument. No significant difference was observed between the spectra of the pure compounds and the blends since only a minimal amount of the "stabilizer" was added.

Two methods were explored to polymerize the monomer blends. The first method which involved irradiating the monolayer on the trough under air or nitrogen atmosphere with UV light (254 nm) proved unsuccessful. In the second method, Langmuir-Blodgett monomer films were exposed to a ^{60}Co γ-ray source. The **I+II** blend was exposed to γ-irradiation dosage of 160 Mrad. The GPC data showed that the deposited **I+II** blend reacted to form in 21% conversion an oligomer that was approximately 10 repeat units long, along with very much smaller portions of high molecular weight polymer. The GPC was calibrated with polystyrene standards. The percent conversion is similar to the results found for bulk polymerization. Without further characterization, the identity of the oligomer could not be made.

This work has demonstrated Langmuir film and multilayer deposition properties of **I**. The monolayer properties of the compound were significantly improved by blending with a suitable co-surfactant. Furthermore, attempts to polymerize the compound by γ-irradiation gave similar results as that observed in the bulk. Compound **I** by itself does not form Langmuir films which will support a significant amount of surface pressure at room temperatures. However, if the temperature of the subphase is lowered below 17°C, surface pressures up to 20 mN/m were seen before collapse. Langmuir films of this pure compound were not stable at any surface

pressure. On the other hand, compound **II** was known to form stable Langmuir films. In addition, this compound bears some structural characteristics in common with the other compound. Now, it has been shown that blending these compounds leads to the production of stable Langmuir films. Following the model put forward by Ishii,[74] it may be said that the "interactant" compound affects the equilibrium behavior of the mixed monolayer, not the dynamic spreading behavior.

The stable blended monolayers were successfully transferred to quartz substrates in Z-type and Y-type depositions. Blend **I+II** showed Z-type dipping behavior.

LBK Film-forming Properties of 4-hydroxy biphenyl-4'(11-undecynoate), **III**

The previous section has shown that compound **I** may be processed with the Langmuir-Blodgett-Kuhn technique[9] only by blending with other compounds such as **II** or by cooling the subphase temperatures below 10°C.

Based on this experience, compound **III** was designed and synthesized. Compound **III** was found to be an improvement compared to **I** because it does not require either blending or low temperatures while being processed with the LBK technique. Figure 2-10 shows the isotherm (27°C) for compound **III**. From the isotherm, extrapolation to zero surface pressure gives the area per molecule in the

monolayer as 23.5 $Å^2$. This value indicates that the molecules are oriented perpendicular to the air-water interface. The monolayer of **III** at the air-water interface was stable (ΔmMa < 0.8 $Å^2$/molecule during 1 hour) at constant surface pressures up to 25 mN/m.

As the film was compressed, the plot of the effective dipole moment indicates that the molecules are beginning to orient closer to the normal with the interface beginning at approximately 42 $Å^2$/molecule. The effective dipole becomes more negative as the molecules become closely packed. The effective dipole becomes negative rather than positive because the acetylene group has a considerable dipole moment opposing the dipole of the hydroxyl group and also the carbonyl in the ester linkage must contribute to the negative value as the molecule orients perpendicular to the water surface.

Attempts to polymerize compound **III** were made by irradiating the material both as LBK multilayers and as a monolayer on water with γ ray dosages up to 160 Mrad. Characterization with UV spectroscopy and GPC indicated the formation of a small fraction of dimer and trimer. Also the bulk crystals in an evacuated capillary were irradiated with γ ray and characterized but no polymer product was found.

For dipping, the subphase temperature was controlled at ca. 27°C with an applied surface pressure of 20 mN/m. The

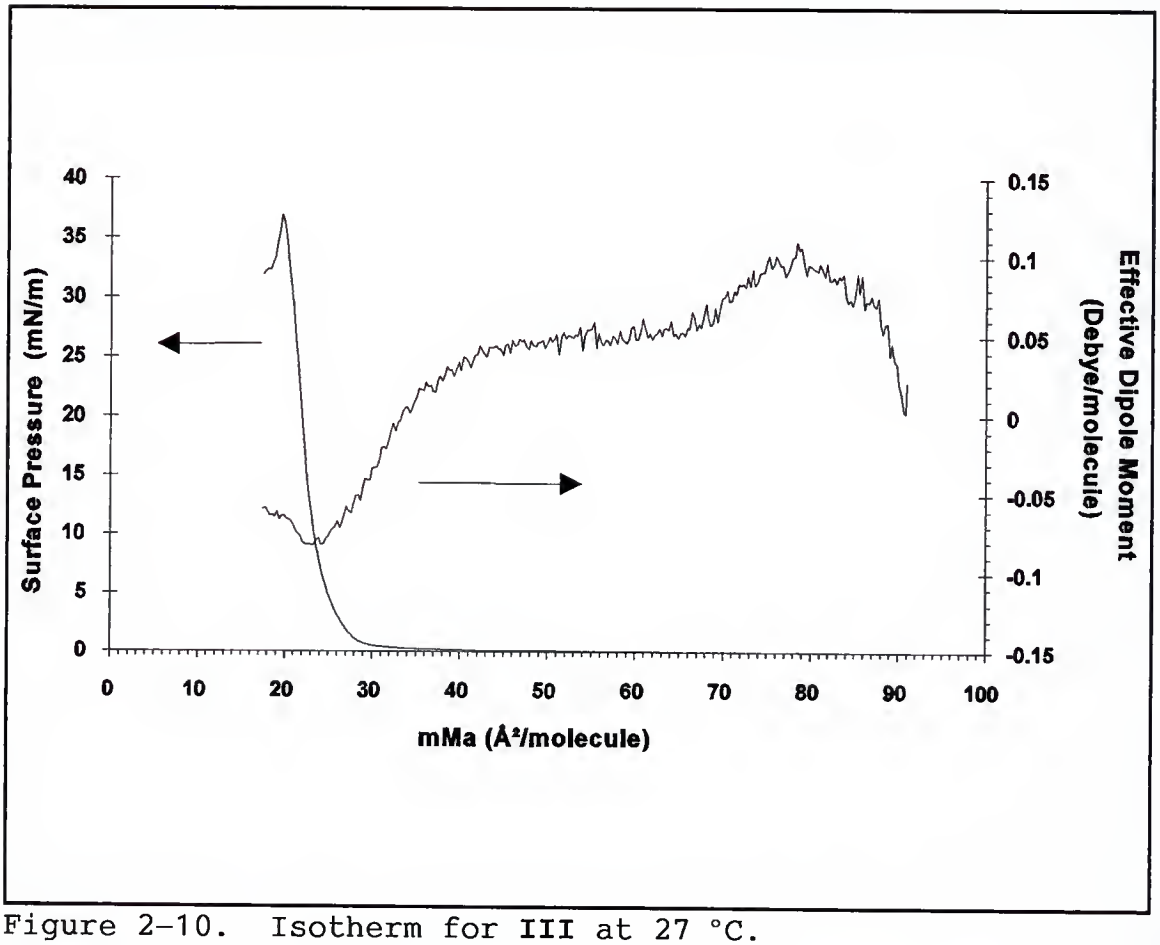

Figure 2-10. Isotherm for **III** at 27 °C.

automated dipping speed was maintained at 0.5 mm/min in both directions. The dipping motion was delayed at the top of its travel for 10 minutes to allow time for the previously deposited layers to dry in the air. The transfer ratio and surface pressure were monitored and recorded during the dipping process. Deposition of **III** on hydrophobic quartz plates was Y-type with a average transfer ratio of 0.96 on the downstroke and 1.03 on the upstroke. The lack of polymer formation despite the good quality LBK deposition

indicated that the acetylene functional groups are not oriented correctly for the desired reaction to take place.

LBK Films of Mesogen-substituted Phenylacetylene Monomers

LBK Film-forming Properties of 4-hexadecyloxyphenyl-4-ethynylbenzoate, VI

Compound **VI** was provided by R. C. Advincula. The compounds **VI** and **V** are different from the other monomers in that the acetylene group functions as the hydrophilic part of the amphiphile. Also, the acetylene is attached directly to the mesogen, so the orientation of the acetylene will be constrained along the director of the liquid crystal. The isotherm of **VI** is shown in Figure 2-11. From the isotherm, extrapolation to zero surface pressure gives the area per molecule in the monolayer as 28 $Å^2$. The monolayer stability of **VI** was found to be -6.2 $Å^2$/molecule at 20 mN/m surface pressure in 50 minutes and -2.1 $Å^2$/molecule at 15 mN/m surface pressure in 70 minutes. These monolayer stability values are not as good as **III** or **IV** because the acetylene group does not have a strong affinity towards the water surface. However, the appreciable surface pressures seen in the isotherm indicate that the monolayer gains considerable stability through efficient packing of the monomers at the interface. The efficient packing is also indicated by the viscous nature of the monolayer. Dipping on hydrophilic quartz gave transfer ratios less than 0.1 at dipping speeds

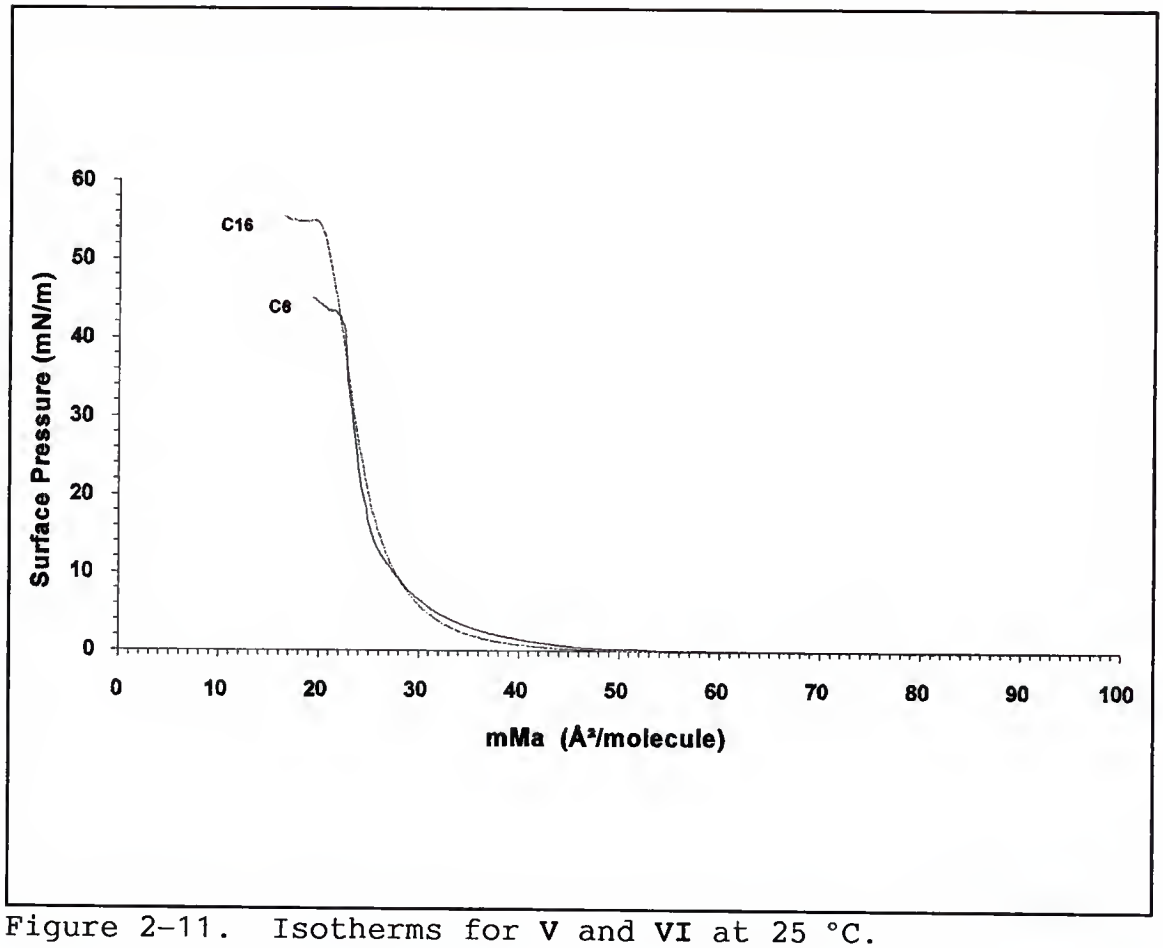

Figure 2-11. Isotherms for **V** and **VI** at 25 °C.

down to 0.1 mm/min. Polymerization by irradiation was not attempted with this compound because the homolog reported in the next section was more processable.

LBK Film-forming Properties of 4-octyloxyphenyl-4-ethynylbenzoate, **V**

Compound **V** was also provided by R. C. Advincula. As with **VI**, the hydrophilic group in this molecule is the acetylene group due to its significant dipole moment. The isotherm for compound **V** is shown in Figure 2-11. From the

isotherm, extrapolation to zero surface pressure gives the area per molecule in the monolayer as 27 $Å^2$. All of the ethynylbenzoate compounds exhibited large hysteresis on repeated compression and decompression cycles such as that seen for **V** in Figure 2-12. In this hysteresis experiment, the monolayer was compressed beyond the collapse point and the results indicate that during decompression the collapsed regions remain aggregated because the subsequent compression cycle begins its rise in surface pressure at the point where the previous cycle reached. The monolayer stability of **V** was found to be -1.7 $Å^2$/molecule at 20 mN/m surface pressure in 80 minutes. This stability is higher than that seen with **VI** because the shorter hydrophobic tail, thus weakerhydrophobicity, is better balanced with the weak hydrophilicity of the acetylene group. As with **VI**, **V** monolayers gain considerable stability through efficient packing and the resulting intermolecular π orbital interactions.

Dipping onto hydrophobic quartz gave transfer ratios of 1.0 on the upstroke and 0.6 on the downstroke with a dipping speed of 0.5 mm/min. Using a dipping speed of 0.5 mm/min on the upstroke and 0.3 mm/min on the downstroke gave transfer ratios 1.0 and 1.2, respectively, for the first layer but subsequent layers showed steadily degrading transfer ratios until by the eighth layer, the transfer ratio on the upstroke was 0.8 and 0.6 for the downstroke. Note that the

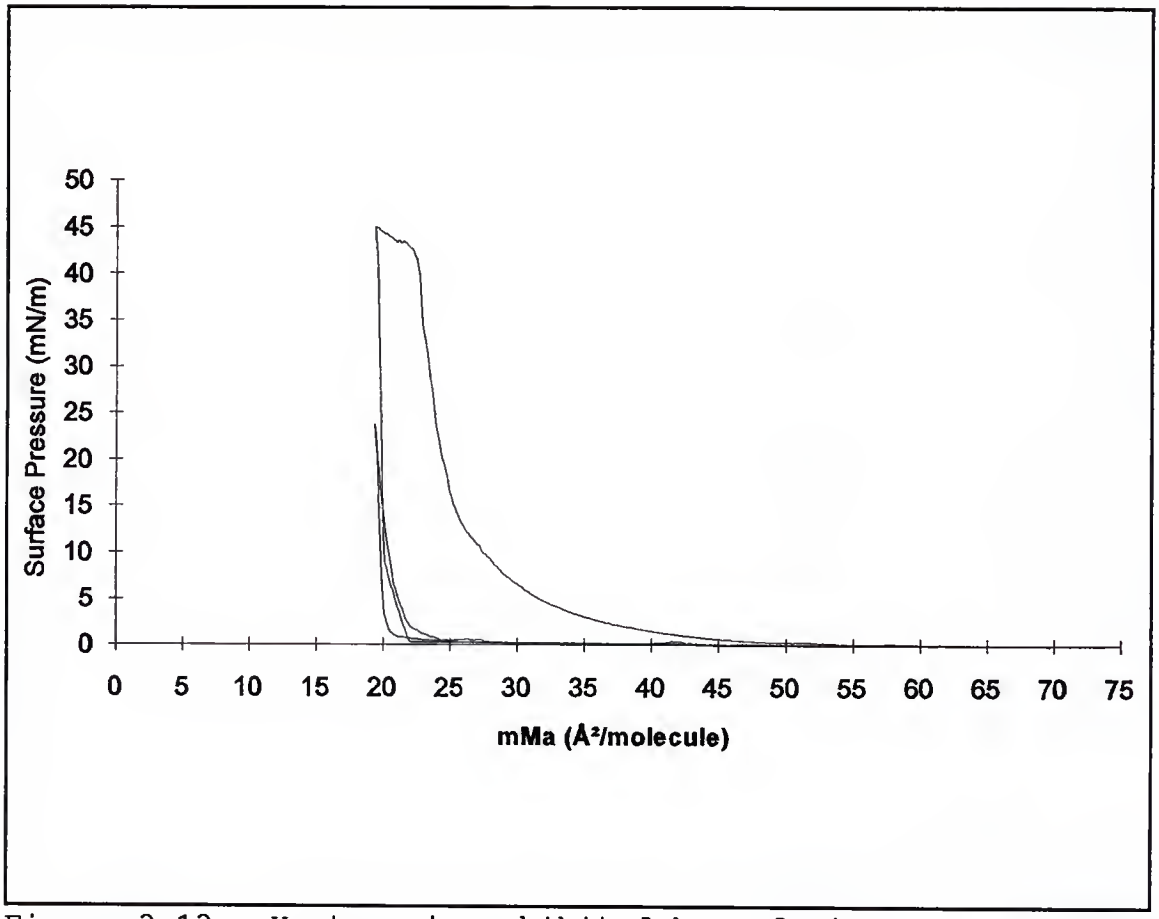

Figure 2-12. Hysteresis exhibited by **V** during a compression and decompression cycle.

dipping speed used was very slow compared to more common dipping speeds of over 5 mm/min. The slow dipping speed was necessary due to the viscous nature of these monolayers.

Polymerization of the LB films was attempted with γ irradiation and also by UV irradiation of the monolayer at the water surface. GPC characterization indicated that only degradation products were obtained. The lack of polymer formation may be due to incorrect orientation of the

acetylene functional groups to allow the desired reaction to take place.

LBK Film-forming Properties of 4-(4'-ol-biphenyl-4-decanoxy)-phenylacetylene, **IV**

As described above, compound **IV** was intended to combine the good film forming performance of **III** with the potentially greater reactivity of a phenylacetylene. The relatively short spacer length makes this compound insoluble in the usual spreading solvents. Thus the spreading solution was made up a mixture of 1 part THF and 9 parts chloroform. This solvent mixture supported a 0.01 mg/ml solution concentration of **IV**. The isotherm (23°C) for the compound is shown in Figure 2-13. From the isotherm, extrapolation to zero surface pressure gives the area per molecule in the monolayer as 25 $Å^2$. This value indicates that the molecules are oriented perpendicular to the air-water interface. The monolayer at the air-water interface was stable (ΔmMa=-0.8 $Å^2$/molecule during 1 hour) at constant surface pressures up to 20 mN/m. This stability is comparable to that found with **III** and may attributed to the strong hydrophilicity of the phenolic OH and the excellent packing of the molecules.

A series of experiments were done to see if irradiation of the compound **IV** at the air/water interface would yield any polymer. The surface pressure was maintained at 5 mN/m

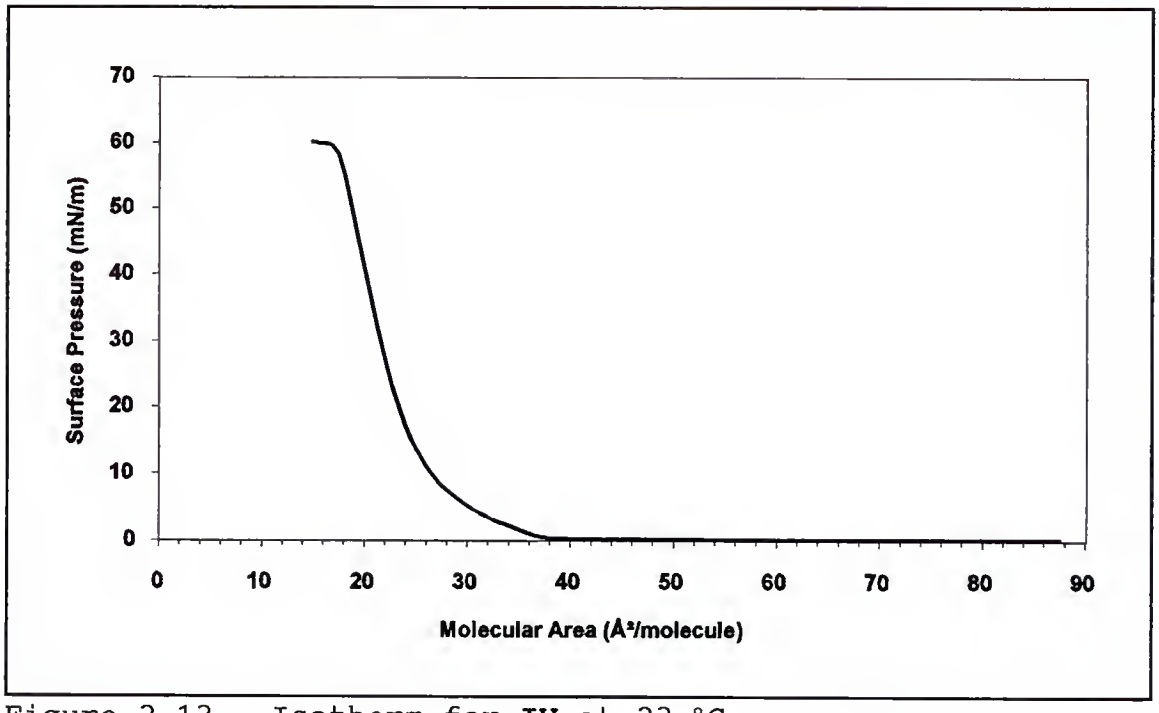

Figure 2-13. Isotherm for **IV** at 23 °C.

while the monolayer was irradiated with a UV mercury pen lamp held within 1 cm of the water surface. Observation under the Brewster angle microscope revealed that the usual stiff irregular shaped domains were fluidized under the influence of the UV lamp. To check if this was due to a heating effect, a quartz heating lamp was held near the monolayer, but the domains were not fluidized by the heat.

Next multilayers of **IV** were irradiated at the argon/water interface for 10, 20 and 60 minutes and the material collected with a fritted glass for subsequent GPC analysis. Injection of the monomer into the GPC gave a retention time for the monomer of 18 minutes. Injection of

the irradiated material showed the presence of the monomer and a lower molecular weight material which elutes after a retention time of 20 minutes. The relative peak height of the lower molecular weight material to the monomer peak increases with the length of the irradiation time. The GPC results clearly showed that the monomer was degraded at the argon/water under the irradiation by UV.

For dipping, the subphase temperature was controlled at ca. 23°C with an applied surface pressure of 15 mN/m. The automated dipping speed was maintained at 5 mm/min on the downstroke and 3 mm/min for the upstroke. The dipping motion was delayed at the top of its travel for 10 minutes to allow time for the previously deposited layers to dry in the air. The transfer ratio and surface pressure were monitored and recorded during the dipping process. Deposition on hydrophobic plates was Y-type with a average transfer ratio of 0.7 on the downstroke and 0.5 on the upstroke.

The UV spectra of the compound shows a series of peaks at 210, 235, 240, 245, 250, and 260 nm corresponding to aromatic transistions of the phenylacetylene and biphenol groups. Following irradiation with a mercury pencil lamp for 30 minutes under argon, the UV spectra exhibits a broad peak centered at 280 nm and tailing out to 400 nm. For characterization with the GPC, the irradiated LB layers were dissolved in a minimum of THF. The monomer elutes with a

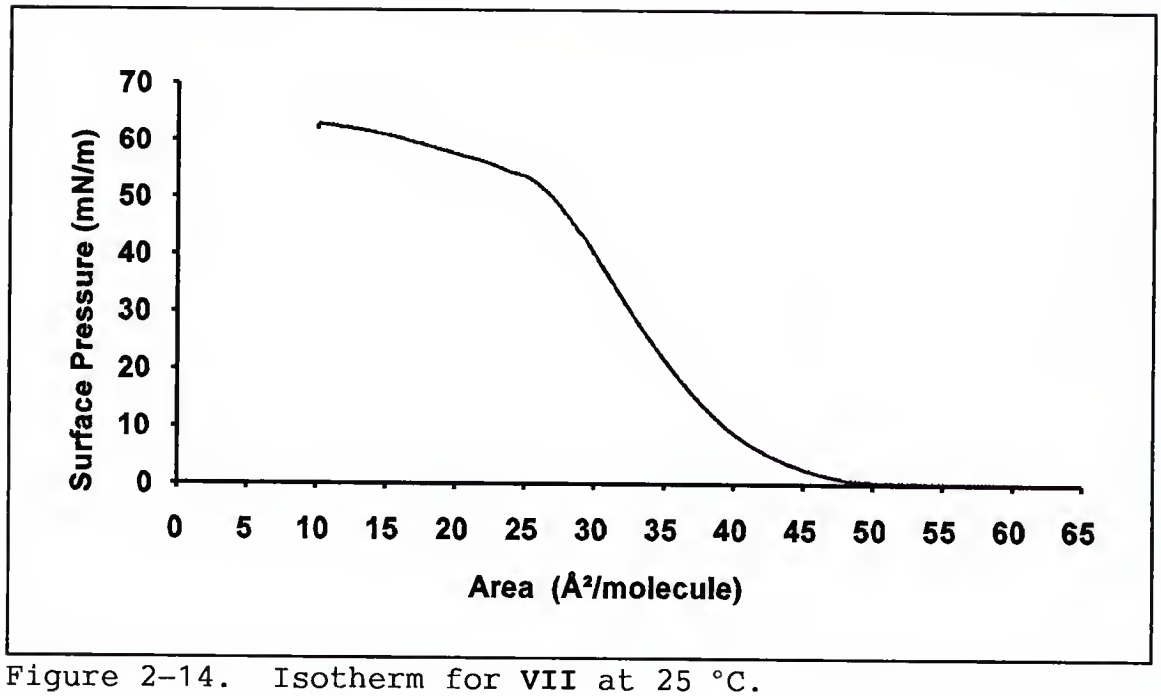

Figure 2-14. Isotherm for **VII** at 25 °C.

retention time of 18 minutes. The irradiated LB layers showed a broad shoulder extending from the monomer peak down to a retention time of 15 minutes. According to the calibration with polystyrene standards, a retention time of 15 minutes corresponds to material with a molecular weight of 4700 g/mol. This molecular weight is consistent with a degree of polymerization of 10 repeat units. The irradiated LBK layers also have a large peak eluting at 19.5 minutes indicating the formation of degradation products similar to that obtained by irradiation at the argon/water interface.

Preliminary Langmuir Film Properties of 2-(10-(4'-ol-biphenyl-4-oxy) dodecanoxymethyl)-anthryl)-trimethylsilylacetylene, **VII**

The first isotherm of **VII** as obtained by Mr. Wei Shen and Dr. Thomas Servay is shown in Figure 2-14. The shape of the isotherm suggests a phase transition from a liquid-expanded to a liquid-condensed phase with a collapse pressure of 52 mN/m. Extrapolation of the isotherm to zero pressure gives an area per molecule of approximately 41 $Å^2$. This is a reasonable value for anthracene compounds with this substitution pattern.[75]

Conclusion

In this chapter, the synthesis of a mesogen-substituted alkylacetylene, **III**, phenylacetylene, **IV**, and a anthrylacetylene, **VII**, has been reported. Compounds **III** and **IV** form stable monolayers at the air-water interface. The Langmuir film work with compound **VII** is not complete yet due to time constraints but this work will be continued by Mr. Wei Shen who has also been involved in the synthesis work.

All of the compounds (except **VII**) have been processed with the LBK technique. The biphenol-undecynoate, **III**, was found to have superior LBK deposition behavior compared to the other compounds in this chapter. The ethynylbenzoate, **V**, gives respectable transfer ratios but the rate of transfer is very slow.

Polymerization was attempted by irradiation of all of the compounds (except **VI** and **VII**). The phenylacetylene, **IV**, had the highest degree of polymerization of the compounds studied here. The UV spectra and GPC retention times of the LBK films was changed by irradiation with a UV lamp in a manner consistent with the formation of oligomers with molecular weight equivalent to 10 repeat units as well as some degradation products. Thus the incorporation of the phenyl ring does increase reactivity because **III** could only be initiated with γ-irradiation. The other compounds gave mainly degradation products. The modest success obtained with **IV** may be related to its strong crystal forming tendency as evidenced by its low solubility in most organic solvents.

The quality of the LBK films for **IV** were not high. If the film quality can be increased perhaps by the introduction of an interactant or by varying the pH of the subphase, then higher degrees of polymerization may be obtained. Thus, future work should include attempts to improve the quality of the LBK films of **IV**. Before undertaking the synthesis of **IV** it is suggested that the chain length of the alkyl spacer be increased so that the solubility is increased and thus the ease of handling of the material. Also the Langmuir film properties of the anthrylacetylene, **VII**, should be determined. The effect of gamma irradiation, heat, or the presence of a free radical

initiator on the films of **IV** could be studied. The surface pressure during LBK film deposition can influence the tilt of the monomers in the monolayers and thus the functional group orientation. Therefore, the effect of applied surface pressure on reactivity could be studied. The photochemistry of the phenylacetylene is an important factor in the improved reactivity of **IV** but equally important is the packing of the reactive groups. Compounds **V** and **VI** are also phenylacetylenes but apparently the packing geometry is not correct for polymerization to occur with those compounds. Generally, better understanding of the polymerization mechanism may be important to optimize structure for reactivity. Based on the results of this chapter, new compounds should be more closely related to the structure of **IV**. The obvious next step would be to synthesize analogues with different types and lengths of spacers, for example, ethylene oxide chains. New monomer design should first look closely at the work of Stupp and Litt both of which have achieved some success in crosslinking liquid crystalline monomers. A smectogen incorporated into the monomer design rather than the nematogens reported here may help to maintain the necessary monomer orientation.

Future work might also include use of a catalyst such as $TaCl_5$ to polymerize the acetylenes either at a liquid/liquid interface or as LBK films immersed in a suitable solvent.[39] Polymerization during transfer might

also be tried though the experimental details such as irradiation time, duration, and location should be considered as well as the problems with elimination of O_2 at the gas/water interface.

CHAPTER 3
PROPERTIES OF SOLUBLE DERIVATIVES OF POLYPHENYLENE-ETHYNYLENE IN LANGMUIR FILMS

Introduction

A recent report[76] from the National Research Council entitled "Polymer Science and Engineering: The Shifting Research Frontiers" suggests high priority for investigations of polymer surfaces and interfaces to permit making smaller structures, thin films, and nanophase materials that have the same scale as the morphological features of polymers.

The nonlinear optical (NLO) response of materials is known to be dependent on molecular ordering parameters.[77] The Langmuir-Blodgett-Kuhn technique is one method by which molecules may be pre-oriented for creation of a well-ordered thin film.[78] Thus, basic studies of the Langmuir film-forming properties of NLO polymers can provide important clues toward an optimal molecular design.

Microscopy techniques, such as Brewster angle microscopy (BAM) and epifluorescence microscopy, facilitate the morphological study of Langmuir films.[79,80,81,82,83,84,85] In the present work, BAM and epifluorescence microscopy were used to examine Langmuir films of soluble derivatives of

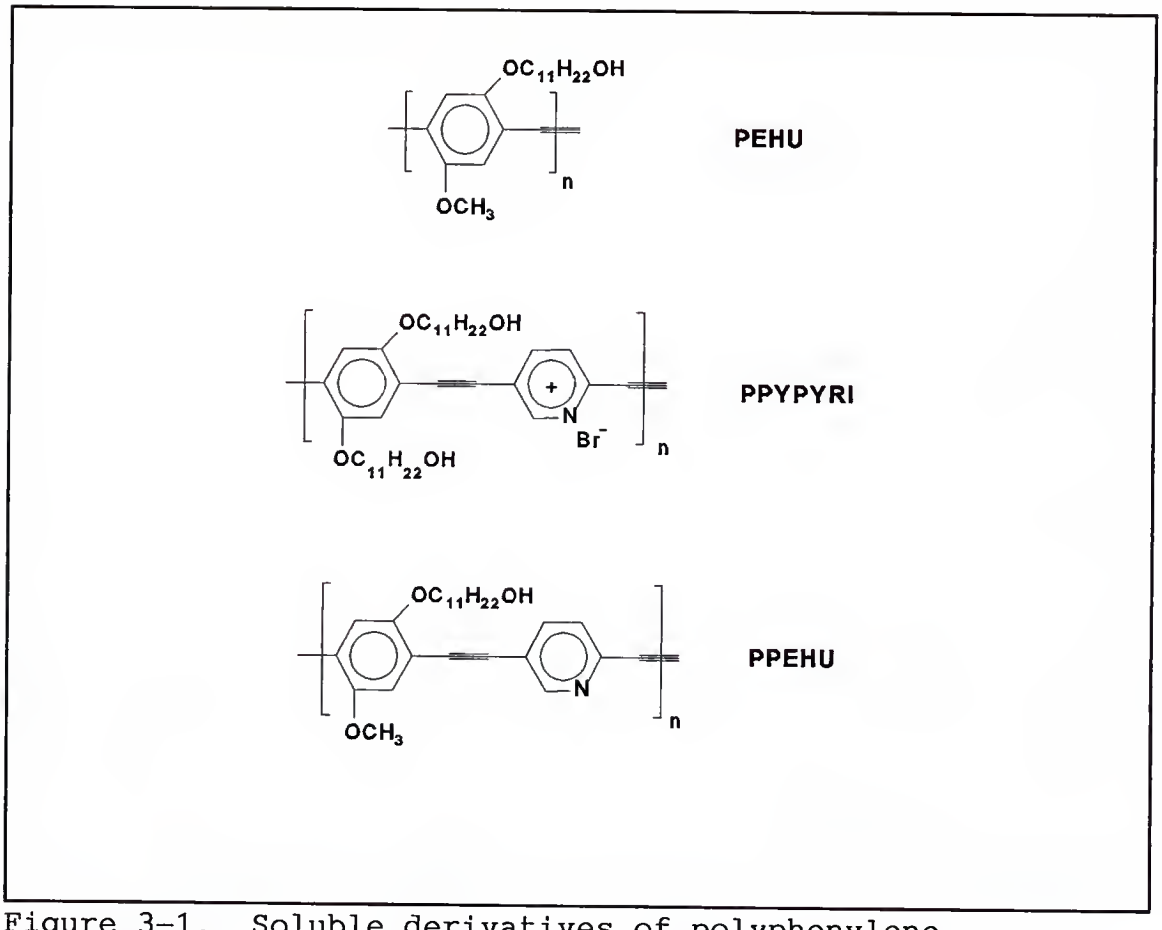

Figure 3-1. Soluble derivatives of polyphenylene ethynylene.

polyphenylene-ethynylene (Figure 3-1). The surface concentration dependence of the surface pressure and surface potential along with microscopy are used to suggest a nanoscale model for the conformation of these polymers at the air-water interface. These polymers are part of a general class of rigid rod polymers designed for nonlinear optics.[86]

Theoretical Considerations

Monolayers of Rigid-Rod Polymers

It is well known that a solution containing rodlike molecules spontaneously forms isotropic and anisotropic domains.[87] Theoretical models such as Flory's discrete lattice model[88] (DLM) explain phenomena such as the isotropic to anisotropic transition on the basis of hard-core repulsive forces only. DLM ignores attractive forces between molecules as perturbations on the athermal model. Flory's DLM represents the rods as sequences of occupied lattice cells, with each sequence oriented parallel to a preferred domain axis. The free energy of the system is expressed in terms of the orientational and the positional entropy. The positional entropy is derived from the probability of finding an occupiable vacancy within the system for a rod with given disorientation from the preferred domain axis.

The existence of true long-range order in a 2D system of rodlike molecules has been the subject for debate, with many but not all arguments being made against it.[89] Thermal fluctuations tend to break up the long range order.

Increasing axial ratios (length/width) favor anisotropic domains as does increasing the concentration of rods. High axial ratio rods create less wasted space than do low axial ratio rods. Monte Carlo simulations of hard

needles revealed only short range order in which orientational correlations die out over a distance smaller than the length of a needle at all but high number densities.[90] Void area becomes negligible as the density of rods is increased because individual rods may slip and rotate to fill all available space.

Cellular Networks

Many examples of 3-dimensional (3D) cellular network structures exist, such as, metal grain boundaries, soap foams, and magnetic bubbles.[91] The properties of 2D slices of these 3D structures are the subject of a mature body of literature.[92,93,94,95,96] These diverse examples of disordered cellular systems suggests that their formation depends, in part, on universal guiding principles independent of short range forces such as molecular interactions. Metal grain arrays and soap froths are topologically similar systems because they contain the same geometrical elements of cells, edges, and vertices. The driving force for coarsening in both systems is capillarity. The main kinetic difference between the two systems is the existence of two time scales of evolution in the soap froth, while only one has been found in metal grain growth. In metal grain arrays, boundary shape and area changes follow the same kinetics. Grain boundary motion is local, where local velocity is

controlled by local curvature. Thus, grain boundaries move locally and if straight do not move.[97]

Alternately known in the literature as 2D foams, cellular structures, or bubble patterns; cellular networks in Langmuir films have been investigated by several research groups, though most of these studies have been of a qualitative nature. The research group of Knobler did preliminary studies of the topology and kinetics of fluorescent probe labelled stearic (octadecanoic) acid '2D foams'. With regard to topology, they found that the average number of cell sides was six with a non-Gaussian distribution skewed toward larger sizes. They found the growth rate of the cell diameter to be more typical of 2D grain growth in metals ($t^{1/2}$) rather than the t^{1} behavior usually seen with 2D slices of soap foams.[98]

Libchaber and coworkers studied the topology and kinetics of fluorescence labelled pentadecanoic acid '2D bubble patterns'. They noticed two different regimes depending on the percentage of 'gas phase' in the monolayer. At high gas coverage (~75%) they observed polygonal gas bubbles separated by thin liquid lines like a 2D soap froth. These polygonal bubbles follow a $t^{1.0}$ time evolution of the mean area. They also found that most of the polygonal cells had 6 sides with a second moment of the cell sides distribution of 1.4. At intermediate gas coverage (~50%) they observed circular gas bubbles which grow at a slower

rate with $t^{0.6}$ evolution of the mean area. The probability distribution for bubble areas broadened continuously.[92]

Rondelez and coworkers studied '2D foams' of a surfactant fluorescent dye, 4-(hexadecylamino)-7-nitrobenz-2-oxa-1,3-diazole. They focussed on discussion of the analogous behavior between the 2D monolayer foams and 3D foams. For example, the line tension between the gas and liquid 2D phase regions plays a role similar to that of the surface tension in conventional foams. The line tension determines the thinning of strips of liquid monolayer phase which separate the gas cells. They believe a lower surface pressure in the corner regions causes the equivalent of Plateau border suction. Also they speculate that a gradient in line tension can lead to a slowing of the thinning process when the gradient opposes the monolayer flow. A gradient in the line tension could come about if a 1D equivalent of the surface activity exists.[99]

Stine and coworkers studied the 'foam morphology' of stearylamine in the coexistence region between liquid-expanded and liquid-condensed phases in Langmuir monolayers. The fluorescent probe, 4-(hexadecylamino)-7-nitrobenz-2-oxa-1,3-diazole, was added in a concentration of 0.3 molepercent. This work is notable because the foam morphology observed consists of two liquid-like phases.[100]

Mann and coworkers studied the great variety of domain shapes formed in monolayers of polydimethylsiloxane

at the air/water interface. Also they observed '2D foams'. It was not possible to follow the foam with time because it coarsened quickly and reached characteristic sizes larger than the maximum field-of-view which was limited to the size of the laser beam in their Brewster angle microscope. One interesting observation in their work was that the reflectivity of the regions of the monolayers dense in polymer was less than the reflectivity of the pure water surface. Thus the polymer dense regions appeared dark in the Brewster angle microscope images. They estimated the line tension of the PDMS to be on the order of 10^{-13} N by observing the time required for distorted isolated domains to relax to the equilibrium circular shape.[101]

Seul and coworkers studied 'bubble domains' in Langmuir films of a mixture of dimyristoylphasphatidylcholine and dihydrocholesterol. The coarsening dynamics were monitored for 90 hours using computer controlled time-lapse video recording. The cell areas and other data were automatically generated from the images with image processing software. They found that the average cell area followed a $t^{0.56}$ growth rate. They also found the cell radii had a Gaussian distribution about the mean radius. Plots of the average cell area versus the number of cell sides were linear in accordance with Lewis law, described below (although deviations from linearity occurred on some experiments due to unreliable statistics of

4 and 8 sided cells). The Aboav-Weire law (described below) was found to be followed as well with the fitted parameters closely matching those of a random Voronoi lattice.[102]

Goldstein and Jackson[103] have reformulated a theory of pattern formation in magnetic fluids to describe the shape instabilities of isolated domains in Langmuir domains. They analyzed the data of Seul to calculate a value for the line tension from the relaxation times for distorted bubble domains of dimyristoylphosphatidylcholine and cholesterol. They found a value for the line tension of 1.1×10^{-13} N.

During the past ten years, McConnell and coworkers have developed the theoretical basis for the variety of domain shapes observed in coexisting phases of Langmuir films.[104,105,106,107,108,109,110,111] The present theory on 2D 'bubble' phases may be described as follows. The theory is simplified by assuming the separated phases are isotropic and there is a sharp well-defined boundary between the phases. The free energy of mixture is given by

$$F_{\phi}=F_{o}+\gamma l$$

where F_o is the bulk (uniform) free energy contribution, γl is the energy cost of creating the wall in 2D, and ϕ is the mole fraction.

If all the dipoles point along the direction normal to the surface, they interact pairwise by means of a repulsive

dipole-dipole electrostatic interaction. The dipole-dipole interaction contribution to the free energy is given by

$$F_d = -\frac{\mu^2}{2}\iint |\vec{r}-\vec{r}'|^{-3}\, dA\, dA'$$

where integration is taken over all possible dipole pairs in areas A and A' and where $\vec{r} - \vec{r}'$ is the distance between points within the domain. For simplicity, the dipole moment in one phase was set to zero and so μ is the dipole moment in the second phase.

The combined shape-dependent part of the free energy is then

$$F = F_\phi + F_d$$

F_ϕ is reduced by an increase in domain size but F_d is reduced by the continued subdivision of domains. Thus the overall free energy, F, favors the formation of domains of a preferred size.

Topologically, cellular networks are defined by a coordination number of 3 at each vertex and a conservation law (Euler's equation). Euler's equation is defined as $N_F - n + V = 1$ for a 2D planar surface, where N_F is the number of faces, n is the number of edges, and V is the number of vertices. Weire and Rivier[91] stated that when the short-range forces are less important in creating the structure than the constraint of space-filling, a disordered cellular

structure results. In a Langmuir film, the short range forces are primarily those due to line tension at phase boundaries and dipole repulsion between molecules within each phase. In addition, there are entanglements of polymer main chains and side chains as well as the steric repulsion between rigid rods.

As a non-equilibrium structure, the cellular network degrades over time. The driving force for the dynamics of the cellular network is the minimization of the line tension within the topological constraints. Beyond the topological constraints, it ceases to be a network.

In the model of Weire and Rivier, statistical entropy of a network is a function of the deviation from an ideal hexagonal network. As shown in Figure 3-2, there are at least three processes which affect the statistical entropy of a cellular network.[91] T1 is a cell neighbor switching process. During a T2 process, a cell disappears into a vertex. This process has been observed in soap cell networks. The third process, cell coalescence, is preceded by an edge-thinning process during which an individual edge releases material to its vertices. Usually, the thinned edge breaks close to one vertex.

Several empirically based models describe the topological and dynamic properties of 2D cellular networks. Topological laws include Lewis, Aboav, and the perimeter law. Lewis' law, which predicts that the mean area of n-

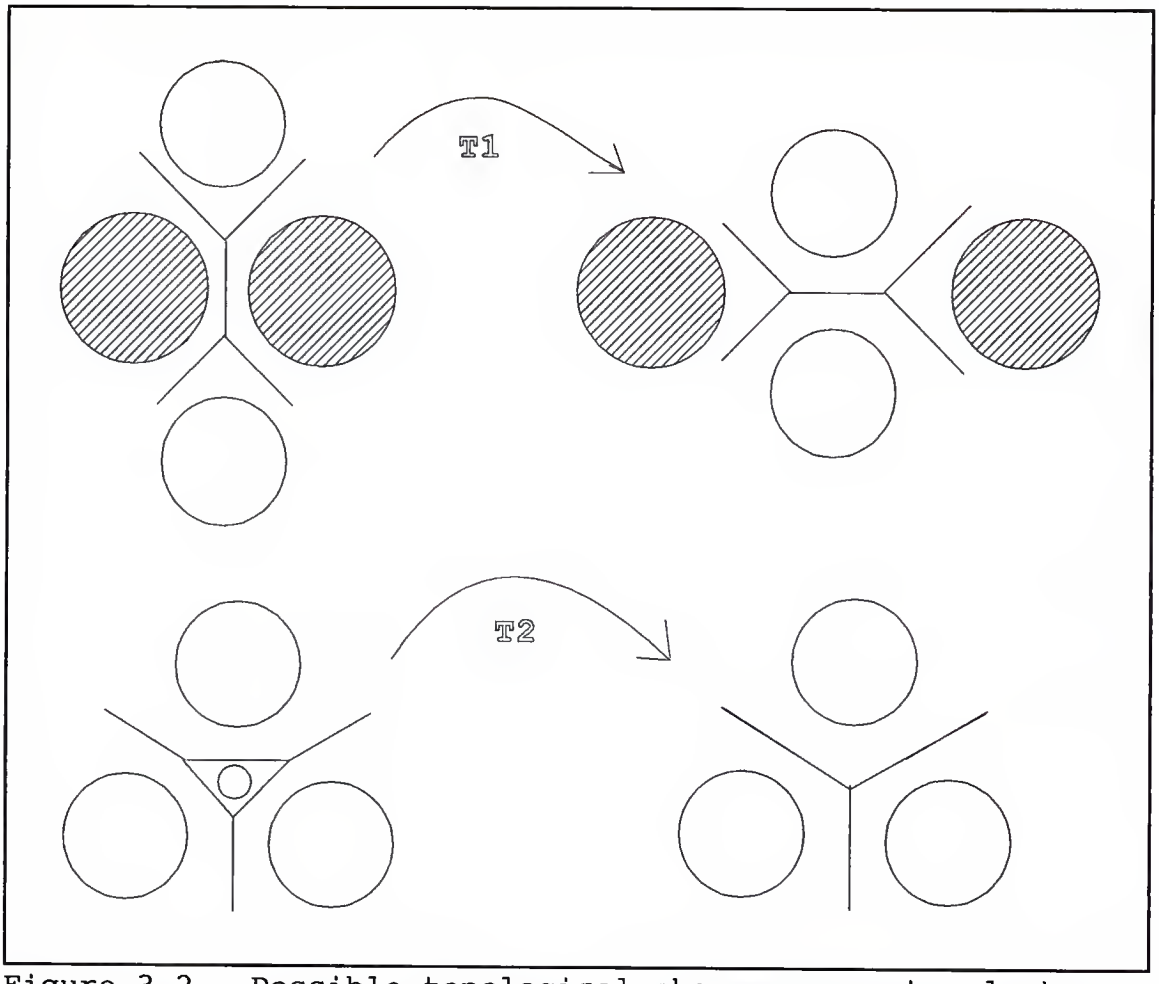

Figure 3-2. Possible topological changes occuring during coarsening of a cellular network. Cell coalescence is a third such change.

sided cells varies linearly with n, has been shown to be an equation of state for cellular structures in statistical equilibrium, where statistical equilibrium is defined as the most probable distribution.[91] Aboav's law relates the number of sides of a cell, n, with the average number of sides of its neighbors, m, through the equation, $mn = 5n + 6$.[112] This equation was later modified by Weire by the

addition of a term, μ_2, for the second moment of the cell side distribution.[91] In their model, the evolution of the cellular network is driven by entropy, and so μ_2 is expected to increase with time. Empirical dynamic laws include Von Neumann's Law which states that the rate of growth of a soap foam cell is proportional to its number of sides minus 6.[113] It predicts that many sided cells should grow in area, few sided cells should shrink and six-sided cells should have a constant area. Previous workers have performed numerical simulations of cellular network dynamics.[114,115]

Cell growth consists of two different simultaneous processes. The first process is the evolution of cell geometry, that is shape and size, which occurs continuously. The second process includes the associated topological rearrangements which occur instantly.

Most simplified theoretical models are uniform boundary models which neglect local differences in cell boundary energies and mobilities, for example, von Neuman's law holds for systems with uniform boundaries and mobile vertices.

Cellular networks were observed in Langmuir films of two of the polymers reported in this chapter. The topology and dynamics of one of the polymer's cellular networks have been quantified. Its behavior (discussed below) fits remarkably well into the existing theory.

Experimental Methods

The polymers studied were provided by Mr. Marc Moroni and Dr. Jacques Le Moigne of the Groupe des Materiaux Organiques, Institut de Physique et Chimie des Materiaux de Strasbourg in Strasbourg, France. They removed the smallest oligomers by preparative GPC. The molecular weight of the resulting polymers is too large to be measured by mass spectrometry. GPC could not be used accurately because evidence of aggregate formation was seen. The molecular weight of the resulting polymers is estimated to be on the order of 10^4 g/mol based on the GPC results. The solid polymers are deep red in color with paste-like texture. The polymers are near perfectly alternating copolymers due to the synthetic scheme.[116]

Spectroscopy

A Perkin-Elmer Lambda 9 UV/Vis/NIR spectrophotometer was used to obtain UV spectra of the chloroform solution and a thin film cast on a quartz slide. A SPEX Model 1680 Double Spectrometer was used to measure fluoresence of the chloroform solution and a thin film cast on a quartz slide.

Trough Setup

Langmuir film balance studies were carried out on a KSV 5000 system (KSV Instruments). Surface pressure

(defined as the difference in surface tension between the clean interface and the film-covered interface) was monitored with a paper Wilhelmy plate suspended from the constant-height balance at a point equidistant from the two moving barriers and approximately 2 cm from the edge of the 10 cm wide trough. Surface potential was measured by a vibrating electrode device. The vibrating electrode is 4.5 cm diameter. The thermostatted PTFE trough (10.0 cm x 32.4 cm) was used with two hydrophilic polyamide barriers for symmetric compression of the monolayer. The subphase was water obtained from a Milli-Q water purification system (Millipore). The film balance system was mounted on vibration isolation table under a downflow hood. The hood fan was turned off during experiments.

Formation of a Cellular Network

The 2D foam-like morphology was generated by compressing the film at a barrier speed of 20 mm/min (0.084 nm^2/repeat unit/min) to an area of 0.25 nm^2/repeat unit. After compression, the direction of the barrier motion was immediately reversed so that the film was decompressed at a speed of 200 mm/min (0.84 nm^2/repeat unit/min) until the desired point along the isotherm is reached. For the dynamics studies, time zero of foam formation was set at the moment when the barriers were stopped. Also, the surface pressure change was monitored over time.

Brewster Angle Microscope

When an air-water interface is illuminated by plane polarized light incident at the Brewster angle (53.1° from normal), the presence of a film changes the refractive index at the interface and thus increases the reflectivity. This property is exploited by the Brewster angle microcope (BAM) technique. The BAM1 system (Nanofilm Technologies) was mounted on a motorized X-Y stage so that different regions of the film could be imaged. The BAM was set up to image at a point equidistant from both moving barriers and approximately 3 cm from the edge of the 10 cm wide trough. The BAM images a 1 mm^2 area of the film by monitoring changes in reflectivity of a He-Ne laser beam that is incident at the Brewster angle for the clean water/air interface. Each pixel corresponds to 4 μm^2. The BAM has a polarizer (analyzer) between the objective lens and the CCD camera so it is possible to check for birefringence in the film by setting this analyzer at 90° to the usual polarization of the reflected beam.

Epifluorescence Trough

A 8 x 17 cm PTFE trough with a quartz window in the bottom and enclosed in a plexiglass box was attached to the stage of a Nikon DIAPHOT-TMD-EF inverted epifluorescence microscope. A single PTFE barrier was used to compress the

film. The microscope was fitted with the B-2A filter block which provides excitation wavelengths between 450 and 490 nm and allows observation of emission wavelengths greater than 500 nm. Photographs were taken on Kodak TMAX P3200 TMZ 135 black and white film using a Nikon F4 camera. Exposure time was in the range of 12 to 14 seconds. In addition, the dynamics of the cellular network were recorded on videotape using a Optronics VI-470 Remote-Head Microscope Camera (Optronics Engineering).

Image Processing

Microscope images were recorded on videotape (JVC) and subsequently transferred to a Sun Sparcstation 1 using a VideoPix image capture board for image analysis. Image analysis software (PV~Wave) was used to correct the images for geometric distortion caused by the viewing angle between the line of sight of the BAM's objective lens and the plane of the interface. Data extracted from captured images with the image analysis software were the relative total reflectivity and the areas corresponding to either of the two phases. The total reflectivity was calculated by summing the grey scale values over all pixels in images captured from videotape. The total relative reflectivities were calculated as the ratio of the total reflectivity of the film over the total reflectivity of the clean water surface. A second image analysis software (SaoImage) was

used to gather data such as cell areas and number of cell sides.

Results and Discussion

Langmuir Film Properties of Poly(2-(11-hydroxyundecanoxy)-5-methoxyphenylene-ethynylene), PEHU

Poly(2-(11-hydroxyundecanoxy)-5-methoxyphenylene-ethynylene), PEHU, as shown in Figure 3-1, dissolves slowly in chloroform. The UV absorbance spectra of PEHU in the solution (Figure 3-3) shows maxima at 387 and 301 nm. The solid cast film shows corresponding maxima at 392 and 303 nm (Figure 3-4). The *in situ* UV spectroscopy of the PEHU Langmuir film at the air/water interface shows a maximum at 410 nm (Figure 3-5). Thus there is a shift of the maximum absorbance to longer wavelengths in the Langmuir film under lateral compression. This may indicate increased conjugation along the main PEHU backbone is induced by the conformation changes forced by the increased surface pressure. It is not clear from the spectrum in Figure 3-5 whether or not the long wavelength side of the peak is also shifted to longer wavelengths. This would be further proof of increased conjugation. The shift in the maximum may also be due to interchain interactions of the π clouds analogous to the formation of H aggregates.

The dissolution rate was increased by adding a drop of trifluoroacetic acid to the chloroform spreading solution.

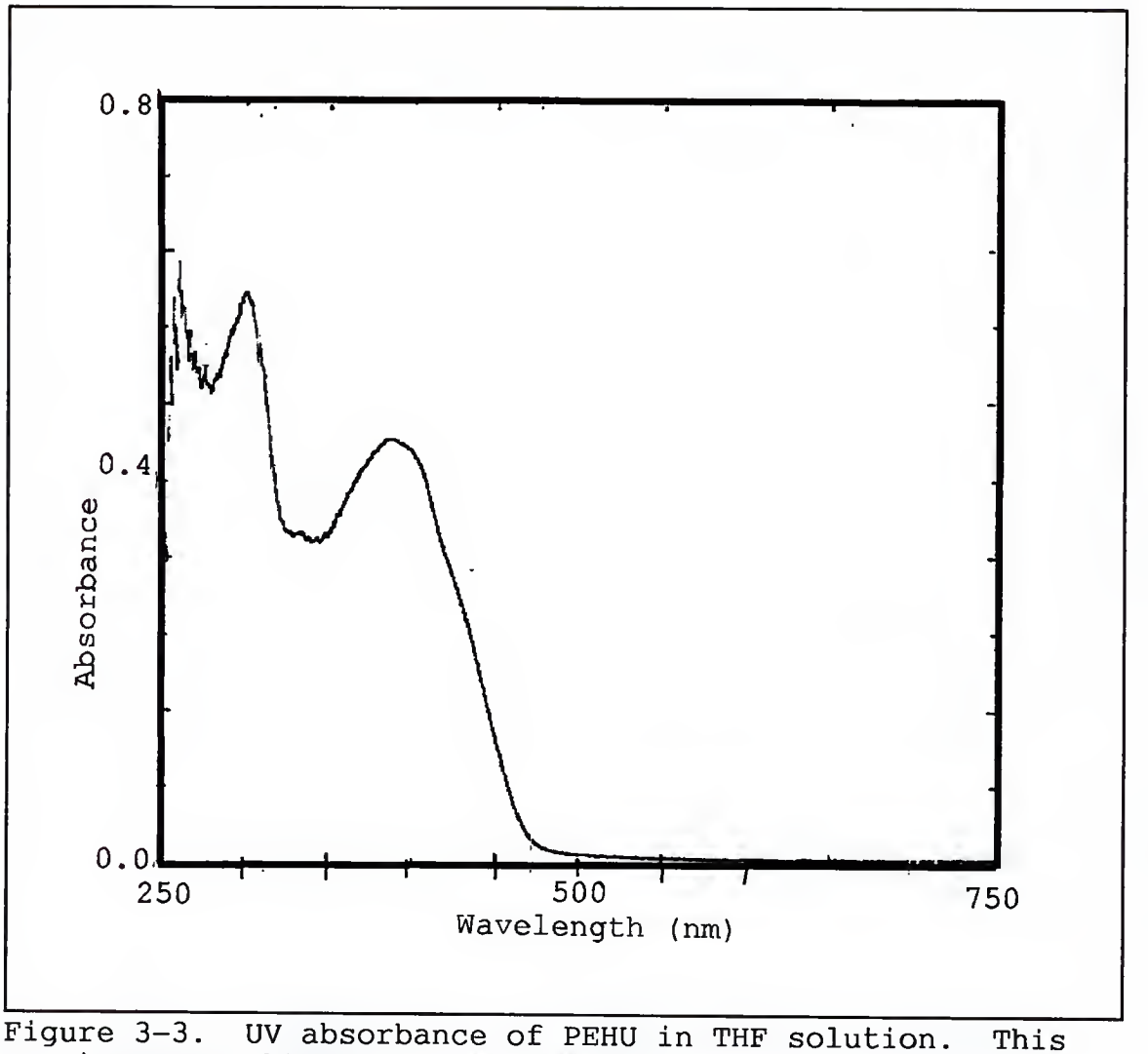

Figure 3-3. UV absorbance of PEHU in THF solution. This spectrum was obtained by Marc Moroni.

The addition of the trifluoroacetic acid changes the color of the 0.47 mg/ml solution from reddish to greenish in color possibly due a loss of conjugation length in the polymer. The loss of conjugation length may be due to changes in conformation.

The isotherm for PEHU is shown in Figure 3-6. The

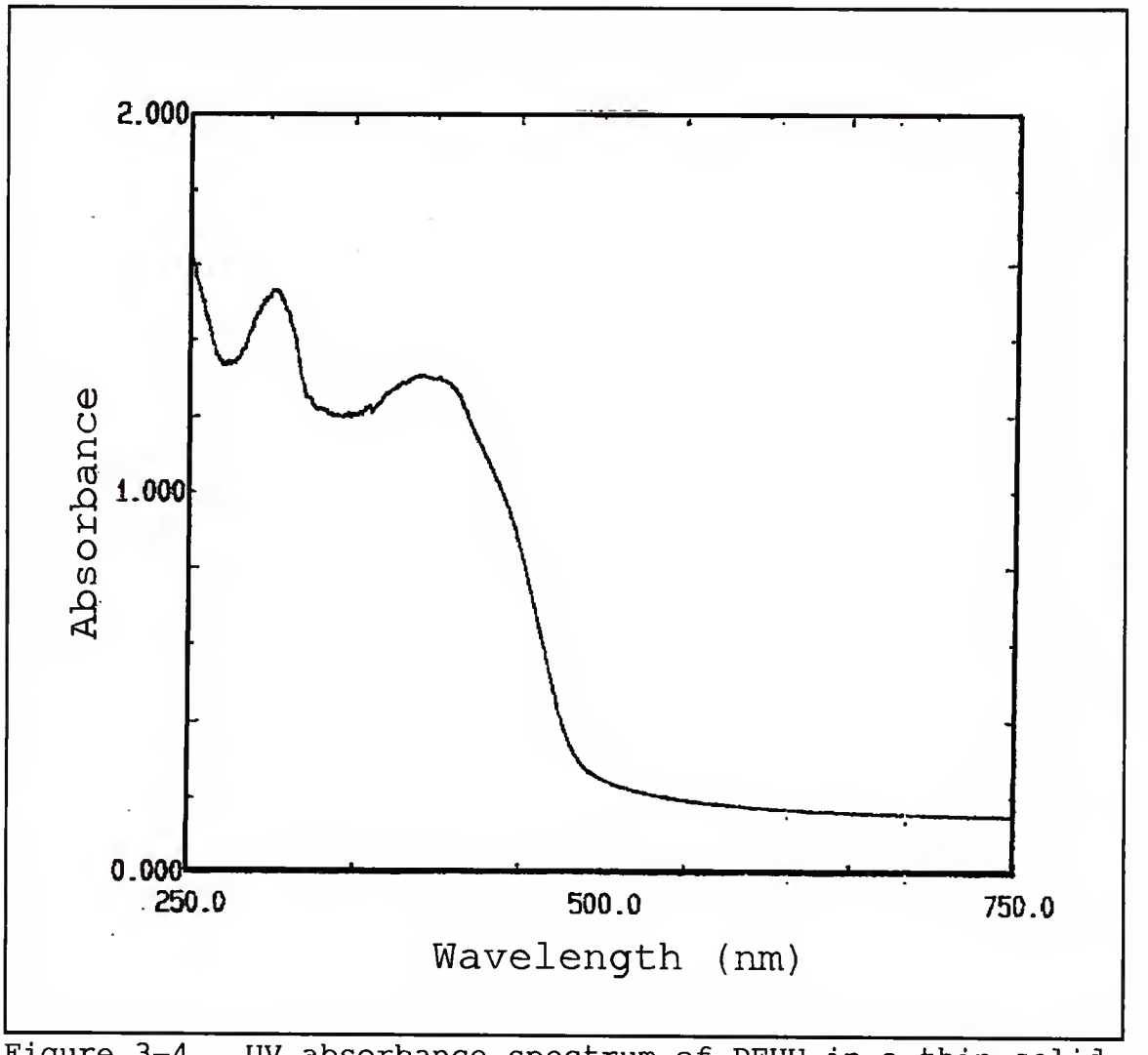

Figure 3-4. UV absorbance spectrum of PEHU in a thin solid film cast on quartz. This spectrum was obtained by Marc Moroni.

shape of the isotherm suggests a compressible film with a collapse surface pressure over 16 mN/m.

Observation of the film with the Brewster angle microscope reveals the film is homogeneous and fluid at repeat unit areas in the range between 0.25 and 0.46 nm^2.

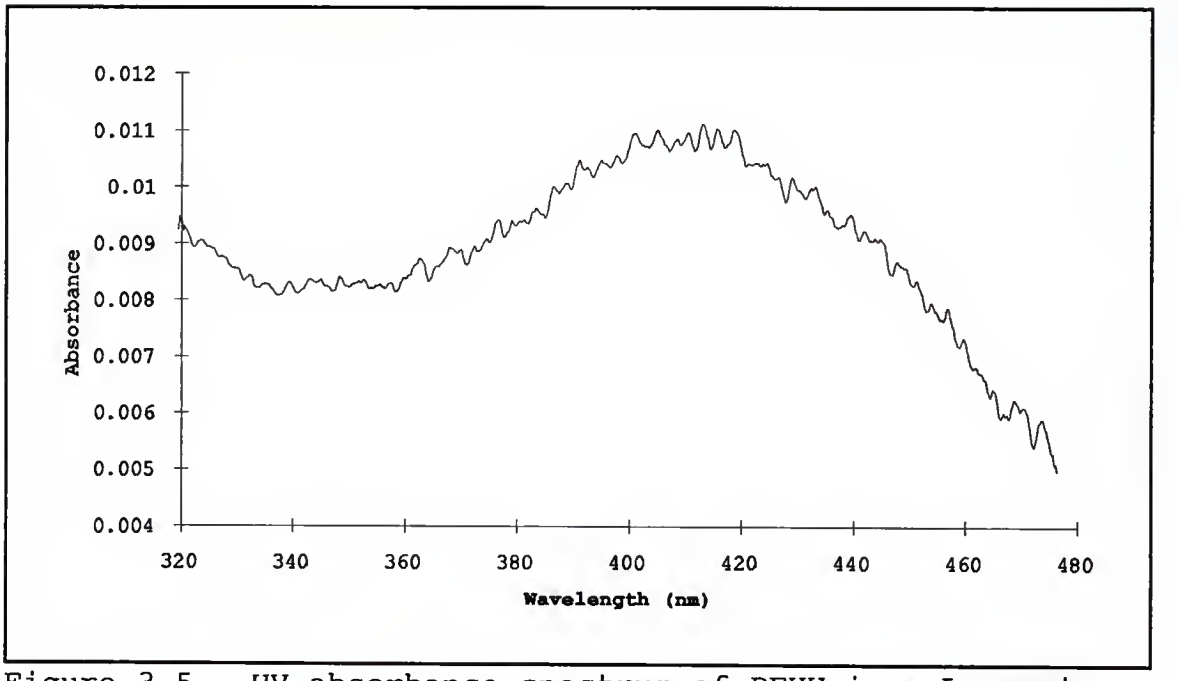

Figure 3-5. UV absorbance spectrum of PEHU in a Langmuir film during compression between 0.2 and 0.45 nm^2/repeat unit.

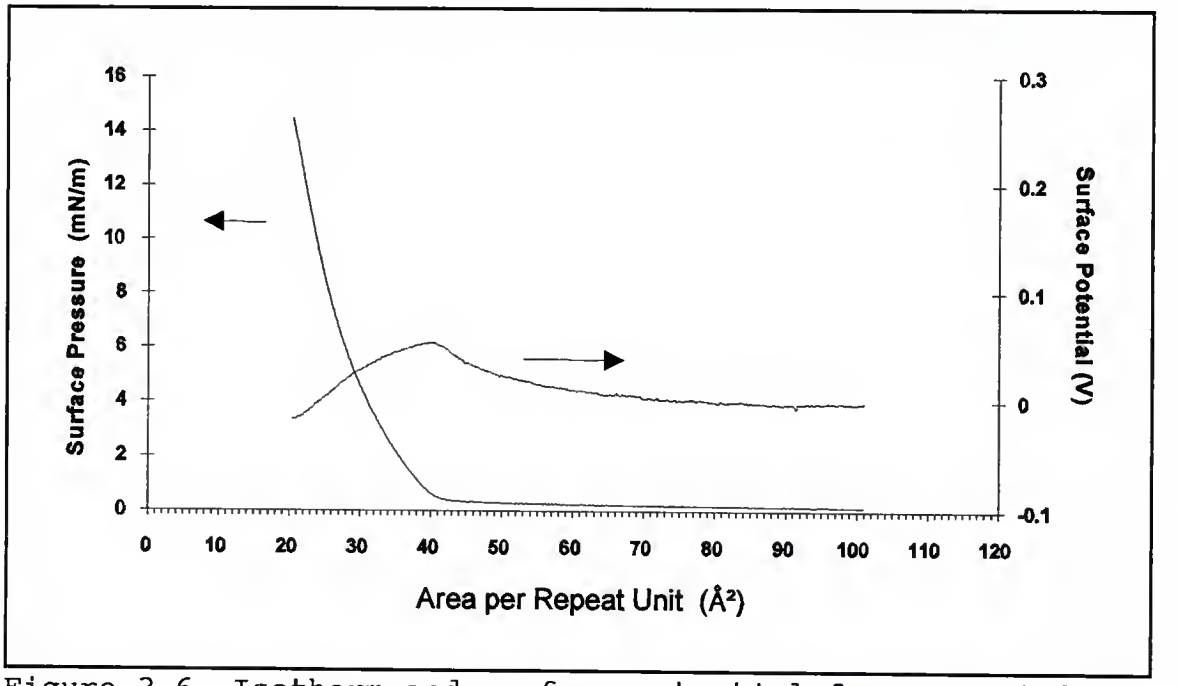

Figure 3-6. Isotherm and surface potential for PEHU at 25°C.

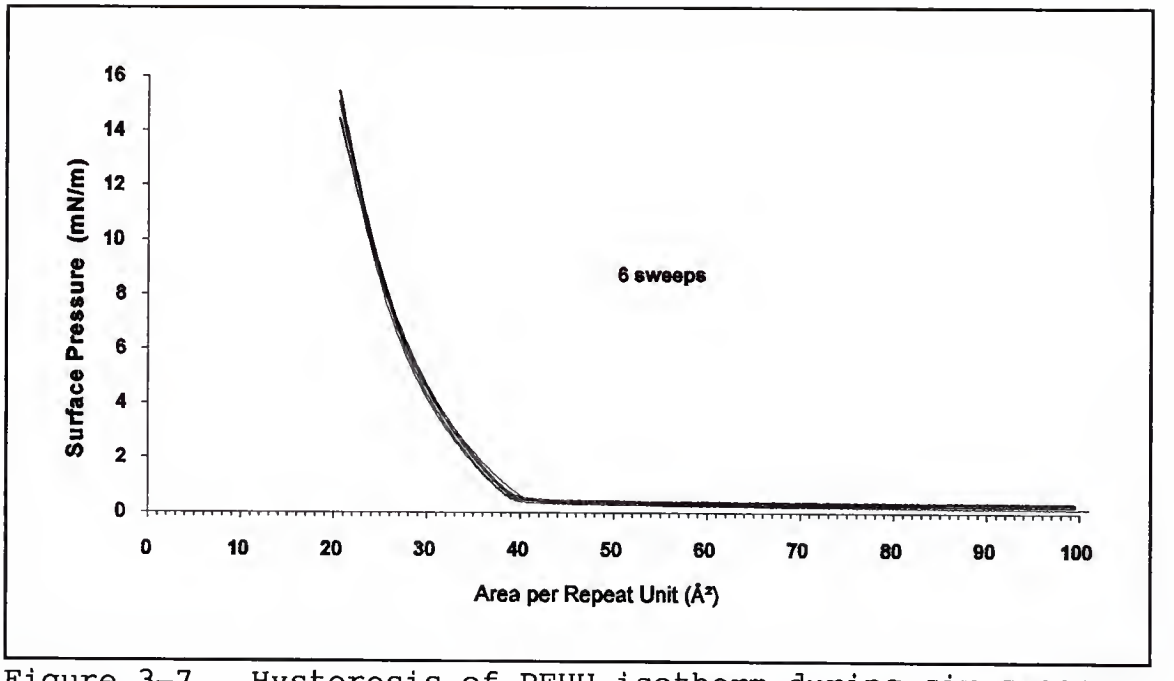

Figure 3-7. Hysteresis of PEHU isotherm during six sweeps at 25°C.

Below 0.25 nm^2 the film becomes rigid. Re-expansion of the film recovers the homogeneous, fluid film. Note, unlike the other polymers reported in this chapter, this material does not form a cellular network on decompression. Repeated compression and decompression cycles reveal the hysteresis behavior of this material (Figure 3-7). *In situ* monitoring of the UV spectra during compression (Figure 3-5) of the film indicates a decrease in the effective absorbance of the main chromophore possibly through reorientation of the chromophore normal to the water surface (Figure 3-8). This is further evidence that the shift in the UV maximum absorbance is due to interchain interactions rather than

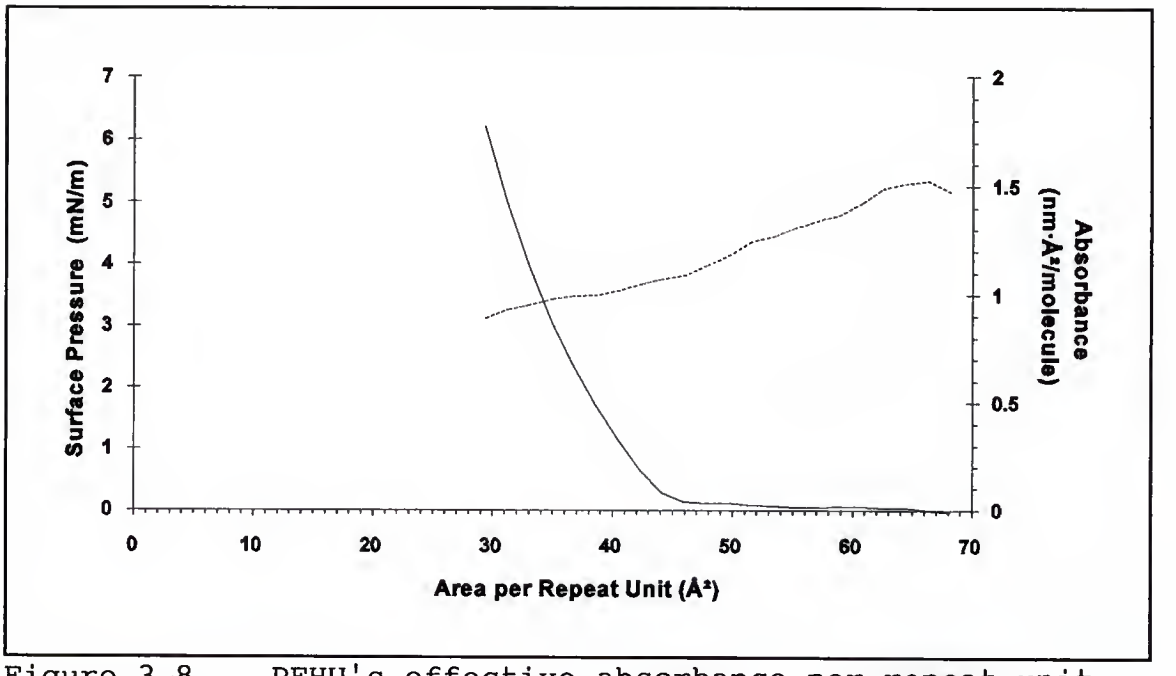

Figure 3-8. PEHU's effective absorbance per repeat unit decreases with compression at 25°C.

increased conjugation lengths. The surface potential goes through a maximum at the point where the surface pressure begins to increase. The shape of the surface potential is reversible on repeated compression and decompression of the film. The stability of the film, determined by maintaining a constant surface pressure of 10 mN/m and following the change in area, was -0.001 nm^2/repeat unit during 8 minutes. During Langmuir-Blodgett-Kuhn processing, the transfer to hydrophobic quartz plates was 0.9 for the first downstroke and upstroke, but transfer degraded to near zero with continued processing. Allowing layers to dry for up to 30

minutes, did not improve the transfer. The best dipping speed was found between 3 and 5 mm/min.

Langmuir Film Properties of Poly(2-(11-hydroxyundecanoxy)-5-methoxyphenylene-ethynylene-pyridine-ethynylene), PPEHU

The behavior of Poly(2-(11-hydroxyundecanoxy)-5-methoxyphenylene-ethynylene-pyridine-ethynylene), PPEHU, at the air-water interface is interesting in several aspects, such as, the coexistence of two fluid condensed phases under certain conditions. The morphology observed depends strongly on the history of the monolayer. For example, compression of the monolayer to a surface pressure within the phase coexistence region results in the formation of domains of the more condensed (MC) phase dispersed in the more expanded (ME) phase (Figure 3-9). Whereas, compression of the polymer Langmuir film to a surface pressure where the more condensed (MC) fluid phase is uniform and equilibrated and then expanding the film until the two condensed fluid phases are coexistent leads to the formation of a microscopic morphology reminiscent of a foam, emulsion, or, in more general terms, a cellular network (Figure 3-9). A key feature of this two-dimensional (2D) microstructure is the continuous random network of the MC fluid phase which typically occupies 10 to 30 area percent and separates the cells of the more expanded (ME) fluid phase. The cellular network completely covers the area of the Langmuir trough in

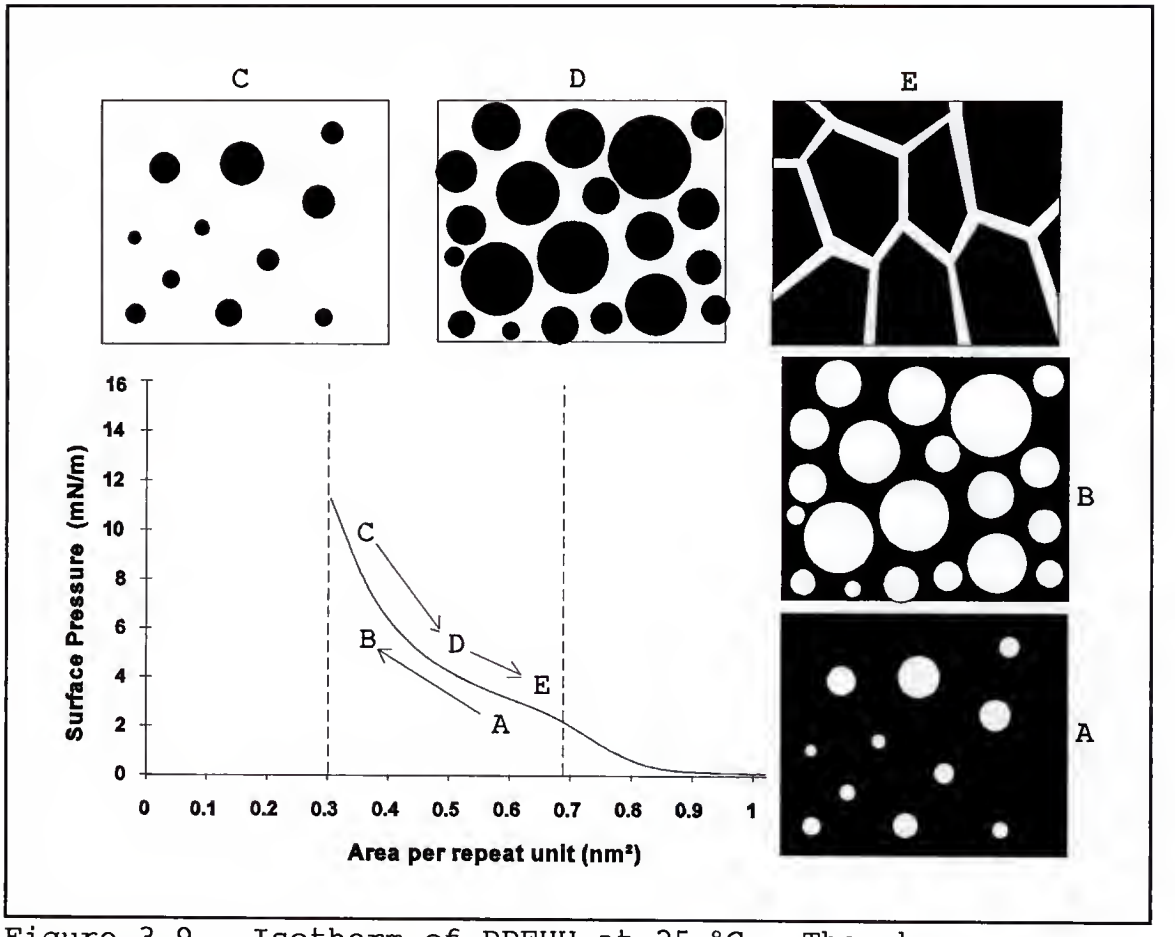

Figure 3-9. Isotherm of PPEHU at 25 °C. The phase coexistence region was observed at the specific areas between the dashed lines. The boxes, A and B, represent the observed morphology at the corresponding points on the isotherm during compression of the monolayer (white=MC phase, black=ME phase). The morphologies in C, D, and E are seen only on decompression of the monolayer.

which it is formed. The average cell diameter can vary widely from about 10 to 1000 μm. The average cell shape can vary from nearly circular to nearly polygonal depending on the relative area fraction (Figure 3-9).

The morphology seen in Figure 3-28 is analogous to 2D cellular structures, or 'foams', occurring in Langmuir monolayers of fatty acids or lipids.[117] At the smallest structural scale, the "energy" required for a polymer molecule to "jump" from one phase to the other tends to stabilize the network morphology by detering the coalescence of neighboring cells. However, the cellular network microstructure is not stable with time or outside applied forces. Furthermore, the network is not in equilibrium. Over time, the two monolayer fluid phases continually move to minimize the line energy by direct coalescence of neighboring cells and also by a coarsening process. Topologically, the transient monolayer network structure consists of cell walls enclosing the cells from the sides, but not the top or bottom. Indeed, the 2D cellular network represents a novel physical arrangement of polymer chains. In this chapter, the properties of this foam-like morphology are compared with those observed in monolayers of low molecular weight amphiphiles.

Electronic Spectra

UV excitation spectra were obtained by setting the fluorometer to monitor the emission at 496 nm. The UV excitation spectra of a cast film shows a broad peak at 385 nm which corresponds to a $\pi \rightarrow \pi^*$ transition over a conjugated chromophore made of the phenyl ring through the

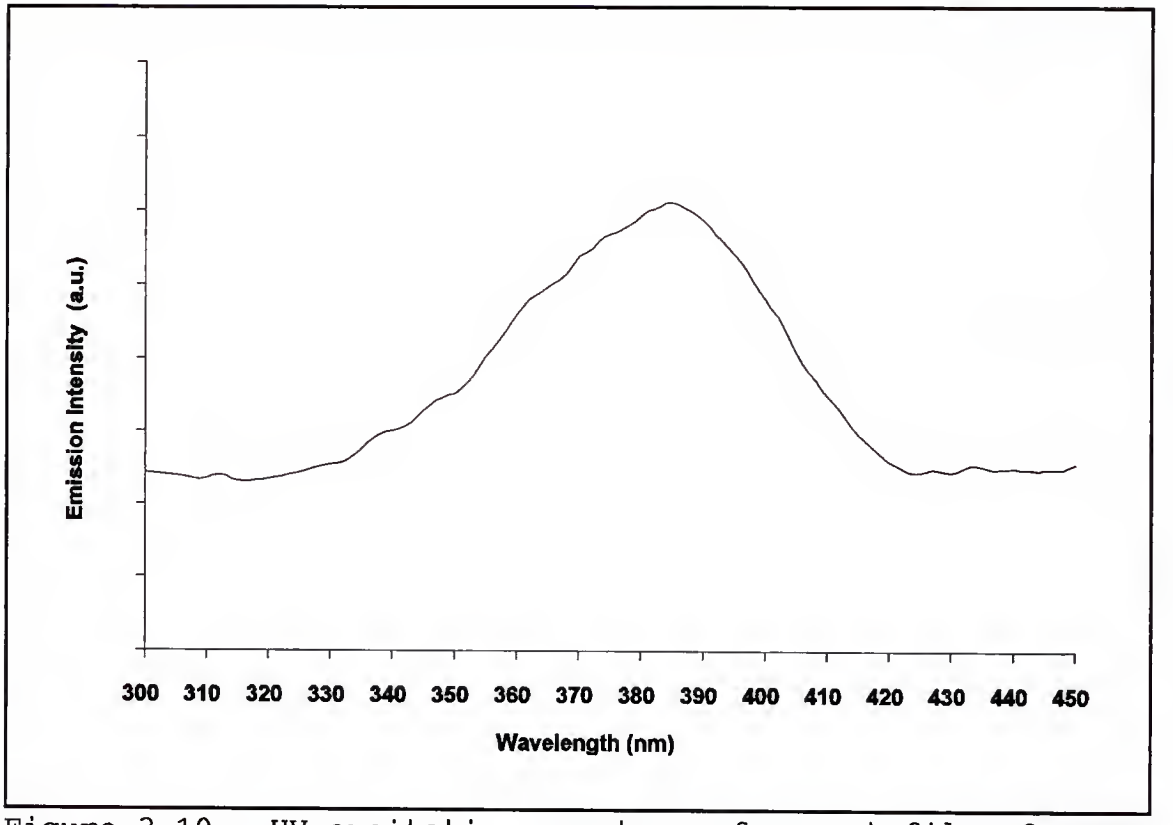

Figure 3-10. UV excitation spectrum of a cast film of PPEHU on quartz (emission monitored at 500 nm).

acetylene bond and including the pyridine ring (Figure 3-10). The UV excitation spectrum of a chloroform solution is shown in Figure 3-11. The chloroform solution of the polymer gives a peak fluorescent emission at 456 nm when excited at 436 nm (Figure 3-12). The thin solid film cast on quartz from chloroform gives a peak fluorescence emission at 492 nm when excited at 385 nm (Figure 3-13). This shift of the excitation peak to higher energy between the solution

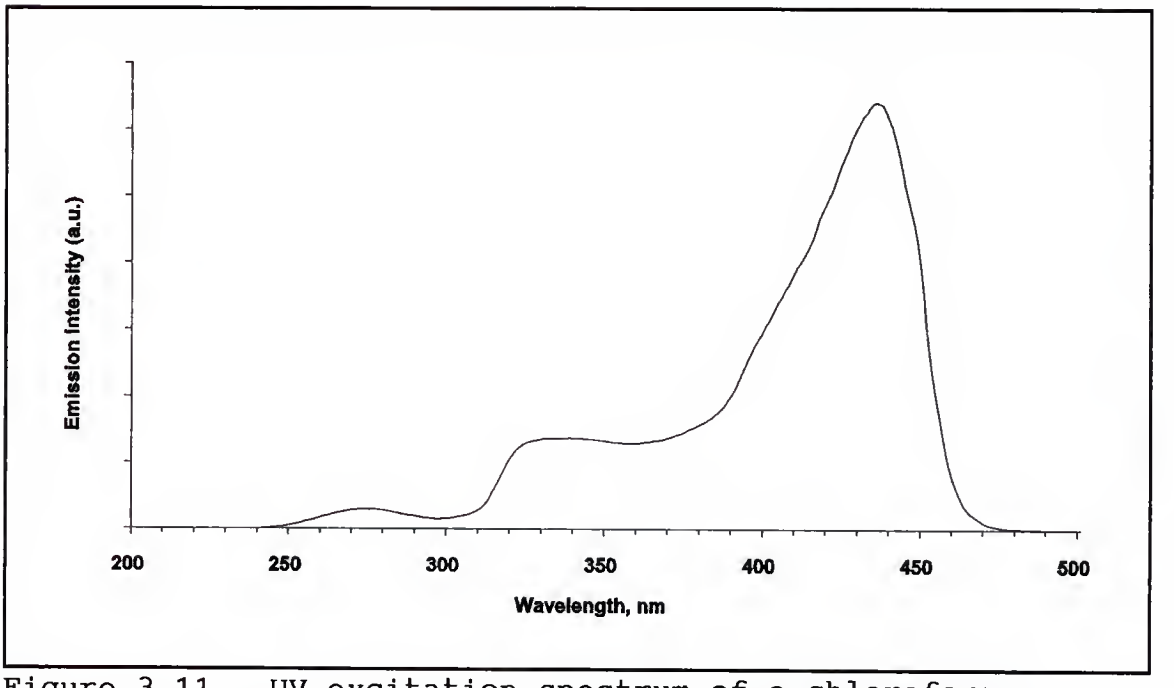

Figure 3–11. UV excitation spectrum of a chloroform solution of PPEHU (Emission monitored at 456 nm).

and the solid film can be explained by the probable formation of aggregates in the solid.[118] It is notable that fluorescence is not quenched in the solid films. This indicates that at least some of the main chains are separated by the side chains sufficiently to avoid interchain quenching or self absorption. The UV spectrum of PPEHU in a Langmuir film is shown in Figure 3–14, where the maximum absorbance was found at 398 nm. The maxima in the cast film and THF solution of PPEHU were found at 402 and 391 nm, respectively. Thus the PPEHU under compression while in the MC phase (0.35 nm^2/repeat unit) has UV absorbance more like the solid film. These results are

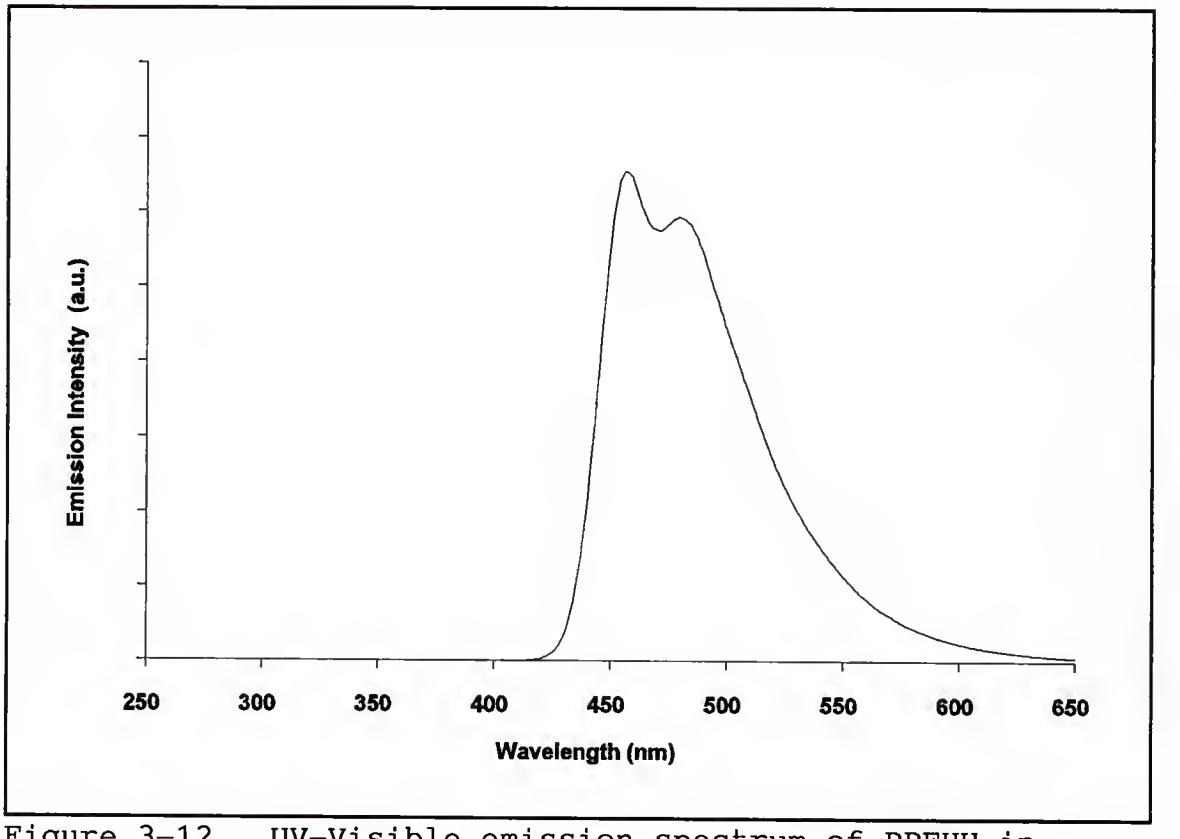

Figure 3-12. UV-Visible emission spectrum of PPEHU in chloroform solution.

discussed further in the section about the epifluorescence microscopy images later in this chapter.

Isothermal Surface Pressure versus Area Diagrams

The isotherm of PPEHU at 25°C has certain characteristic features including a somewhat flattened section which corresponds to a monolayer liquid-liquid phase coexistence region. As the temperature of the subphase is

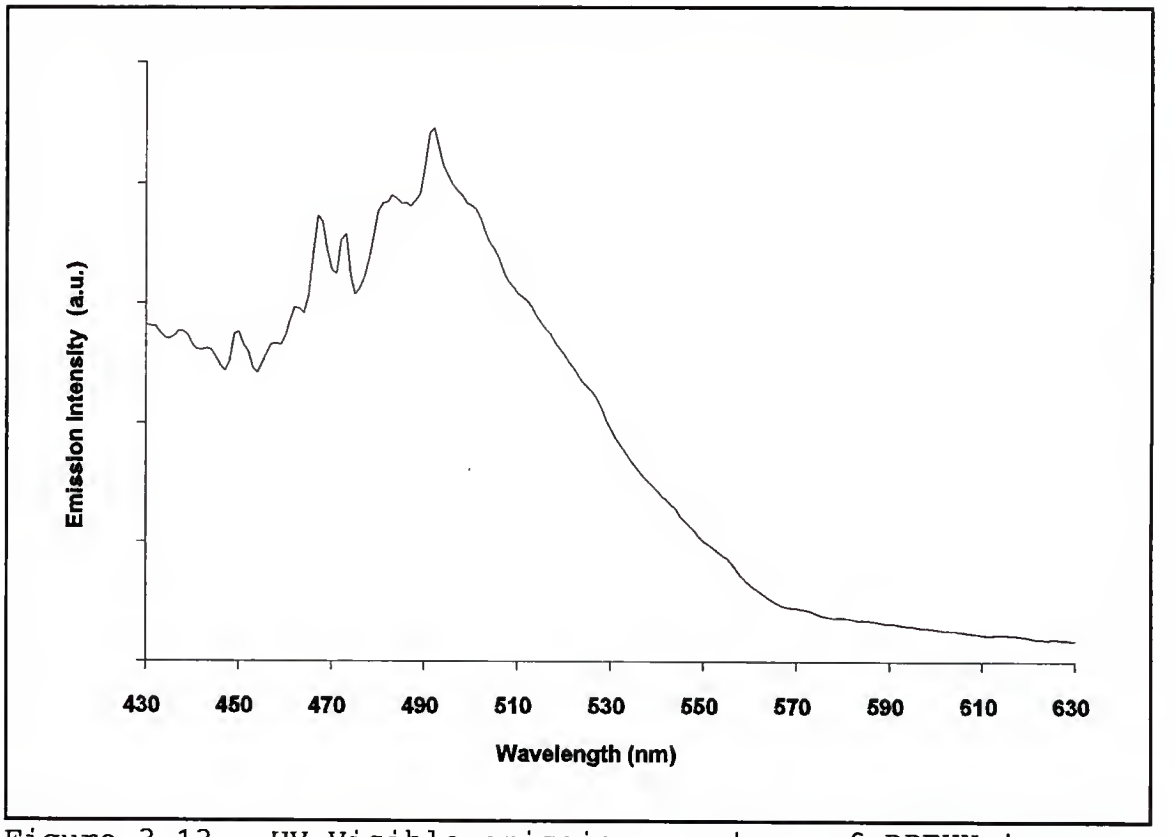

Figure 3-13. UV-Visible emission spectrum of PPEHU in a cast film on quartz.

increased, the phase coexistence line moves to greater surface pressure and increases in slope (compression speed was 0.042 nm^2/repeat unit/min) (Figure 3-15). This temperature dependence is typical of long-chain compounds having highly polar groups such as fatty acids or alcohols. For those low molecular weight compounds, there is a transition from the so-called liquid expanded (L_1) state to the liquid condensed (L_2) state.[119] For PPEHU, the low density boundary of the apparent phase coexistence region

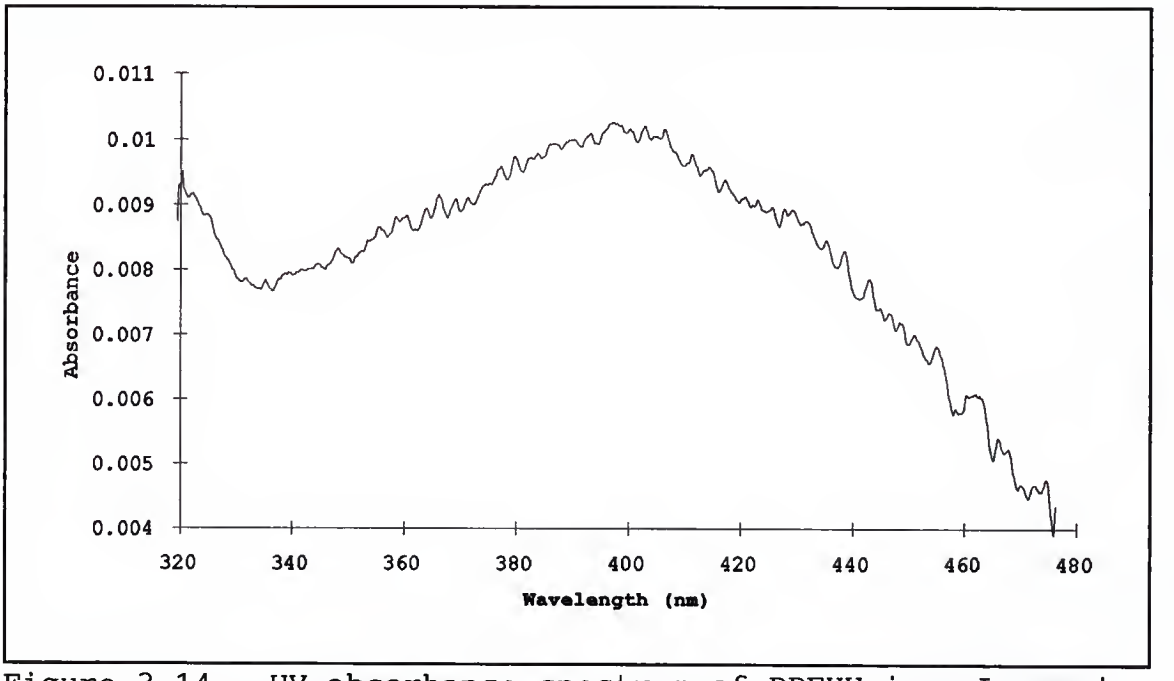

Figure 3-14. UV absorbance spectrum of PPEHU in a Langmuir film during compression at 0.35 nm^2/repeat unit.

shifts to higher area with increased temperature. This apparent shift is different from the typical L_1–L_2 biphasic region which shifts to lower areas as the temperature is increased (Figure 3-16). The increasing temperature causes decreased compressibility of the film. As temperature increases the probability cone for each alkyl chain is expanded. In addition, the frequency of rotation and the amplitude of wagging motions of the phenyl and pyridine rings along the main chain also increases.

Repeated compression-decompression cycles measured at a series of barrier speeds between 0.0084 and 0.042 nm^2/repeat unit/min, show that the shape of the isotherm was

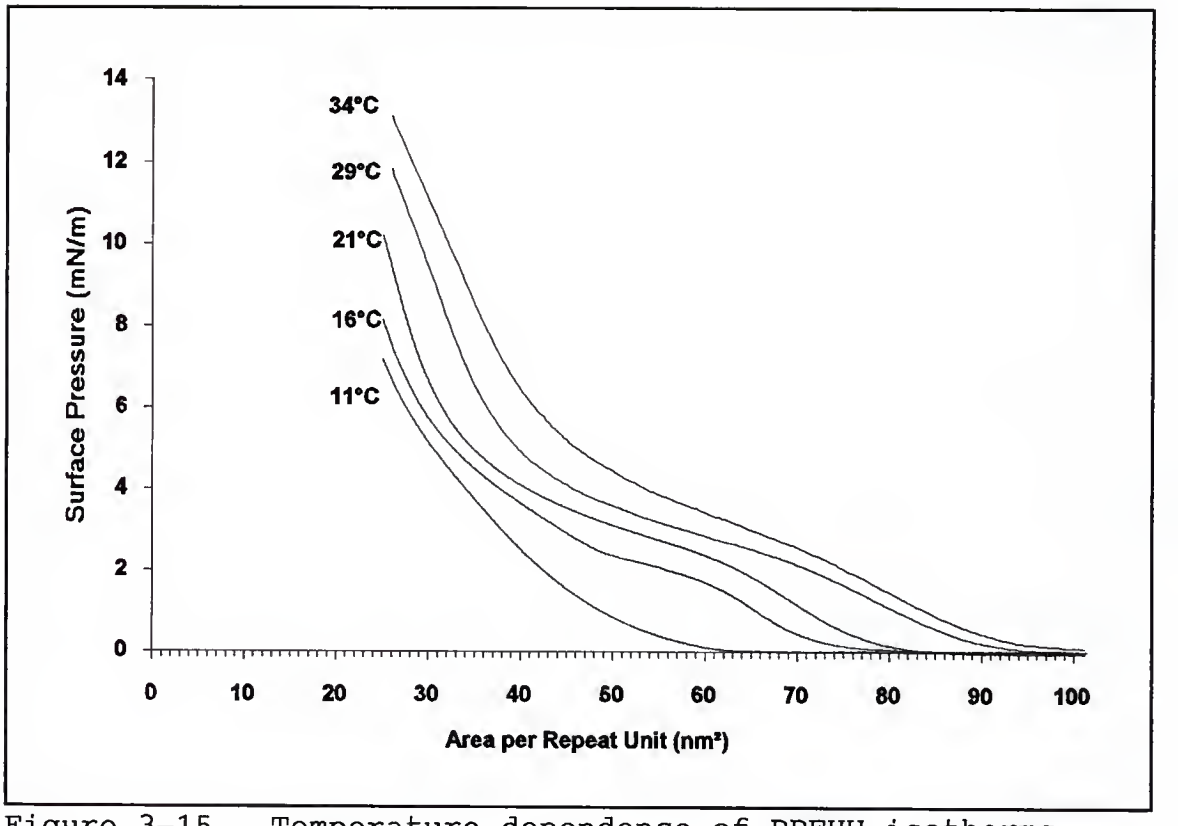

Figure 3-15. Temperature dependence of PPEHU isotherms.

unchanged with negligible hysteresis. This indicates that the stress relaxation processes for PPEHU are nearly as fast as the movement of the barrier.

The effective dipole moment ($\mu_\perp$) was calculated from the surface potential using the Helmholtz equation (Figure 3-17). The Helmholtz equation assumes the interface may be modelled as a capacitor. The molecules in the monolayer are assumed to be an oriented dipole array with their more positive end away from the water surface. The degree to which the real molecules approach the ideal model leads to

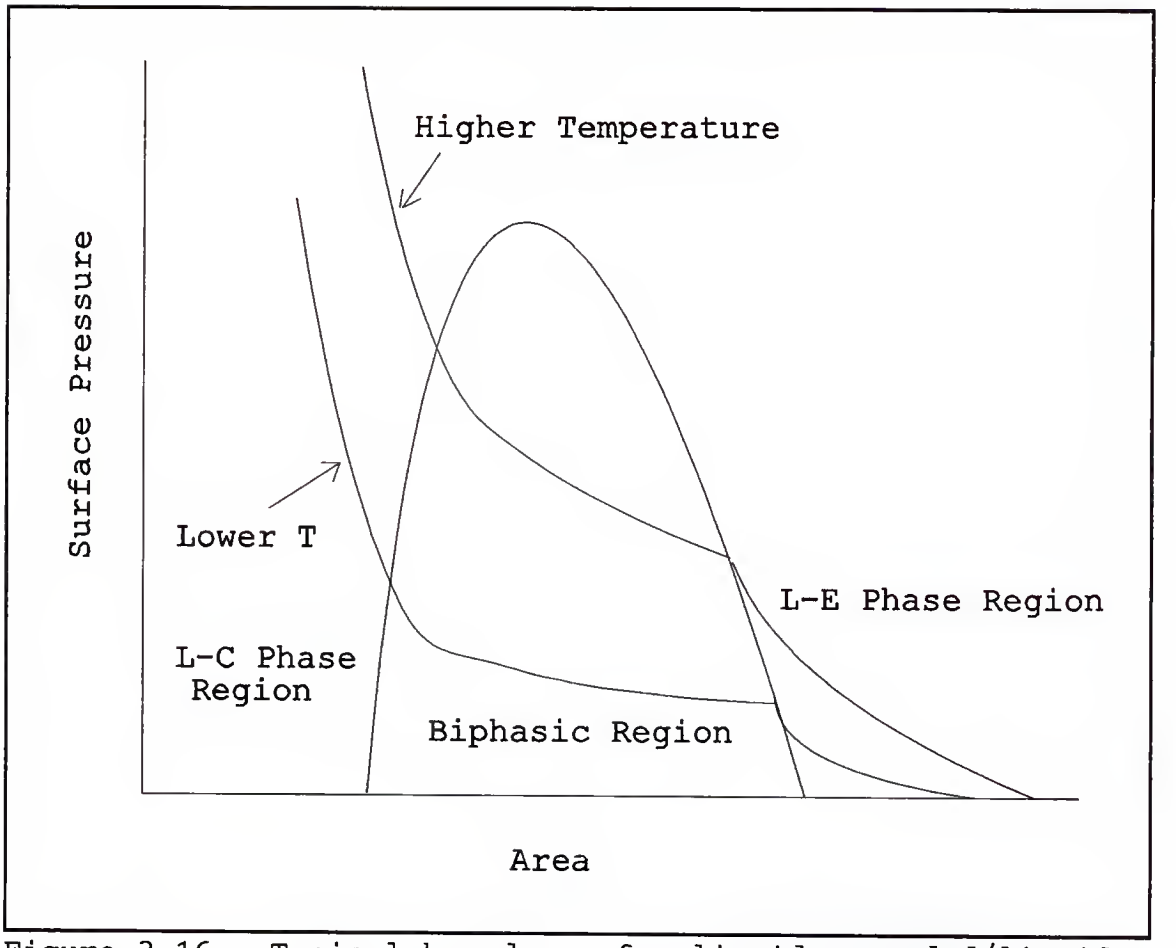

Figure 3-16. Typical boundary of a liquid-expanded/liquid-condensed phase coexistence envelope seen for Langmuir films of long-chain fatty acids or alcohols.

more positive values for the calculated $\mu_{\perp}$. The interesting feature of Figure 3-17 is the steep rise in $\mu_{\perp}$ prior to the increase in surface pressure, that is, once the point corresponding to a close-packed monolayer is reached, $\mu_{\perp}$ peaks and falls linearly as the film is compressed through the phase coexistence region.

There are three functional groups in the polymer,

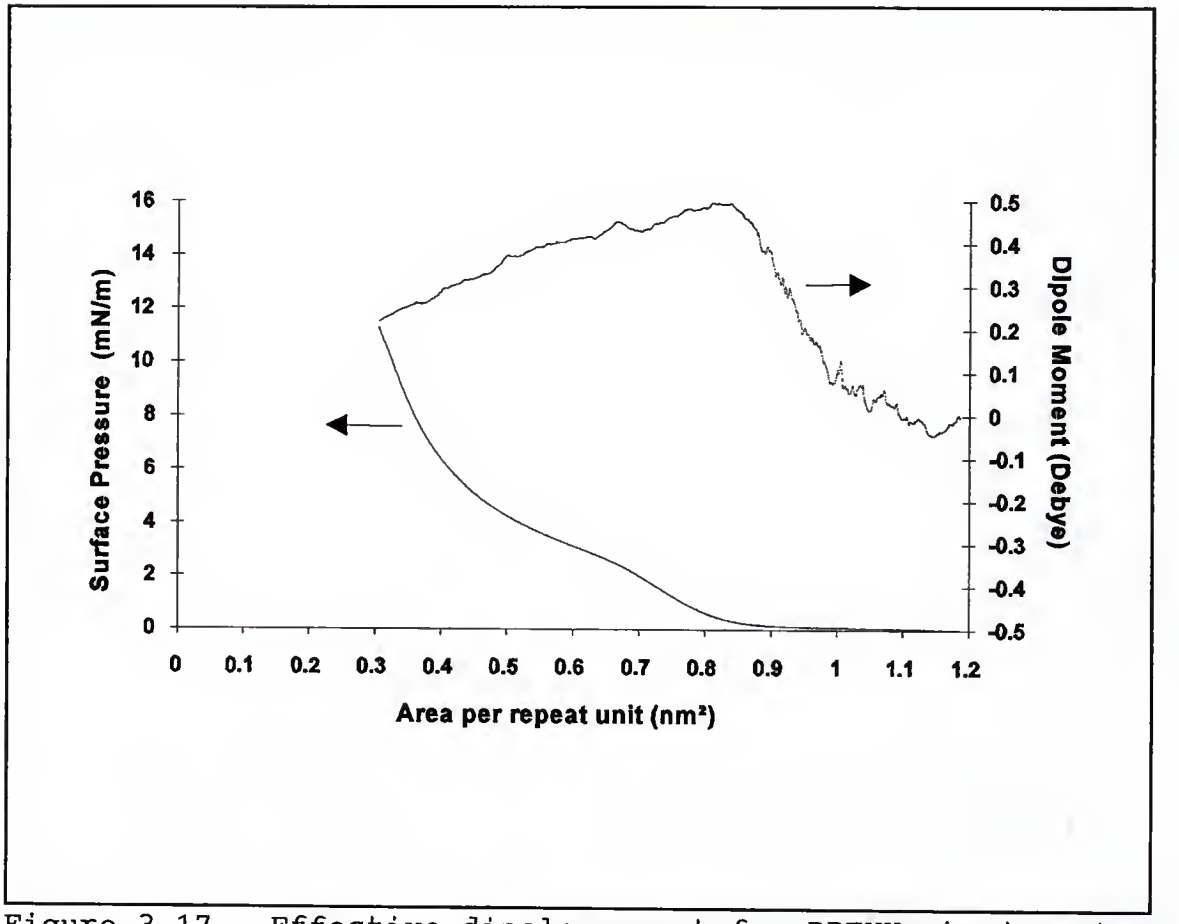

Figure 3-17. Effective dipole moment for PPEHU at air-water interface.

PPEHU, which may affect $\mu_\perp$. One functional group contributing to $\mu_\perp$ is the hydroxyl group at the end of the alkyl chain with a dipole moment of approximately[120] 1.7 Debye. The ether linkage dipoles are at opposite sides of the phenyl ring and thus cancel each other out. The last group that contributes significantly to $\mu_\perp$ is the pyridine ring. The dipole moment of an isolated pyridine ring is 2.3 Debye, but because the pyridine rings in the polymer, PPEHU,

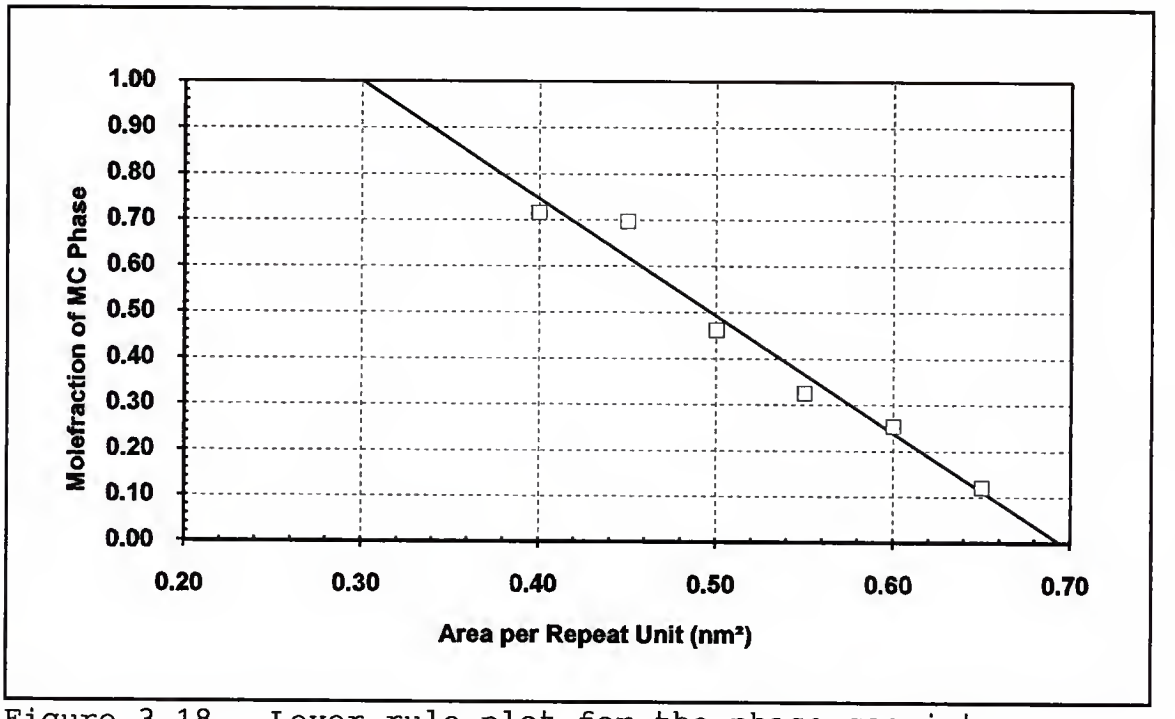

Figure 3-18. Lever rule plot for the phase coexistence region of PPEHU at 25°C.

experience some conjugation, the dipole of this group will be lower in magnitude. By comparing this result with the observed BAM images it was possible to assign the brightly fluorescing regions to the ME phase and the dark regions to the MC phase.

Lever Rule

In general, the densities of the two phases in low molecular weight amphiphiles is much greater than that observed with the PPEHU material. The lever rule was applied to compare the density of the two monolayer

phases.[121] The area fraction of the MC phase was calculated from BAM images at five points within the coexistence region of the isotherm. Assuming that the phase transition begins at an area density of 0.69 nm^2/repeat unit (based on observation under the BAM), the MC phase area density was found to be 0.30 nm^2/repeat unit (Figure 3-18). These densities are consistent with the densities of condensed phases rather than a vapor-like phase.

Now, a simplified model for the orientation of the functional groups of PPEHU may be described as follows (Figure 3-19). Initially, before the Langmuir film of PPEHU is compressed, the polymer chains are isolated from each other. Neighboring chains repel for steric reasons, and because both the polymer backbone and alkyl side chains are more attracted to the water molecules than to each other. Within each polymer main chain, the pyridine rings orient with the nitrogen towards the water surface. As the initially isolated polymer chains are pushed together, the alcohol side chains are forced into a hairpin conformation nearly perpendicular to the water surface. As compression continues the OH-terminated side chain are forced out of direct contact with the water subphase. Since $\mu_\perp$ falls linearly throughout the phase coexistence region, then the alcohol side chains pushed up away from the water surface must adopt a conformation such that the dipoles within this overlayer cancel each other out and thus the overlayer

contributes little to the overall $\mu_{\perp}$ through the film. As with any interpretation of surface potential results, it is important to point out the contribution of unknown magnitude to the surface potential caused by the reorientation of the subphase water molecules.

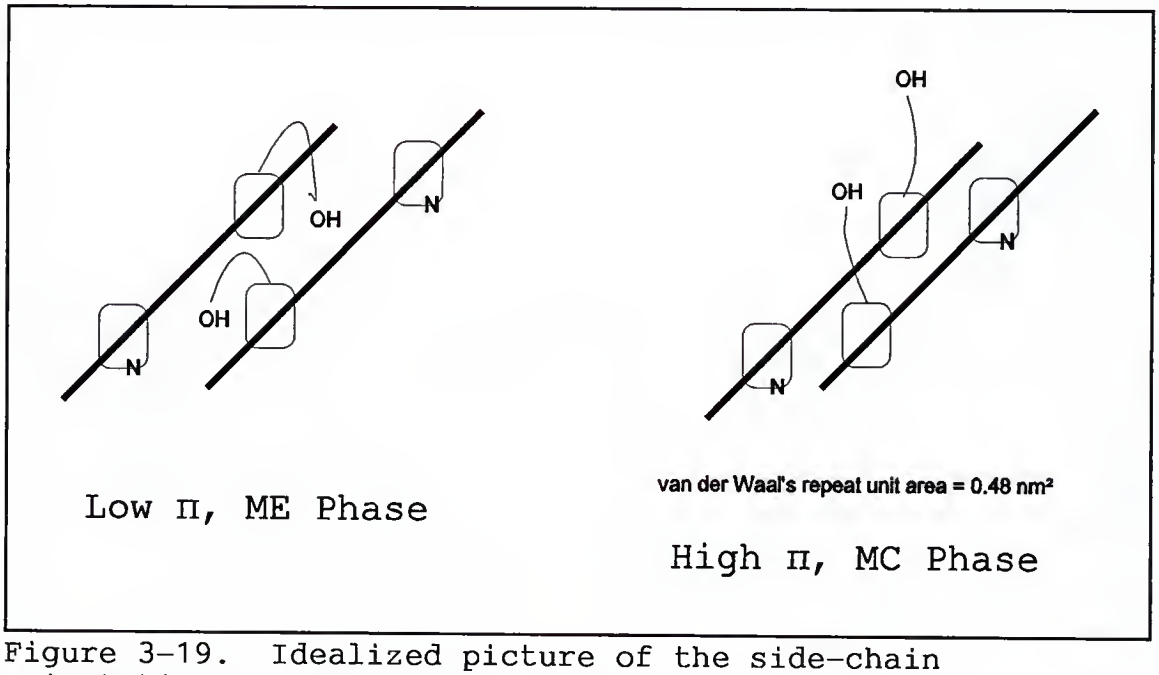

Figure 3-19. Idealized picture of the side-chain orientation of the PPEHU phases.

This emerging picture of the orientation of the polymer molecules within the two phases can also be used to help explain the atypical temperature dependence of PPEHU isotherms. There are two strong hydrophilic groups in each repeat unit of PPEHU, namely, the pyridine ring and the OH group at the end of the alkyl side chain. As the film is compressed, OH groups are removed from the water surface,

allowing the polymer main chains to interact. Since the main chains are rigid-rods, nearly all of the alkyl-OH groups must be pushed out of the way before any two main chains can interact closely. This can explain why the surface pressure increases through the biphasic region. The initial surface pressure onset moves to higher areas with increased temperature. Increasing temperature increases higher energy side chain motions thus expanding the monolayer area. In other words, from the point when the compression of PPEHU begins to a point just outside the low density boundary of the two-phase envelope, the PPEHU might be expected to behave like a 1:1 mixture of an alkyl-substituted poly(phenylene-acetylene-pyridine-acetylene) and a long chain alcohol. Thus the onset pressures move to lower densities as the temperature is increased. Thus, this analogy can explain why the low density side of the two-phase envelope shifts to higher areas. Once a point within the two-phase envelope has been reached, the continued compression is removing the long chain alcohol from the water surface and leaving the alkyl-substituted poly(phenylene-acetylene-pyridine-acetylene) at the surface, so the mixture ratio is continually changing toward increased concentration of the polymer.

Thus at the molecular level, the MC phase consists of OH-terminated alkyl chains as an amorphous or liquid-like overlayer covering the close packed polymer main chains.

The ME phase has the alkyl side chains in a hairpin-like conformation and the OH groups in contact with the water subphase between neighboring polymer main chains. Since the polymer molecules are constrained to the 2D interface, their interactions are 2D. For a polymer molecule of the MC phase, a ME phase molecule 'looks' like a different type of polymer. Thus, the Flory-Huggins rule for polymer blends may be invoked to explain the strong tendency toward demixing and separation of the MC and ME phases. This is an interesting ramification of the alkyl side chains acting as a "bound solvent" [122] in affecting the film-forming properties of these materials. As such, the thermodynamics of the transition may be more akin to a pressure induced phase separation, analogous to temperature dependent ones seen in block copolymers, than a typical isotropic to liquid condensed phase transition.

Based on the observed isotherm results, the nature of the two phases can be deduced, as well. Extrapolation of the isotherm to zero pressure gives an area per repeat unit of 0.49 nm^2/repeat. Using the van der Waals packing radius,[123] gives a calculated area of 0.48 nm^2/repeat for the main chain exclusive of the side chains. This supports a model for the phase transition in which the alkoxy side chains are squeezed out to form an amorphous overlayer during the compression of the film.

Further evidence is provided by close inspection of

the hysteresis of the isotherm during slow compression and decompression. The hysteresis is unusual in that the surface pressure on decompression is slightly higher than the surface pressure on compression (Figure 3-20). This behavior can be explained in light of the present model. When the film is compressed completely into the MC phase, most of the alkyl chains are interacting within the liquid-like overlayer described previously. As the film is decompressed to a point just inside the high density boundary of the two-phase envelope, gaps open up between the rigid-rod main chains. The OH terminated alkyl chains must then make a transition from a cone of probable conformations to a more constrained range of conformations, bound by the quasi-1D narrow (but widening) gap between the main chains as the OH group adsorbs to the water surface. This represents a considerable loss of degrees of freedom for the alkyl side chain, a minimal gain in degrees of freedom for the backbone, the entire process being driven by the favorable energy of adsorption. This explains why the surface pressure is slightly higher during decompression through the two-phase envelope than it was during the previous compression step. These gaps between the main chains are nucleation points for the ME phase because a main chain at a phase domain boundary will be more free to move away from its MC phase neighbors than a main chain surrounded by MC phase. If the number of nucleation points

could be plotted as a function of the rate of decompression, more could be said about whether it is more energetically favorable for the monolayer as a whole to either create more nucleation sites or allow the existing domains to grow. It is clear the reverse process has many nucleation points because of the observation of such during the recompression of the monolayer. This indicates that at least for compression the creation of new domains is not much less favorable than growth of existing boudaries.

The line energy between the phases might be defined as the difference in energy between the molecule uniformly surrounded by one phase, say the MC phase, its energy while within the boundary between the phases. So for the present model, then this energy difference is energy required to desorb the alcohol terminated side chain.

The total energy required to put the monolayer into the MC phase may be calculated by taking the difference between the area under the isotherm on compression and decompression. According to the hysteresis curve obtained, it takes more energy to take the monolayer from the uniform MC to the uniform ME phase than the reverse process. Because the work required is greater on expansion is due the deaggregation of the main chains and the change in conformation of the alcohol side groups in order to readsorb to the water surface. In short, on compression the monolayer experiences a favorable change in entropy due the

desorption of the alcohol side group which gains degrees of freedom, while on decompression, the entropy change is unfavorable because of loss of degrees of freedom but the adsorption energy overrides the negative entropy change.

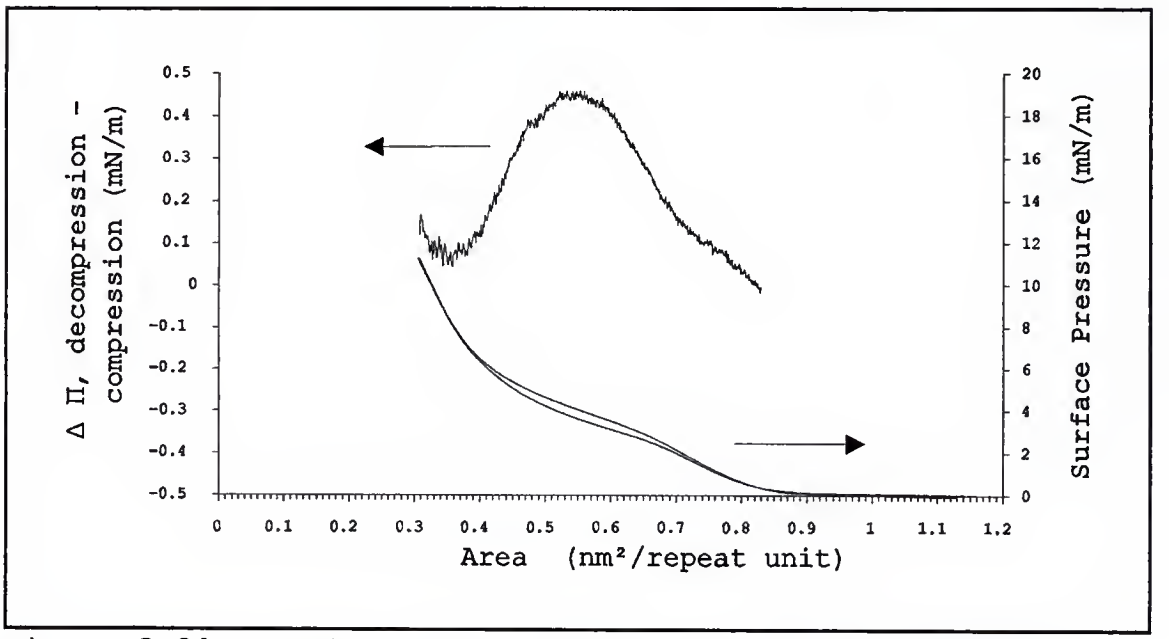

Figure 3-20. Hysteresis of PPEHU at 25°C and a barrier speed of 2 mm/min (0.0084 nm^2/repeat unit/min). The plot shows the difference in surface pressure between the compression and decompression sweeps within the biphasic region.

Film Stability

The film stability of PPEHU was quantified by recording the surface pressure change with time at constant area after rapid decompression from 0.25 nm^2/repeat unit. The change in surface pressure with time was found to be less than -0.2 mN/m over 30 minutes in the range of 0.50 to

0.75 nm^2/repeat unit. The magnitude of the film stability data is roughly 1/2 of the hysteresis discussed in the previous section. The small discrepancy is probably due to the difference in the barrier speeds used in the two different experiments. This data indicates that throughout the phase coexistence region, the relaxation processes occuring within the film are more rapid than the rate of stress induced by the decompression of the film. This is expected for such a rigid rod polymer as the main polymer chain does not have any conformational degrees of freedom which would lead to entanglements. Entanglements occurring within the side chains are quickly undone due to their relatively short length and high degree of flexibility. This implies that the measured surface pressure is a thermodynamic quantity with a minimal but definite kinetic component, especially on expansion. Furthermore, the measured surface pressure is not strongly influenced by the cellular network which is continually coarsening during these stability measurements.

Brewster Angle Microscope Images

Within the phase co-existence region, light and dark domains corresponding respectively to MC phase and the ME phase were observed in the BAM images.

The total relative reflectivity of the film was plotted versus area in Figure 3-21. This shows that the

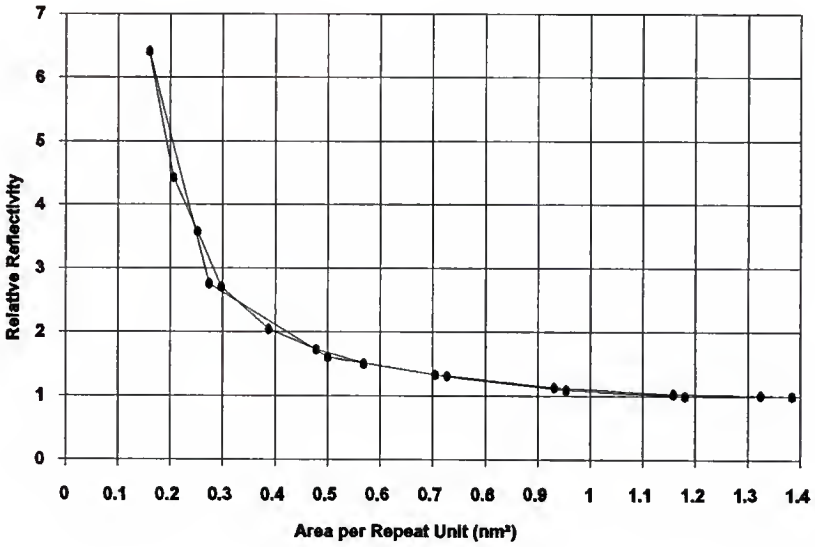

Figure 3-21. Relative total reflectivity calculated from BAM images of PPEHU during one compression/decompression cycle.

reflectivity is a continuous function of the polymer concentration at the interface. The reflectivity of the cell walls was found to be on average, 1.8 times the reflectivity of the cell centers. However, both the cell walls and the cell centers become darker as the entire film is decompressed. The vertices remain bright relative to the rest of the cell walls.

The reflectivity of a real interface at the Brewster

angle for p-polarization depends on three factors; the thickness of the interface, the roughness of real interfaces, and the anisotropy of the monolayer. To find how the reflectivity varies with film thickness begin by noting the two components of the incident electric field from the laser are

$$E_p^i = E_o \cos\phi \cos(\omega t)$$

and

$$E_s^i = E_o \sin\phi \sin(\omega t)$$

where ϕ is the angle between the polarization of the light and the plane of incidence (usually set close to 0°). The reflected field for optically isotropic domains is

$$E_p^r = E_o \, r_s(\theta_B) \cos\phi \, \overline{\rho}_B \sin(\omega t)$$

and

$$E_s^r = E_o \, r_s(\theta_B) \sin\phi \sin(\omega t)$$

where $\overline{\rho}_B$ is the ellipticity given by

$$\overline{\rho}_B = \frac{\pi}{\lambda} \frac{\sqrt{n_1^2 + n_2^2}}{n_1^2 - n_2^2} \int_{-\infty}^{+\infty} \frac{[n(z)^2 - n_1^2]\,[n(z)^2 - n_2^2]}{n(z)^2} \, dz$$

The thickness of the interface is z, and the refractive indices of both media and the interface are represented by n. Since the intensity, $I = E^2$, then

$$I_r = (E_p^r + E_s^r)^2 = I_o \, |r_s(\theta_B)|^2 \, [\cos\phi \, \bar{\rho}_B + \sin\phi]^2$$

With p-polarized light incident, $\phi = 0°$, so

$$I_r = I_o \, |r_s(\theta_B)|^2 \, \bar{\rho}_B^2$$

Assuming the refractive index of the interface is constant over its thickness allows the integration of the ellipticity to give

$$\bar{\rho}_B = \frac{\pi}{\lambda} \frac{\sqrt{n_1^2 + n_2^2}}{n_1^2 - n_2^2} \frac{[n^2 - n_1^2] \, [n^2 - n_2^2]}{n^2} \, Z$$

Grouping all the constants in one defined constant, K, allows the intensity of the reflected beam to be written as

$$I_r = I_o \, K \, Z^2$$

Imagine two sections A and B of a film made up of the same material with different thicknesses and their consequent reflected intensities then the ratio of the reflected intensities is given by

$$\frac{I_r^A}{I_r^B} = \frac{Z_A^2}{Z_B^2}$$

From this relation, it is easily seen that a doubling of the thickness of the idealized film will cause the intensity of the reflected beam to increase fourfold. In terms of this model then, the cell walls would be, on average, 1.3 times

thicker than the cell centers. This evidence helps to dismiss an alternative model for the nature of the two phases in the Langmuir films of PPEHU, which would have the MC phase as a bilayer and the ME phase as monolayer. Again, it is important to emphasize the assumptions which were made to arrive at the quadratic dependence of the reflected intensity on the film thickness; optical homogeneity across the breadth and through the thickness of each phase, and uniform roughness in both phases.

When the film is compressed to 0.45 nm^2 and maintained at that area, domains of the MC phase dispersed in the ME phase are seen to form, Figure 3-22. Over time, the circular MC phase domains coalesce and thus increase in average diameter (Figure 3-23).

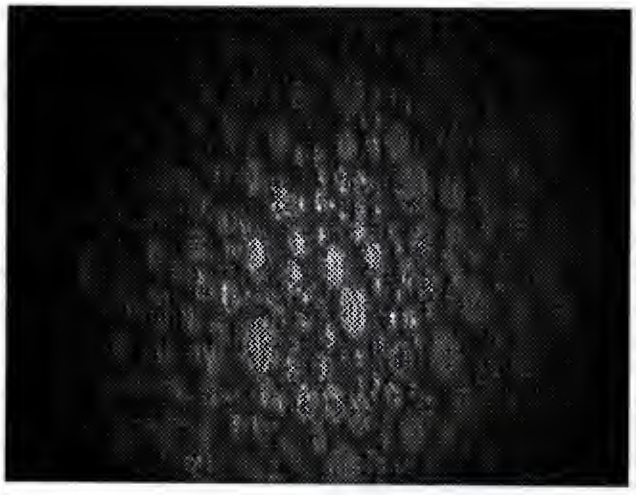

Figure 3-22. Domains of MC phase dispersed in the ME phase at 0.45 nm^2 and 25 °C.

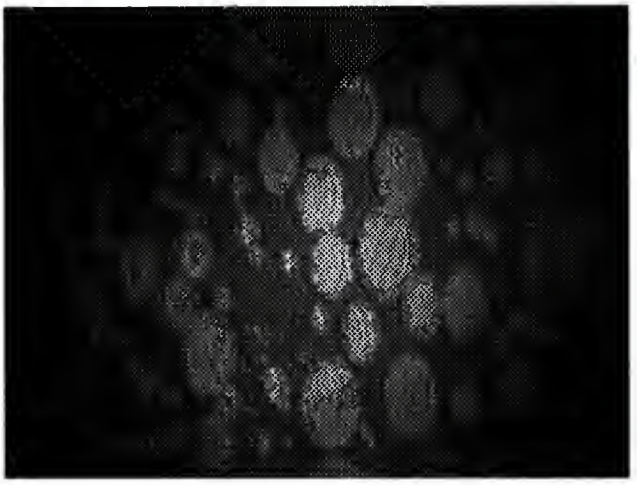

Figure 3-23. Domains of the MC phase dispersed in the LC phase 30 minutes compressing and holding at 0.45 nm^2 and 25 °C.

Compression of the PPEHU film to 0.25 nm^2/repeat followed by rapid decompression to mean repeat unit areas between 0.35 and 0.65 nm^2/repeat causes the formation of cellular networks. Cellular networks formed at repeat unit areas less than 0.60 nm^2/repeat have circular or elliptical cells of the ME phase (Figures 3-24 to 3-26). Networks formed in the range of 0.60 to 0.65 nm^2/repeat have polygonal cells of the ME phase (Figure 3-28).

One interesting effect, difficult but possible to reproduce, is the creation of metastable free-floating hollow rings of the MC phase material (Figure 3-29). The formation of these hollow rings is achieved through rapid expansion of the film to mean repeat unit areas greater than

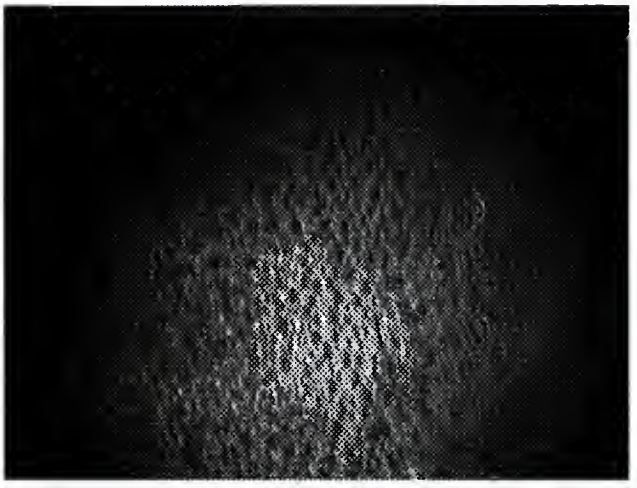

Figure 3-24. Cellular network aged at 0.35 nm^2/repeat and 25°C.

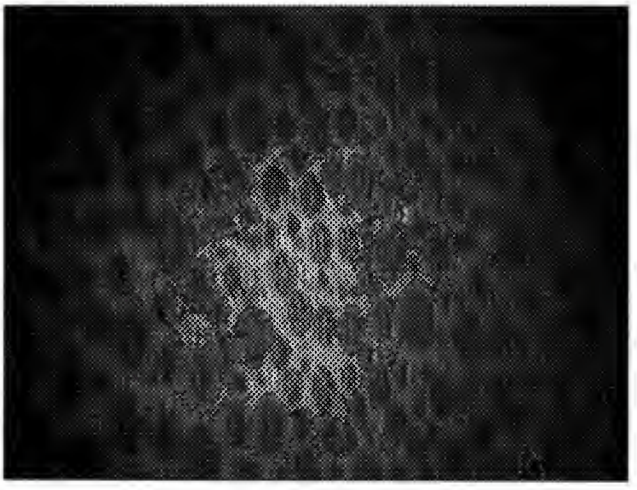

Figure 3-25. Cellular network of PPEHU aged at 0.45 nm^2/repeat and 25°C.

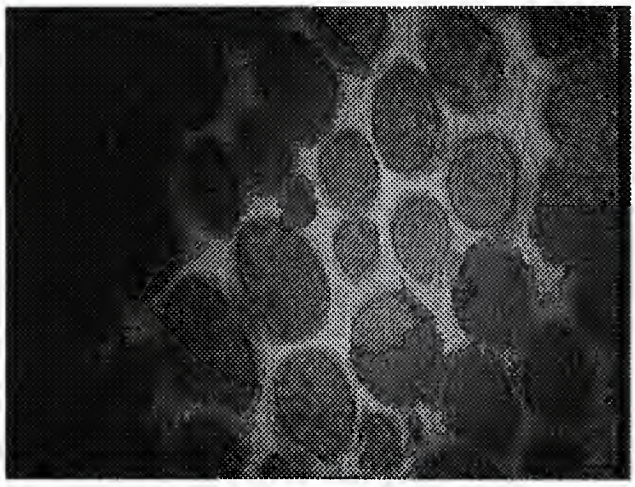

Figure 3–26. Cellular network of PPEHU aged at 0.55 nm^2/repeat and 25°C.

the phase coexistence region. Usually, this results in a disrupted cellular network consisting of short sections of broken cell walls (which quickly become filled circular domains) but if the trough is slightly overfilled with water to the correct level, then hollow rings are formed.

Birefringence was not observed during room temperature hysteresis experiments in which the barriers are always moving. However, when a cellular network of PPEHU is allowed to 'anneal', over an hour, a weak birefringence is seen within the cell walls. Since the resolution of the BAM is only 4 μm^2, the observed birefringence is an indication of long range ordering of the polymer main chains over time. These results are consistent with the Monte Carlo simulations of 2D hard needles described previously. The ME

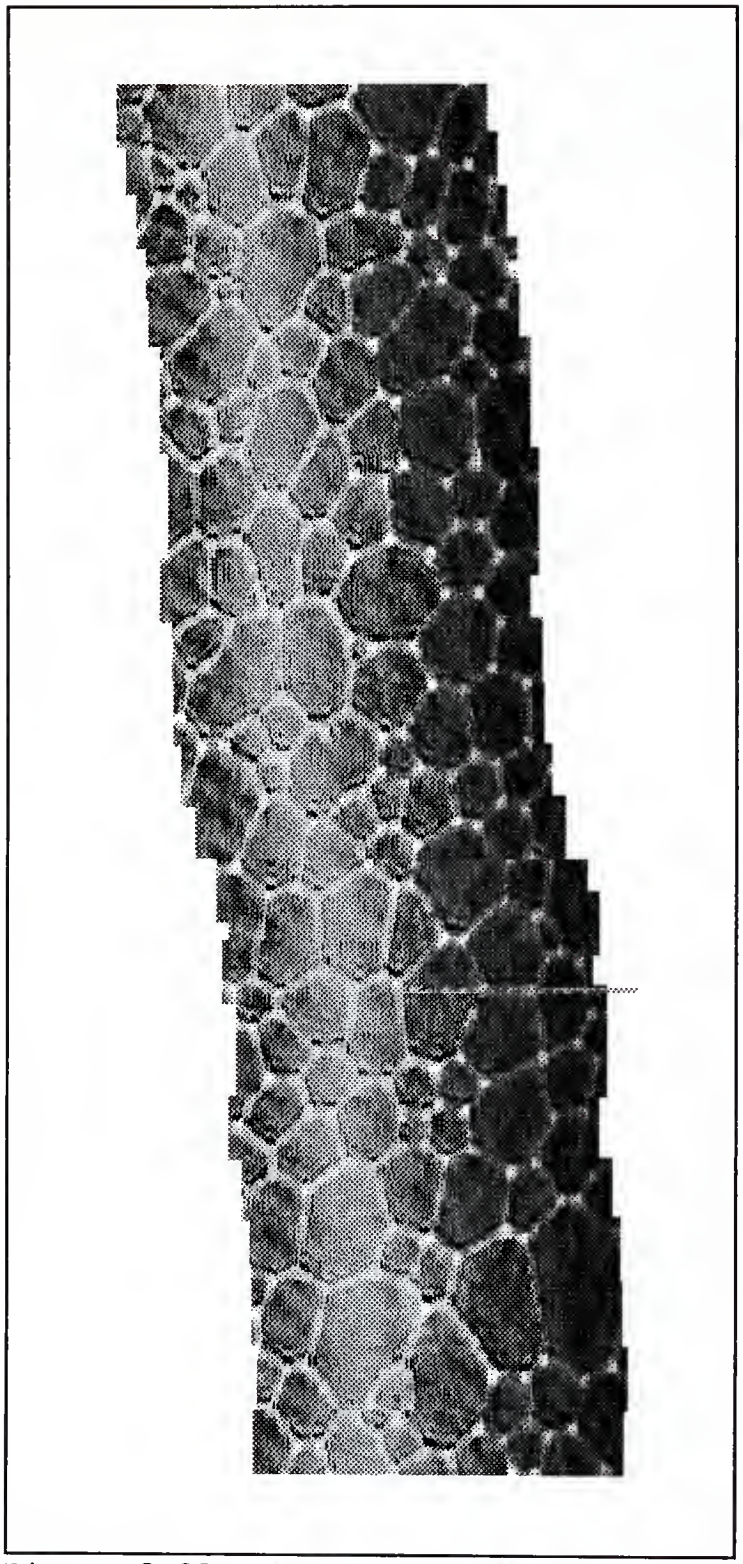

Figure 3-28. Mosaic of BAM images of PPEHU after decompression to 0.62 nm^2 at 25°C. Each strip is 50 µm x 400 µm.

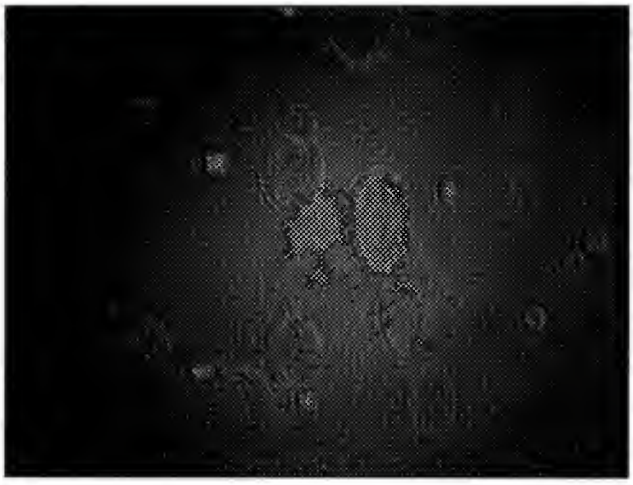

Figure 3-29. Metastable free-floating rings of PPEHU MC phase at 0.75 nm^2/repeat and 25°C. Image size is 1200 μm x 800 μm.

phase does not develop long range order (LRO) because the hydroxy-terminated alkyl side groups are adsorbed to the water surface. Their presence tends to break up LRO. On the other hand, the MC phase does develop LRO. However, the MC phase remains fluid because the solvating effect of the pyridine rings in the main chain coupled to the water subphase is stronger than the interchain attraction.

Observation of the PPEHU Langmuir film with the BAM during compression at temperatures below 15°C reveal the formation of dendrites at mean repeat unit areas below 0.60 nm^2 (Figure 3-30). Large relatively strong birefringent regions are also seen at these low temperatures (Figure 3-31). The director of the dendrites (with the analyzer out) is at a different angle than the director of the

Figure 3-30. Dendrites formed during compression of PPEHU below 0.60 nm^2/repeat and 15°C (no analyzer in plane). Image size is 1200 μm x 800 μm.

birefringent stripes (with the analyzer in, at 90° to the usual plane of polarization of reflected light). The formation of the dendrites is probably due to recrystallization of the side chains as they are squeezed out from between the main chains. It is not clear whether or not the birefringent stripes are due to the crystallized side chains or to long range order induced in the backbones as a consequence of the side chain crystallization. Further

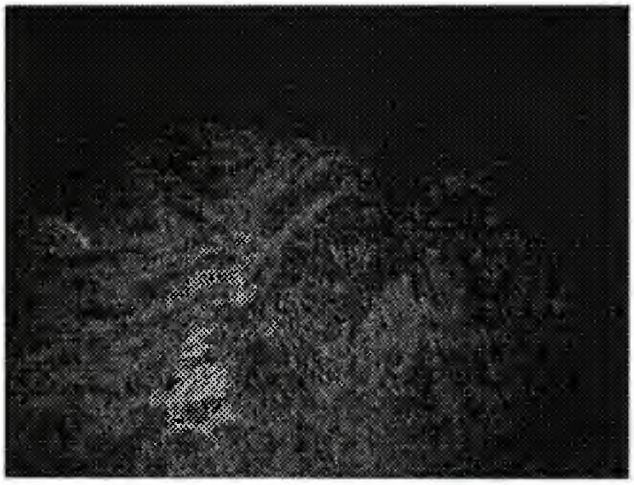

Figure 3-31. Birefringent regions in PPEHU Langmuir film below 0.60 nm^2/repeat and 15°C (analyzer at 90° to usual polarization of the reflected beam). Image size is 1200 μm x 800 μm.

evidence for this side chain crystallization is the observation that a cellular network is not formed on decompression at this low temperature. The side chain crystallization rigidifies the film and inhibits the flow necessary for phase separation. Side chain crystallization has been observed in rigid-rod polymers[124,125,126]. This may be an interesting example of side chain ordering forming a "template" which establishes true 2D LRO of the polymer backbones.

Epifluorescence Microcope Images

The inherent visible wavelength fluorescence of the

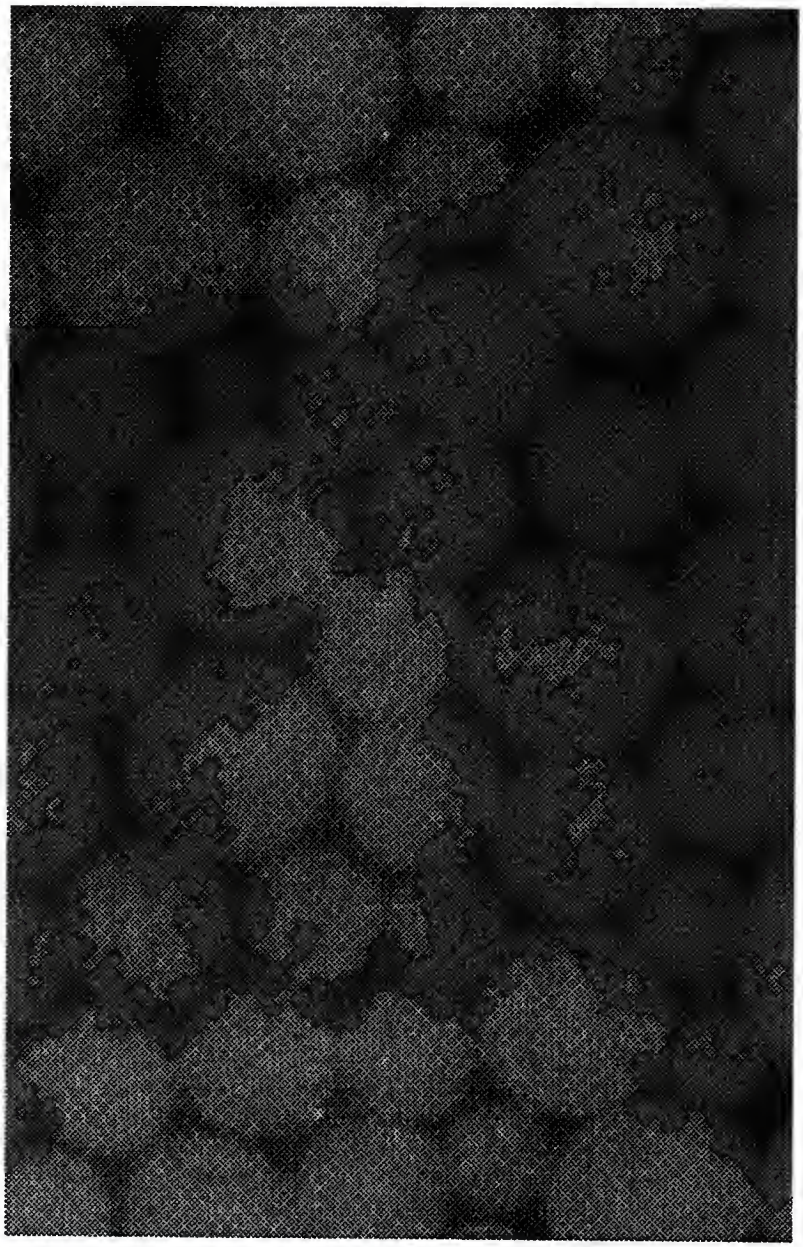

Figure 3-32. Epifluorescence microscope image of PPEHU at 0.60 nm^2/repeat and 25°C.

polymer, PPEHU, allows for imaging with an epifluorescence microscope without the need for a probe molecule. Photographs of the cellular network show that the fluorescence emission from the MC phase walls is much less than the emission from the ME phase cells when the excitation wavelengths are in the range of 450-490 nm (Figure 3-32). Remember this is opposite to that seen with the BAM, where the cells appear dark relative to the walls. This observation is counterintuitive if looked at merely in terms of the fluorophore concentration, but the phenomena may be explained in terms of a fluorescence quenching process.

There are at least two types of possible intermolecular quenching, namely, dynamic and static, or a combination of the two. Dynamic quenching involves interaction between the fluorophore and the quencher through diffusion. Static quenching requires formation of a complex between the fluorophore and quencher. One method to differentiate between these types of quenching is by varying the temperature. Since higher temperatures result in higher diffusion coefficients, the dynamic bimolecular quenching constants are expected to increase with increasing temperature. In contrast, increased temperature is likely to result in decreased stability of complexes and thus lower values of the static quenching constants. One additional method to distinguish static and dynamic quenching is by

careful examination of the absorption spectra of the fluorophore. Collisional quenching only affects the excited states of the fluorophore and thus no changes in the absorption spectra are predicted. In contrast, ground state complex formation will frequently result in perturbation of the absorption spectra of the fluorophore[127]. Remember that the peak excitation wavelength of PPEHU shifts from 436 to 385 nm between the chloroform solution and the solid thin films. Therefore, the conclusion may be drawn that the MC phase consists of aggregated main chains which results in quenched fluorescence in the cell walls. Whereas, within the ME phase the main chains are separated by the hydroxy-terminated alkyl chains and so the cells fluoresce.

Utilizing the CCD camera with the epifluorescence microscope allowed the cellular network to be imaged over time. If the lens was allowed to remain focussed on the same region of the monolayer, there was a marked decrease in the fluorescence intensity in the cells within 40 seconds. Eventually, the fluorescent intensity from the cells became less than that observed from the cell walls (which remained relatively constant). When the microscope remains focussed on the same region this leads to localized heating of the monolayer. The fluorophore consists of conjugated sections of the main chain of the polymer, PPEHU. This leads to the speculation that the heating disrupts the conjugated sections by driving higher amplitude bond rotation about the

main chain axis and thus the fluorophore is lost. As the localized heating is allowed to continue, the material in the cell walls undergoes the phase transition to the ME phase. Thus new cells are observed forming at vertices and within the walls.

Langmuir Film Behavior of Mixtures of Poly(2-(11-hydroxyundecanoxy)-5-methoxyphenylene-ethynylene) and Poly(2-(11-hydroxyundecanoxy)-5-methoxyphenylene-ethynylene-pyridine-ethynylene)

PEHU was found to have higher film stability than PPEHU at surface pressures typically used for deposition of LBK films. Thus mixtures of these two materials were made to determine if the transfer of PPEHU to LBK films could be improved.

The spreading solutions for the series of mixtures used for these experiments were made by taking suitable quantities from solutions of the pure components. For example, to make a molar mixture of PEHU and PPEHU from the 0.492 mg/ml PEHU solution and the 0.226 mg/ml PPEHU solution, the following formula was used to calculate the volume ratio.

$$\frac{V_{PEHU}}{V_{PPEHU}} = \frac{MW_{PEHU}}{MW_{PPEHU}} \frac{C_{PPEHU}}{C_{PEHU}} \frac{X_{PEHU}}{X_{PPEHU}}$$

In this equation, V is volume of pure component solution, C is the concentration of the pure component in its respective

pure component solution, and X is the desired final mole ratio of each component. For the 1:2 PEHU:PPEHU molar mixture, this gives V_{PEHU}/V_{PPEHU} of 0.174. The mixture was made by transferring 100 µl of PPEHU solution and 17.4 µl of PEHU solution to a clean 1/2 dram vial. The top of the vial was sealed with teflon tape to minimize evaporation. In order for the film balance computer software to calculate the mean repeat unit area, the mixture concentration was calculated using the equation,

$$C_{mixture} = \frac{V_{PEHU}C_{PEHU} + V_{PPEHU}C_{PPEHU}}{V_{PEHU} + V_{PPEHU}} .$$

The mixture repeat unit molecular weight was calculated using the equation,

$$MW_{mixture} = X_{PEHU}MW_{PEHU} + X_{PPEHU}MW_{PPEHU} .$$

The isotherm for the 1:1 mixture of PEHU and PPEHU is shown in Figure 3-33. The position and shape of the 1:1 mixture isotherm indicates a complex mixing behavior which depends strongly on the surface pressure. This complexity is due to the presence of at least two phases contributed by the PPEHU fraction each interacting with at least one phase of the PEHU fraction. From the isotherms, it appears that the biphasic region of PPEHU is suppressed by the presence of the PEHU. Furthermore, at pressures below the coexistence region, the mixtures were densified compared

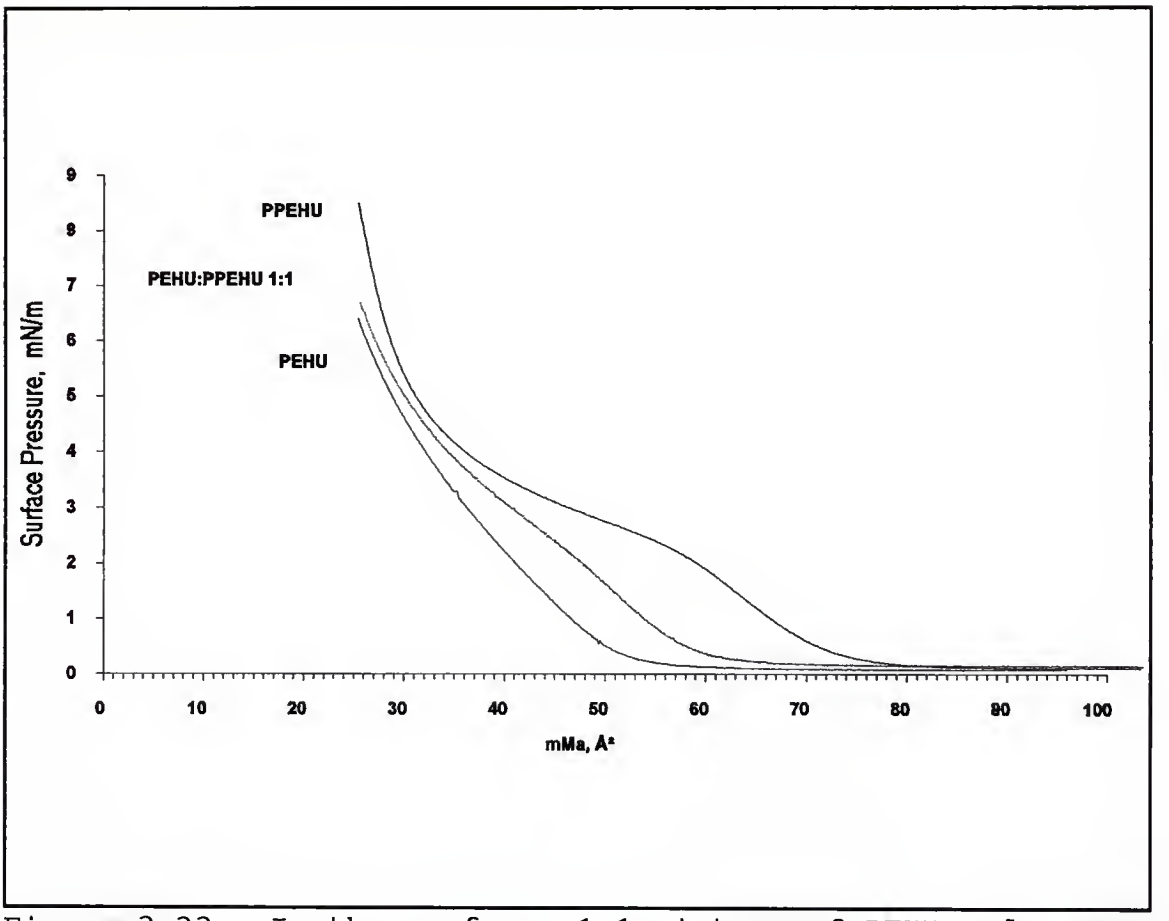

Figure 3-33. Isotherms for a 1:1 mixture of PEHU and PPEHU compared to the isotherm of each pure component at 23°C.

with what would be seen based on an ideal law of mixtures. This is evidence for favorable interaction between the two polymers.

Demixing of the components was indicated by the textured appearance of the film as seen with the Brewster angle microscope (Figure 3-34) at a surface pressure of 5 mN/m. Decompression of the film to 1 mN/m results in more

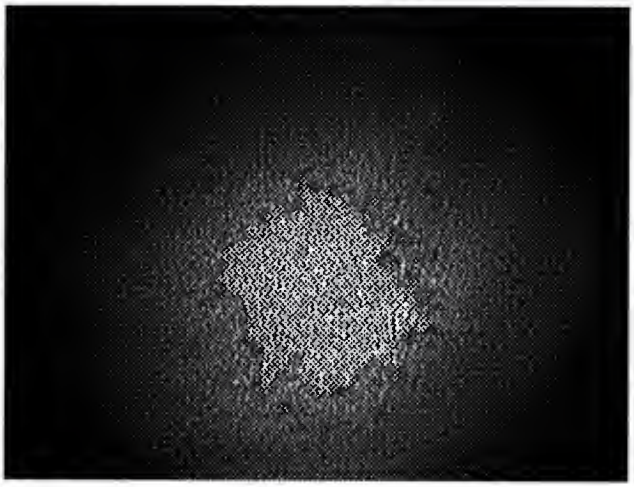

Figure 3-34. BAM image of a 1:1 molar mixture of PEHU and PPEHU at 5 mN/m and 23°C. Image size is 1200 μm x 800 μm.

Figure 3-35. BAM image of a 1:1 mixture of PEHU and PPEHU at 1 mN/m and 23 °C. Image size is 1200 μm x 800 μm.

obvious separation (Figure 3-35). Although demixing is evident, it is interesting to note that cellular networks were not obtained when these mixtures were decompressed.

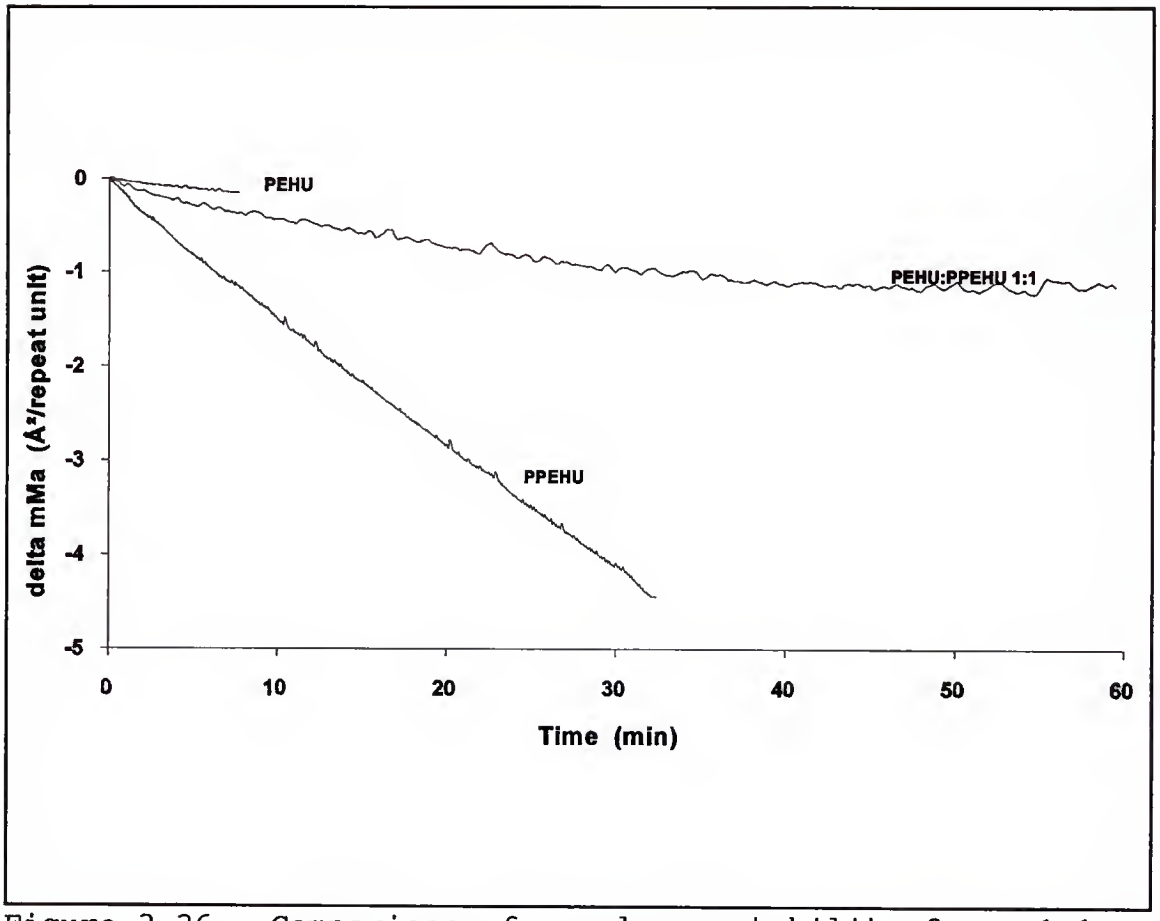

Figure 3-36. Comparison of monolayer stability for a 1:1 mixture of PEHU and PPEHU, and each of the pure components 10 mN/m and 25 °C.

The film stability of the 1:1 PEHU:PPEHU mixture as determined by maintaining a constant surface pressure of 10 mN/m and following the change in area was significantly better than the pure PPEHU (Figure 3-36). This indicates some interaction between the two components which stabilizes the film. PEHU has twice the density of side chains along the main backbone as PPEHU because each arylene ring is substituted.

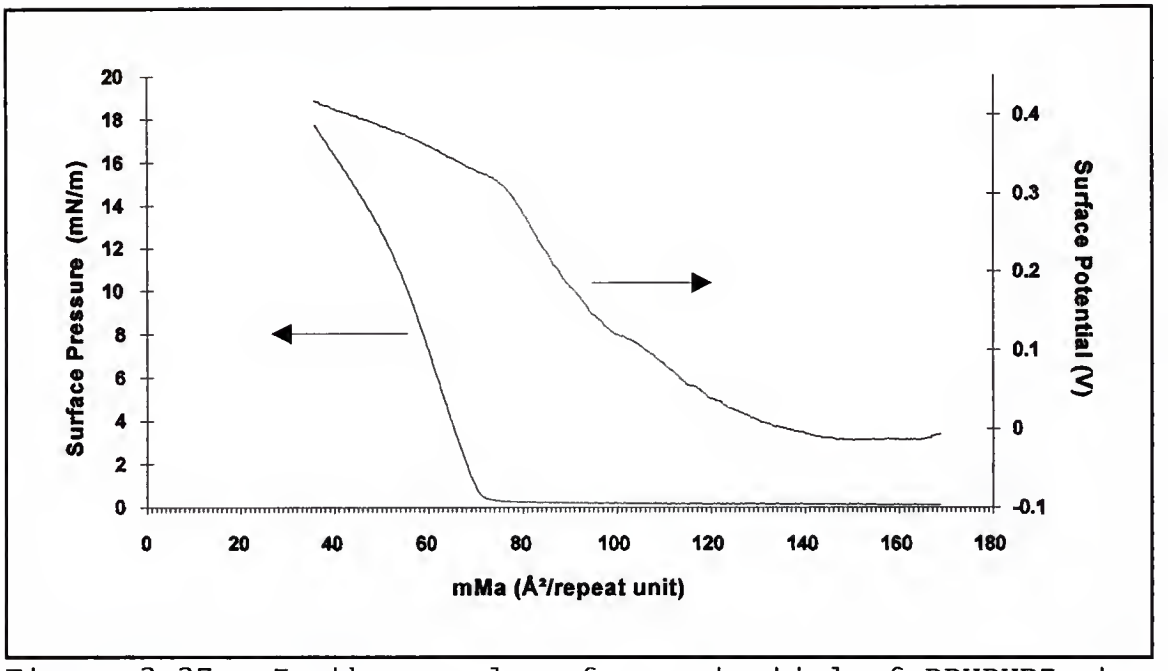

Figure 3-37. Isotherm and surface potential of PPYPYRI at 25°C.

Mixtures of PEHU and PPEHU were also made in the ratio of 1:2 and 2:1. Observation under the BAM during decompression revealed no formation of a cellular network but only demixing of the components. Thus, the interaction between PEHU and PPEHU inhibits the cellular network formation.

Langmuir Film Properties of Poly(2,5-di(11-hydroxyundecanoxy)phenylene-ethynylene-pyridinium bromide-ethynylene)

Poly(2-(11-hydroxyundecanoxy)-5-methoxyphenylene-ethynylene-pyridinium bromide-ethynylene), PPYPYRI, as shown

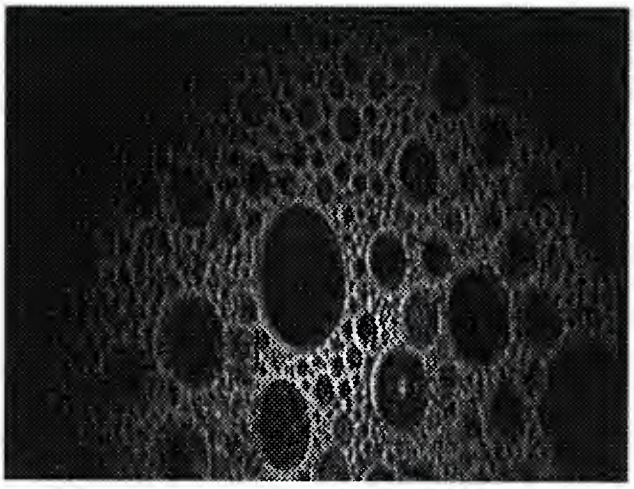

Figure 3-38. BAM image of PPYPYRI as first spread at the air/water interface. Image size is 1200 μm x 800 μm.

in Figure 3-1, dissolves slowly in chloroform. The dissolution rate was increased by adding a few drops of trifluoroacetic acid to give a 0.21 mg/ml spreading solution. The isotherm for PPYPYRI is shown in Figure 3-37. The shape of the isotherm suggests a compressible film with a collapse surface pressure over 10 mN/m. The surface potential curve exhibits a distinct change in slope at the point where the surface pressure begins to increase.

Observation of the film with the Brewster angle microscope reveals the film, as spread at 2.0 nm^2, is fluid with fluid 'rafts' of polymer in a condensed phase interspersed with circular domains of a vapor-like phase (Figure 3-38). As the film is compressed (0.130 nm^2/repeat/min), the vapor-like phase material condenses

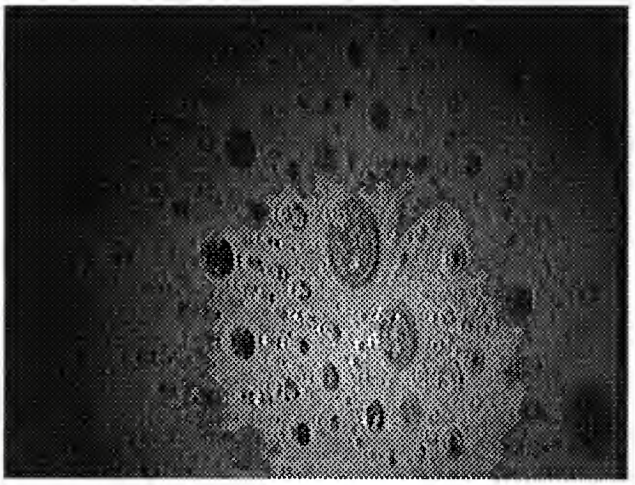

Figure 3-39. BAM image of PPYPYRI during compression at 0.75 nm^2 and 25°C. Image size is 1200 µm x 800 µm.

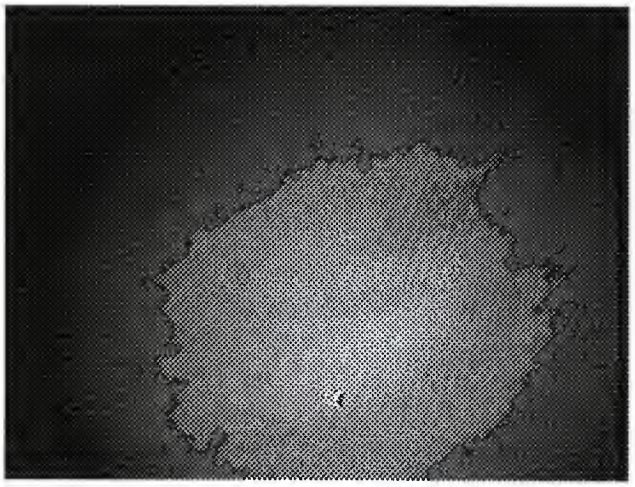

Figure 3-40. BAM image of PPYPYRI under compression at 0.40 nm^2 and 25°C. Image size is 1200 µm x 800 µm.

within the circular domains (Figure 3-39). The appearance is reminescent of spinodal decomposition. Even at the slowest barrier speeds material is seen to condense within the circular vapor-like phase domains. This indicates that

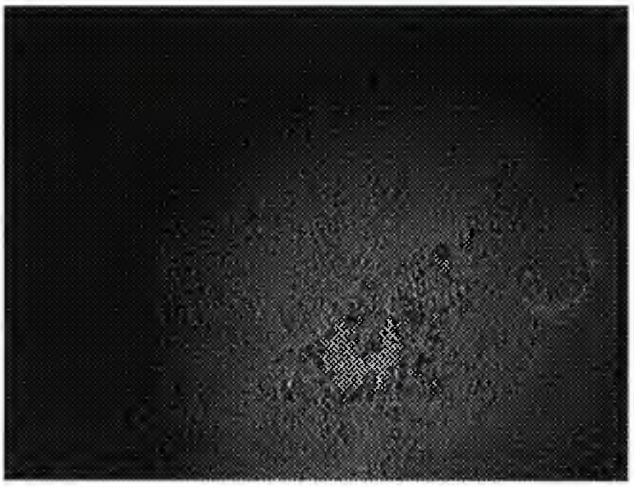

Figure 3-41. BAM image of PYPYRI during decompression at 0.8 nm^2 and 25 °C. Image size is 1200 μm x 800 μm.

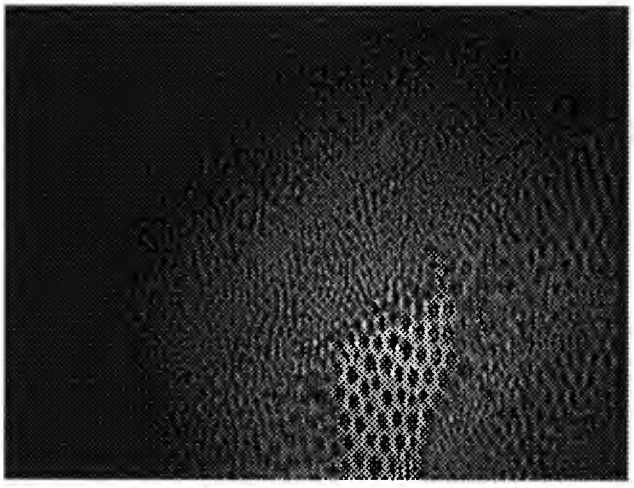

Figure 3-42. BAM image of PPYPYRI during decompression at 1.0 nm^2 and 25 °C. Image size is 1200 μm x 800 μm.

the walls of the domains are not preferential nucleation sites for this process. Similar behavior was observed with PPEHU.

The film appears homogeneous and fluid at repeat unit

Figure 3-43. BAM image of PPYPYRI during decompression at 1.7 nm^2 and 25 °C. Image size is 1200 µm x 800 µm.

areas in the range between 0.40 and 0.70 nm^2 (Figure 3-40). Re-expansion of the film causes the formation of a cellular network morphology above 0.70 nm^2 (Figure 3-41). The cellular network persists with further decompression to 1.0 nm^2 (Figure 3-42) and 2.0 nm^2 (Figure 3-43).

Though not quantified, this cellular network obtained on expansion appears to be less random after aging and more stable than that observed with the PPEHU material discussed below. Coulombic effects cause the ME phase of PPYPYRI to exist at higher areas and also the phase is more gas-like. Like PEHU, PPYPYRI has twice the density of side chains along the main backbone as PPEHU, yet PPYPYRI forms cellular networks while PEHU does not. Again, this shows the effect of the ionic charge. It is important to emphasize that the

types of 2D phases which make the PPYPYRI cellular network are a vapor-like phase and a liquid expanded phase, whereas, the PPEHU cellular network consists of two liquid-like phases.

The stability of the film, determined by maintaining a constant surface pressure of 10 mN/m and following the change in area, was less than 0.02 nm^2 during 30 minutes. During Langmuir-Blodgett-Kuhn processing, the transfer to hydrophobic quartz plates was 1.1 for the first downstroke and near zero on the upstroke, but transfer steadily degraded to near zero on the downstroke as well with continued processing. Allowing layers to dry for up to 30 minutes, did not improve the transfer. The best dipping speed was found to be 2 mm/min.

The PPYPYRI polymer has three strong hydrophilic groups per repeat unit. These are the hydroxyl groups at the ends of the two alkyl side groups and the pyridinium ion in the main polymer backbone. The two alcohol side groups are on opposite sides of the main chain. Thus during compression the side chains balance each other and tend to keep the benzene ring to which they are attached flat on the water surface. This explains the higher onset surface pressure. If the benzene ring were turned on edge during compression, the onset area would be more near to that for PPEHU. The BAM images indicate that the polymer was initially spread at concentrations within a phase

coexistence region. These phases consist of a gas-like phase and a liquid condensed phase. Even when the polymer was spread at mean molecular areas as high as 5 nm^2/repeat unit, the surface pressure rose to 0.2 mN/m, indicating that this was still within the phase coexistence region. In this transition from gas-like to liquid condensed phases, the alcohol side groups are pushed up into a hairpin conformation as the distance between the main chains is decreased. At the point where close packing concentration is reached, the surface pressure rises steeply. The main polymer backbone carries an ionic charge in every repeat unit, so coulombic charge repulsion is a factor in the observed phase behavior. The number of alkyl side groups per arylene ring is the same in PPYPYRI as that of PEHU, yet the presence of the charged main chain of PPYPYRI leads to different phase behavior.

The cellular networks of the PPYPYRI and PPEHU are interesting from the following standpoint. One of the initial motivating factors behind the detailed study of these networks is the possibility of transferring the network intact to a solid substrate. The idea here is that polymer is then pre-arranged into a circuit-like pattern without the need for the usual patterning techniques to create a working device. Several attempts were made to transfer the cellular network of PPEHU to hydrophilic and hydrophobic substrates without apparent success. This lack

of success with PPEHU may be due to its generally poor transfer properties. However, the PPYPYRI material might be processed in this way, though it has not been tried. Another possible use of the cellular networks from a materials science standpoint, would be to mix microfibers into monolayer and then generate the cellular network. The microfibers would orient within the network. This seems plausible due to the observation that dust particles invariably stayed in the MC phase cell walls of the PPEHU material. Some way would have to be found to overcome the natural tendency of the microfibers to form agglomerates, perhaps through surface pretreatment of the microfibers.

Topology of the PPEHU Cellular Network

Two-dimensional cellular networks have been studied in detail in other systems such as magnetic domains or fatty acids and lipids in Langmuir films. Thus it was interesting to see how the PPEHU cellular networks compared to those studied previously. The PPEHU material was chosen first for study (rather than PPYPYRI) because the contrast between the phases in PPEHU was more distinct in the BAM images over the full range of the phase coexistence region. Whereas, the PPYPYRI material becomes quite dark at the areas where polygonal shaped cells are seen.

Histograms of the number of sides at five different times shows that most of the cells have either 5 or 6 sides.

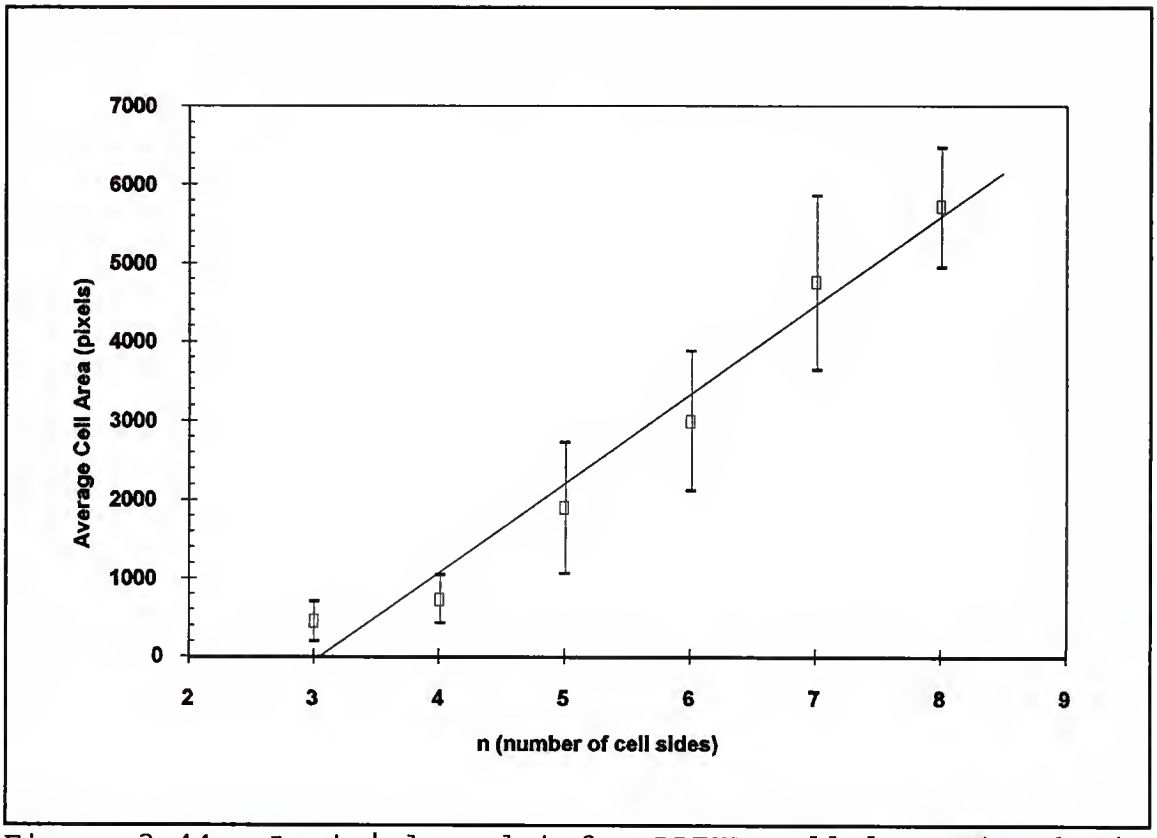

Figure 3-44. Lewis' law plot for PPEHU cellular network at 0.65 nm^2/repeat and 25°C.

The shape of the cells of ME phase are polygonal at 0.65 nm^2/repeat unit while cell shapes at 0.60 nm^2/repeat unit are circular.

To test the cellular network with regard to Aboav's law, linear regression of a plot of mn vs. n was performed, where m is the average number of sides of a cell's neighbors. The slope was found to be 4.9 with an intercept of 8.2. This is consistent with the Aboav's law equation as modified by Weire, since the second moment was found to

be 1.7.

For Lewis' law, Figure 3-44 shows a plot of cell area vs the number of sides. This plot indicates that the cell area is not a linear function of the number of sides because Lewis' law fails for 3 and 4 sided cells. Lewis' law usually works for systems which are more topologically constrained and less physically constrained. It does not always work for soap froths (which experience strong surface forces), and also at least one computer simulation also failed to follow Lewis' law. That the PPEHU random cellular network does not follow Lewis' law indicates that its cellular network is more physically constrained so that the general topological requirement to fill all of the available space is overridden. This last statement is also consistent with the discussion above regarding the hysteresis behavior of the PPEHU isotherm.

For the Perimeter law, a plot of cell perimeter versus the number of sides was made (Figure 3-45). Thus, for this system the perimeter law gives a better fit to the data than Lewis' law. Furthermore, a log-log plot of the cell area versus cell perimeter squared divided by 4, gives a linear regression fit with a slope of 1.08. This so-called convolution index plot gives an indication of the degree of randomness in the cell side structure. A slope of 1.5 would indicate total randomness while a value of 1.0 would indicate a high degree of order in the network.[128] The slope

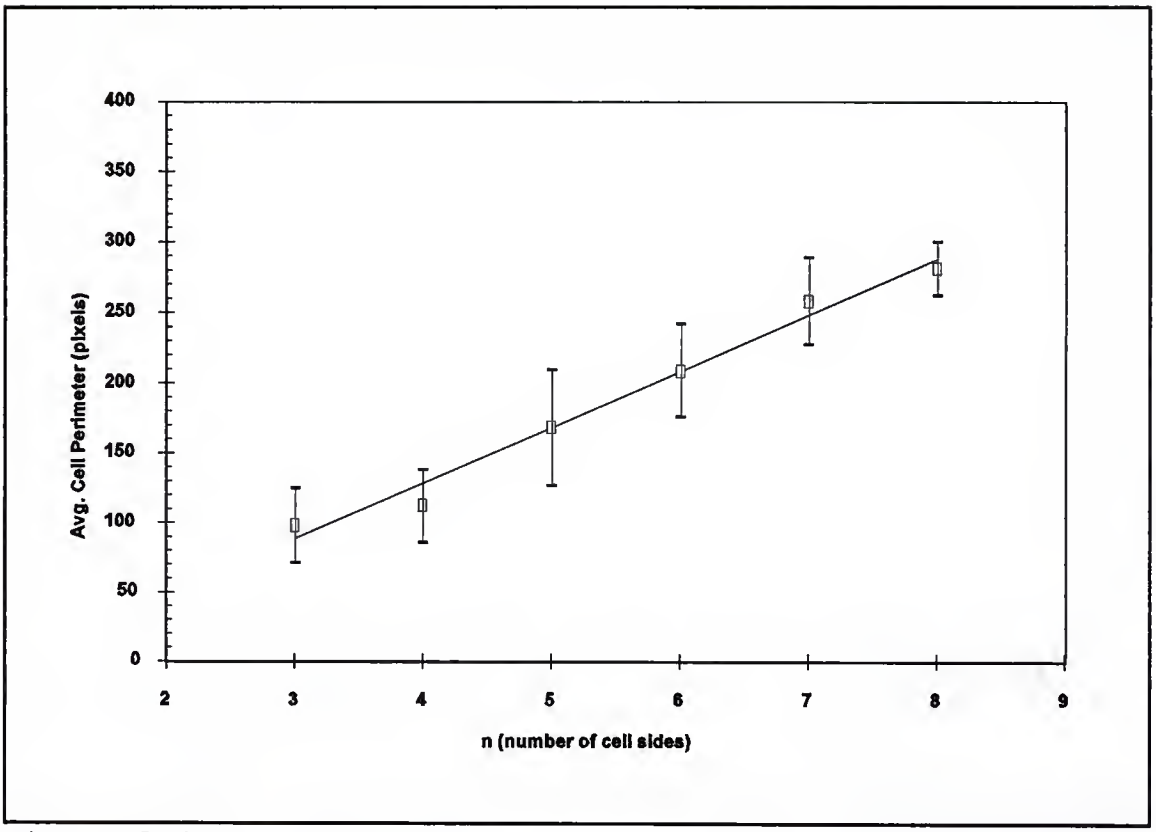

Figure 3-45. Perimeter law plot for PPEHU cellular network at 0.65 nm^2/repeat and 25°C..

can also be taken as a measure of the roundness of the polygons with a slope of unity for circles. A value of 1.03 was found for the surface micelles of polystyrene copolmer of Eisenberg and coworkers.[128] The value of 1.08 for the PPEHU cellular network is consistent with the view that strong surface forces are shaping the domains. These surface forces are the line tension between the phases and dipole repulsion.

In the way of caveats, it should be noted that the

system is not at equilibrium with regard to exchange of water subphase with the surrounding air. Thus there is a constant evaporation of water through the monolayer during the experiments. This "humidity effect" has been shown to be an important factor influencing domain shapes in a Langmuir monolayer.[129]

Cellular Network Dynamics

In order to check whether the cell areas change according to Von Neumann's law, the time rate of cell area change, dA/dt, vs. number of sides was plotted for the repeat unit area of 0.70 nm^2. In general the cell area grows whether or not the number of cell sides is greater than or less than 6. The statistical variation in the rate of growth was greater for cells with more sides (Figure 3-46). According to Von Neumann's model, area is transferred from one cell to the other at a rate proportional to the product of the length of their common edge and the driving force for material transfer, often a pressure difference. This is not observed with these networks. The failure of Von Neumann's law may be attributed to the relatively high frequency of cell coalescence events. Cellular networks which follow von Neumann's law coarsen by the T1 and T2 processes with less frequent cell coalescence. Stine and coworkers attributed the failure of von Neumann's law for their lipid monolayers to the presence of Plateau borders

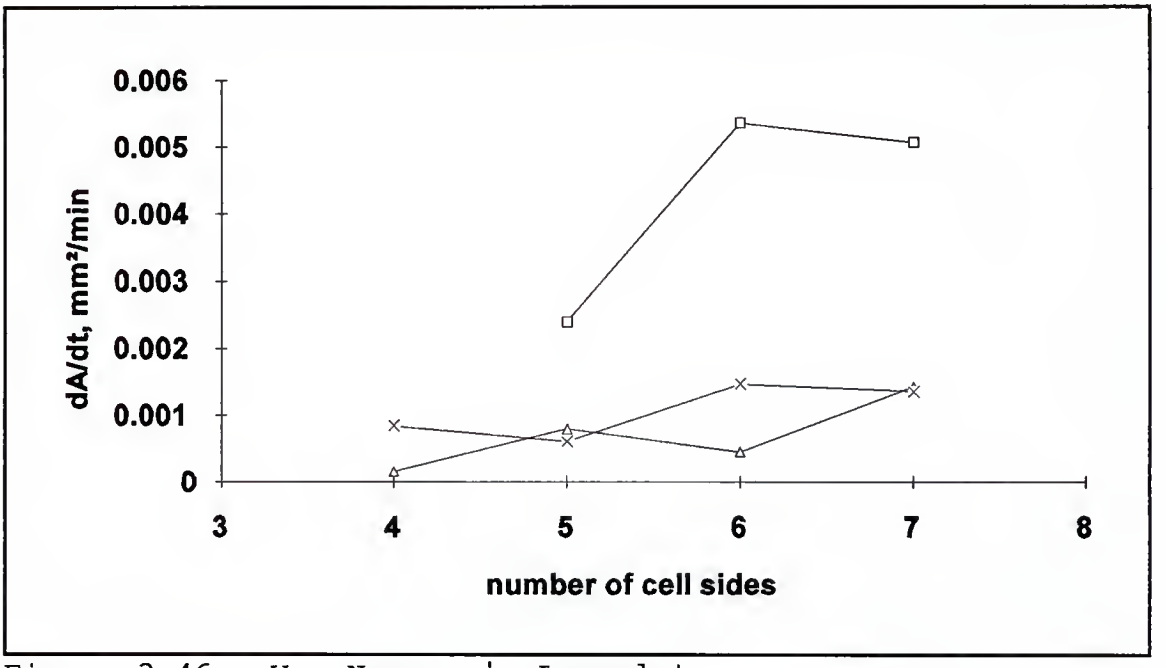

Figure 3-46. Von Neumann's Law plot.

which can cause vertex angle deviations. This may also be the case with the PPEHU cellular network. One of the assumptions in the derivation of the von Neumann's law is the average vertex of 120°, which is the angle which results from a balancing of forces around the vertex. The existence of Plateau border suction, pulls material from the cell edges into the vertex. The accumulation of material at a vertex can reach a point where it tends toward a circular domain shape itself. At this point, the vertex has enough mass to be less affected by the tension force from the cell edge and thus deviations in vertex angle are the consequence. The edge thinning is also the beginning of the cell coalescence process. Therefore, the presence of Plateau borders and relatively high frequency of cell

coalescence events combine to cause the observed deviation from von Neumann's law.

The observed dynamics include motion of the subphase and its coupling with the Langmuir film cellular network. Motion of the subphase is induced by motion of the barriers and soon dissipates. Continuous centimeter-scale motion is driven by air currents.

The relative frequency of T1 and cell coalescence events was observed to depend on the molefraction of the MC phase in the cellular network. As the fraction of the MC phase increases, cell coalescence increases compared to T1 processes. T2 processes were observed in the epifluorescence experiments. In general, for most cellular structures studied previously by other workers, the T1 process is the predominant coarsening process while the T2 process occurs more frequently (though still less than T1) when the diffusion across the boundary between cells is faster, as in gas bubbles. In the case of the PPEHU cellular network, the diffusion is hindered by the large size of the polymer molecules.

A series of experiments were made to determine if the rate of cell growth depends on the relative fraction of the two phases. BAM images were recorded over time for a series of phase fractions. A log-log plot of average cell area versus time was made for each phase fraction. Linear regression was used to obtain a slope for each plot. These

slopes are plotted versus phase fraction in Figure 3-47. The slopes remain fairly constant around 0.6 when the more-condensed (MC) phase fraction is greater than 0.2. The ME phase cells are circular and isolated at MC phase fractions greater than 0.2. The slopes show more scatter at MC phase fractions less than 0.2 but the slopes are clearly lower than those for high MC phase fraction. The ME phase cells are polygonal and interacting at these low MC phase fractions. It is interesting to note that rate of cell growth is greatest at the same mean molecular areas where the PPEHU isotherm shows the greatest hysteresis though there is no similar discontinuity observed there. Clearly, the transition from circular non-interacting cells to polygonal cells is important in any explanation of the discontinuity of growth exponent. The data obtained for the PPEHU cellular network opposes the trend previously observed in lipid monolayers. For lipid monolayer cellular networks, the growth exponent was found to be 0.6 for circular domains,[130] 0.8 for intermediate,[96] and 1.0 for polygonal domains.[99]

The network morphology forms spontaneously upon 2D decompression. The nucleation of the cells within the decompressed film appears to be random and homogenous. Initially, cells nucleate and grow; feeding from the edges of the walls which surround them until the space-filling constraint is satisfied. Beyond this initial formation and

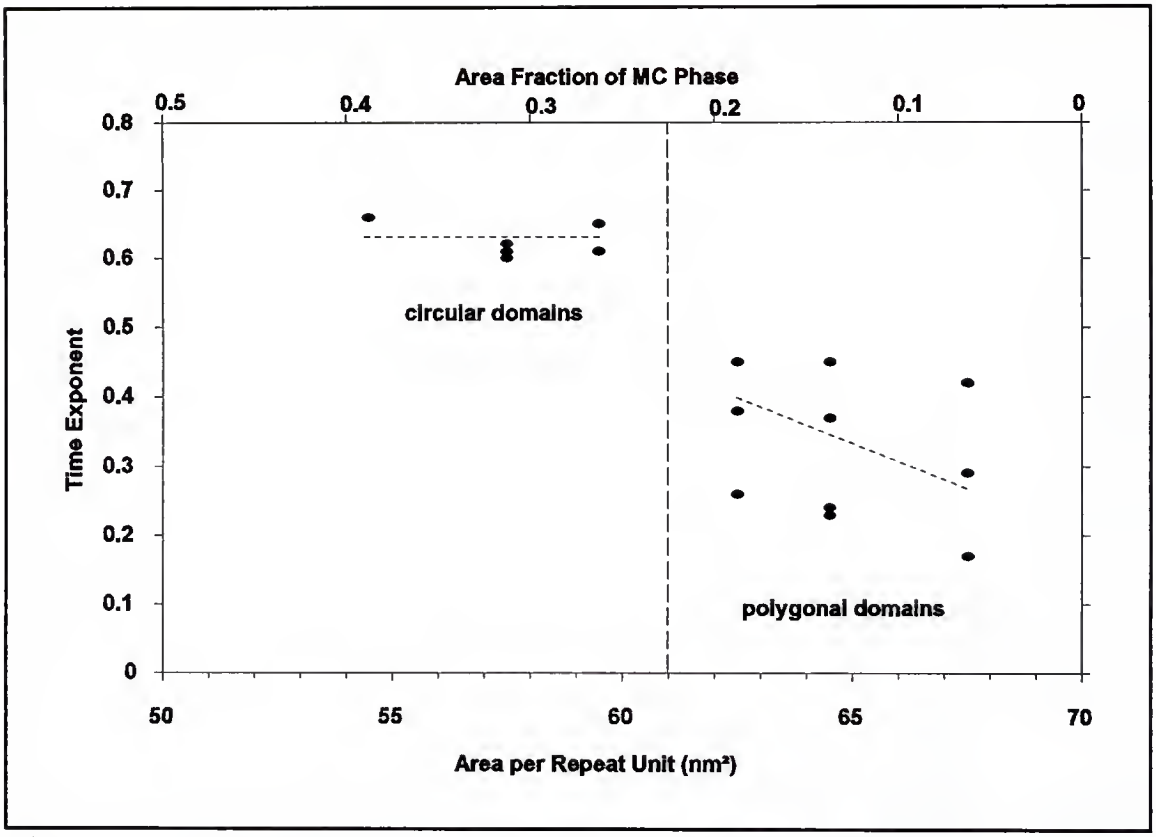

Figure 3-47. Variation of cell growth exponent with relative phase fraction.

coarsening of the cellular network, other processes begin. The cells continue to grow by two ways; namely, a cell neighbor switching process and a cell coalescence process. Ultimately, after approximately 2 hours, the cellular network breaks apart. The remnants of the cellular network appear as circular domains of the MC phase dispersed randomly within the continuous ME phase.

In summary, the rigid rod polymer film cellular network evolves through two main processes; the T1 process

and cell coalescence. As the mole fraction of the MC phase is increased, the relative size of each vertex and the thickness of each edge increases. This causes faster evolution of the cellular network. Also there is an increase in the frequency of cell coalescence relative to the frequency of other processes. The driving force for cell coalescence is minimization of the line energy because a larger cell results which has a lower line energy than the equivalent number of small cells. Given the orientation of dipoles within the ME phase, from an electrostatics standpoint, the PPEHU cellular network is more similar to condensed domains seen in lipid monolayers. The ME phase consists of the alcohol side chains in a tightly packed hairpin conformation. This leads to a strong dipole charge concentration within each cell. As the molfraction of the MC phase is decreased, the edges separating the cells are thinner and so the charge repulsion force is greater according to the usual inverse square law and less charge screening. Thus the separation between cells is maintained due to this charge repulsion. As a consequence, cell coalescence becomes less frequent and this results in a lower growth law exponent. This leads to slower evolution of the cellular network.

Energetics of Cell Coalescence

Although there is no direct evidence, cell coalescence

may begin at corrugations in edge width. Line tension acts against the corrugations but van der Waals forces will favor the generation of wide and narrow parts in a cell edge. If the increase in line Gibbs energy and dipole-dipole interaction energy is exceeded by a decrease in the van der Waals energy then the corrugations will grow in amplitude resulting in breakage of the cell edge and coalescence. Once the edge is broken, both the Gibbs line energy and van der Waals energies drive the material from the broken edge into the vertex. Even if conditions are favorable for the corrugations to grow spontaneously, the growing fluctuation requires time because of viscous resistance against flow. The lifetime of a fluctuation will be long when its wavelength is only slightly larger than the critical wavelength because in that case the driving force for growth is small. On the other hand, when the wavelength of the fluctuation is very large, it will grow slowly because the fluid MC phase has to be transported over relatively long distances.[131]

As observed under the microscope, cell coalescence in the PPEHU cellular network is similar to the bursting of soap bubbles. When the edge between two neighboring cells breaks, it rapidly retracts toward the former vertex. The rapidity of the process is testament to the magnitude of the line tension existing between the two phases. An estimate of the line tension may be made using an analogue of an

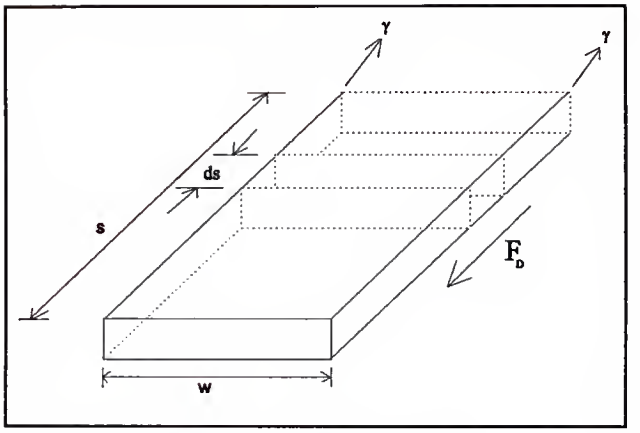

Figure 3-48. Section of ruptured cell edge.

equation first developed by Culick to describe the rim velocity of a bursting soap bubble.[132]

Figure 3-34 depicts a small section of the ruptured cell edge. The ruptured cell edge moves along the axis 's'. An incremental slice of the edge is denoted as 'ds'. The initial width and length define W and S.

The momentum balance, assuming the velocity, U=constant=dS/dt and including the viscous drag force gives

$$\gamma = \frac{1}{2} \left(\Gamma W U^2 + F_D \right)$$

where U is the velocity of the edge, γ is the line tension, Γ is the surface concentration.

There are at least four types of viscosity opposing the retracting edge. These are the surface shear viscosity

of the polymer layer, ν_s; the shear viscosity of the water subphase which may move with the polymer layer, ν_b; the viscosity between the film and the water subphase, ν_{s-b}; and the surface shear viscosity between the retracting edge and the surrounding ME phase which may move, $\nu_{s-s'}$. Typical values found for these viscosities are $\nu_b = 10^{-2}$ g cm^{-1} sec^{-1} and $\nu_s = 10^{-2}$ mg sec^{-1}. The viscosities ν_{s-b} and $\nu_{s-s'}$ would be too high to be a main factor here.

The viscous drag force due to ν_b may be estimated by assuming the retracting edge is a finite flat plate, for which, the Reynolds number is

$$Re = \frac{U \rho S}{\nu_b}$$

where ρ and ν_b are the density and viscosity of water, respectively. The equation for the drag on one side of a finite flat plate oriented parallel to the direction of flow with a Reynolds number less than 500,000 is

$$F_D = \frac{1.328}{2} W S U^2 \rho Re^{-0.5} \quad .$$

Observing U to be 1000 μm/s for an edge 7 μm wide and 100 μm long, the Reynolds number was calculated to be 0.1. With the density and viscosity of water at 1 g/cm^3 and 0.01 g/cm·s the calculated viscous drag force was 1.4×10^{-12} N. The surface concentration of the MC phase was found to be

2.1 repeat units/nm^2, so this leads to an estimated value of 7 x 10^{-10} mN for the line tension. This expression will tend to underestimate the line tension because it does not take into account the effect of adsorbed water molecules, and inelastic collisions as the moving edge tip collides with the stagnant molecules. For purposes of comparison, the line tension calculated by other workers using other techniques is shown in Table 3-1.[133]

The magnitude of the line tension has an important effect on the cellular network dynamics and topology. High values of line tension favor small domain sizes. The value estimated here is intermediate between the low values found for polydimethylsiloxane and the high values found between the solid and liquid phsaes of stearic acid. High values of line tension lead to more circular domains. Thus the convolution index was close to the value for circles but not as close as that found for lipid monolayers. The line tension has only been estimated for one point in the phase coexistence region of PPEHU. Thus it is difficult to speculate about any links between the magnitude found and the proposed molecular model and the effect on the observed hysteresis.

This method for estimating the line tension between 2D phases in Langmuir monolayers is unique though it draws strongly from similar models developed for 3D ruptured soap bubbles. The method of McConnell in which domains are

Table 3-1. Comparison of Calculated Line Tension between Monolayer Domains

Material	Monolayer Phases	Line Tension	Reference
nitrobenz-oxadiazole stearic acid	solid/liquid	10^{-9} mN	Muller and Gallet, 1991
cholesterol/ dimyristoyl-phasphatidylcholine 3:7 mixture	liquid/liquid	10^{-9} mN	Benvegnu and McConnell, 1992
cholesterol/ dimyristoyl-phasphatidylcholine 3:7 mixture	liquid/liquid	10^{-9} mN	Seul, 1993
cholesterol/ dimyristoyl-phasphatidylcholine 3:7 mixture	liquid/liquid	10^{-10} mN	Goldstein and Jackson, 1994
polydimethyl-siloxane	liquid/gas	10^{-10} mN	Mann, Hénon, Langevin, Meunier, 1992
poly(hydroxy-undecanoxy-phenylene-acetylene-pyridine-acetylene)	liquid/liquid	10^{-10} mN	Roberts, Teer, Moroni, Le Moigne, Duran, 1995

intensionally distorted by an air stream into long thin shapes with bolas at each end is mathematically somewhat similar, particularly in its difficulties with unknown

values for the various viscosity coefficients. Estimating line tension based on observed cell coalescence events requires greater patience than other methods because the event must happen within the field of view of the microscope. Also the event must be recorded so that frame by frame measurement of the retracting cell edge may be made. Its main advantage over some of the other techniques is that the monolayer need not be disturbed from its normal state. The accuracy of the technique could be improved by utilizing faster video recorders so that more frames per event would be available and also if better estimates of the viscosity were available.

Future Work

Future work will include attempts to transfer the monolayer to a solid substrate such as quartz in such a way that the 2D foam-like morphology seen on the air-water interface is reproduced on the solid substrate. Such a supported cellular network film might be a preformed optical circuit with the cell walls functioning as waveguides. A number of interesting shapes have been observed within the remnants of the foam-like morphology. How these shapes come about should be elucidated. Also other types of polymers have been observed to produce a 2D foam-like morphology. Studies of these polymers should aid in the continuing

search for understanding of novel 2D structures.

The chemical structure of the repeat unit of these polymers is analogous to the polyphenylenevinylenes (PPV). PPV's have been recently demonstrated to be electroluminescent so it would be interesting to see if the phenylene ethynylenes also have this property. If so, then the cellular networks of these materials could be an advantage as the sizes of cells formed is smaller than the pixels on a typical display screen and thus would give a higher resolution display if the electroluminescence efficiency is high enough, for example.

Work from this chapter that should be extended includes the imaging of the PEHU and PPYPYRI materials with the epifluorescence microscope along with fluorescence spectroscopy as was done with the PPEHU. Work with PPEHU could include the use of a polarizer with the florescence microscope to look for LRO in its Langmuir films. The polarizer could also help to more fully characterize the dendrites seen in the PPEHU Langmuir films at low temperatures.

The growth law for the domains of the PPEHU MC phase when the PPEHU monolayer is initially compressed to various points within the phase coexistence region might be measured. The domains of the MC phase are more directly analogous electrostatically to the cells of other Langmuir film cellular networks. Thus the growth law exponent would

be expected to approach unity as the area fraction of MC phase is increased. This proposed experiment would test the speculations above regarding the slower rate of growth for polygonal ME phase cells.

CHAPTER 4
CONCLUSIONS

The Langmuir film balance technique was used to study the monolayer properties of a series of substituted acetylene monomers and polymers with amphiphilic properties. The Langmuir technique exploits the orienting properties of an interface to induce order in such amphiphilic molecules. The interface utilized, in this dissertation, was the ultrapure water/gas surface. By varying the lateral pressure and temperature on monolayers of amphiphilic molecules, two-dimensional phase changes were produced. Herein, the monolayer properties were discovered through surface analytical methods, such as, Brewster angle microscopy, epifluorescence microscopy, *in situ* ultraviolet spectroscopy, and surface potentiometry. Furthermore, the amphiphilic molecular monolayers were evaluated with regard to the propensity for transfer onto solid substrates. This ability to transfer to solid substrates is important with regard to the materials' potential for use in working thin film devices such as waveguides. In this dissertation the Langmuir film properties of mesogen-substituted acetylene

monomers and polymers were discovered.

As reported in Chapter 2, six different mesogen substituted acetylene monomers were studied with regard to their Langmuir film-forming properties, their processibility for transfer to solid substrates, and finally their reactivity in multilayer solid films. The goal of achieving polymerization within the deposited multilayers places an extreme demand on the quality of the films because reactive groups must be placed in a specific geometry in order for the desired reaction to take place. The synthesis of three of the monomers was reported in Chapter 2. Two of the monomers were alkylacetylenes, three were phenylacetylenes, and one was an anthrylacetylene.

The chemical structure of the alkylacetylene monomers were identical with the exception that one utilized a methoxy group as the hydrophilic part of the molecule while the second molecule utilized a hydroxyl group. Both alkylacetylene monomers used the biphenyl mesogen with an alkyl chain spacer attached to the mesogen with an ester linkage. The second molecule was found to have superior Langmuir film stability under lateral pressure as well as good transfer to solid substrates. Up to 30 layers of the second compound could be deposited with near ideal transfer efficiency. However, both materials were found to be unreactive in thin solid film form under gamma and ultraviolet irradiation.

The phenylacetylene monomers varied in their chemical structure in the type and placement of the mesogenic group. Two of the phenylacetylene monomers, had the phenylbenzoate mesogen with two alkyl chain lengths. The acetylene group was attached directly to the mesogen and functioned as the hydrophilic part of the amphiphiles. The third phenylacetylene monomer had a biphenyl mesogen separated from the phenylacetylene group by an alkyl spacer. The third phenylacetylene used a hydroxy group as the hydrophilic part of the molecule. All three phenylacetylene monomers formed stable films on the water surface but the biphenol substituted monomer monolayer was the most stable. The phenylbenzoate monomers produced highly viscous films which were difficult to transfer to solid substrates though this was achieved through very slow dipping speeds. The biphenol substituted monomer had the best reactivity under UV irradiation, achieving propagation up to ten repeat units according to gel permeation chromatography.

The anthrylacetylene monomer also utilizes a biphenyl mesogen. Preliminary experiments indicate that it also forms stable Langmuir monolayers.

The main conclusions from Chapter 2 are as follows. The synthesis of three new mesogen-substituted acetylenes has been achieved, including an alkylacetylene (biphenol-undecynoate), a phenylacetylene (4-(4'-ol-biphenyl-4-decanoxy)-phenylacetylene), and an anthrylacetylene (2-(10-

(4-(4'-ol-biphenyl-4-dodecanoxymethyl)-anthryl)-trimethylsilylacetylene). The LBK film forming properties of the new alkylacetylene and the new phenylacetylene have been studied and compared to previously synthesized alkyl- and phenylacetylenes. Both new compounds form stable monolayers at the air-water interface but the new alkylacetylene was found to make higher quality films.

Solid state polymerization in LBK films was attempted by irradiation of the mesogen-substituted acetylene monomers. The new phenylacetylene was superior in its solid state reactivity compared to the other compounds. The reason for the improved reactivity of the new phenylacetylene may be due to its packing geometry and/or electronic properties. The quality of the LBK films of the new phenylacetylene was not high. If the film quality can be increased perhaps by the introduction of an interactant or by varying the pH of the subphase, then higher degrees of polymerization may be obtained.

The Langmuir film balance technique was also used to produce monomolecular films of phenylene acetylene rigid-rod polymers. At the air-water interface, two of the pre-formed polymers were observed to form microscopic network morphologies after treatment by a simple processing procedure. These network morpholgies are the result of two-dimensional phase separation. The difference in the phases is due to conformational changes of the hydroxy-terminated

side chains. Careful consideration of data including surface (lateral) pressure versus mean repeat unit, surface potential, Brewster angle microscopy, and epifluorescence microscopy has led to this nanoscale model of the nature of the 2D phases observed. A unique feature of the behavior is pressure dependent phase separation due to changes in the alkyl side chain conformation. This leads to non-typical temperature behavior of this isotherm.

Langmuir films of the third phenylene acetylene polymer did not exhibit phase separation and thus no cellular network. The chemical structure of the third polymer differs from the other two polymers, in that, it does not have the strongly hydrophilic pyridinium moiety in its main chain. Thus the density of alkyl chains along the main chain is greater in this third material. The density of alkyl side-chain substitution as well as the pattern of attachment to the main chain is thought to be important factor in the phase behavior exhibited by these three polymers. The presence of ionic charges along the backbone is also an important factor affecting the 2D phase behavior.

Like the monomers, these polymers were also evaluated with regard to their processibility to solid multilayers. The network-forming polymers did not tranfer to solid substrates. On the other hand, the polymer which did not form the cellular network showed excellent transfer for the first two layers. This difference is attributed to the

greater monolayer stability of the polymer at high surface pressure.

The microscale dynamics and topology of one polymer's 2D cellular network morphology was analyzed in terms of previously developed theory. Such networks generally coarsen over time by a combination of cell coalescence and neighbor-switching processes. The driving force behind these network dynamics is the minimization of the line energy: the line energy being the 2D analog to surface energy. In Chapter 3, a model was presented that allows the calculation of the line tension between the 2D phases by observation of cell coalescence events. The kinetics of the cell growth was seen to follow a power law with the average cell area increases at a $t^{0.6}$ rate when the cells are circular and not interacting. This result is consistent with values found by other workers while working with low molecular weight amphiphiles such as pentadecanoic acid. When the cells are polygonal the growth law exponent is in the range of 0.4 down to 0.2. This result does not follow the trend found with the low molecular weight amphiphiles where the growth exponent was found to be 1.0 for polygonal shaped cells. This contrary trend can be explained on the basis of long range dipole repulsion. The phase making up the polymer cells consists of the alcohol side chains in tightly packed hairpin conformation. This leads to a strong dipole charge concentration within each cell. Thus the

separation between cells is maintained due to this charge repulsion. As a consequence, cell coalescence becomes less frequent and this results in a lower growth law exponent. The nature of the phase within the cells of the low molecular weight amphiphile does not lead to such a dipole charge concentration.

This dissertation has explored the wide range of Langmuir film properties exhibited by mesogen-substituted acetylene monomers and polymers. The results demonstrate the processibility of these materials for potential multilayer thin film devices. In addition, the results point to improvements which may be made in the molecular design.

REFERENCE LIST

1. Fuller, R. Buckminster *Critical Path* St. Martin's Press, New York, 1981, 73.

2. Wong, K. S.; Han, S. G.; Vardeny, Z. V. *Synthetic Metals* 1991, 43(1-2), 3209-12.

3. Butcher, P. N.; Cotter, D. *The Elements of Nonlinear Optics* Cambridge University Press, Avon, 1990, 19.

4. Marder, S. R.; Gorman, C. B.; Meyers, F.; Perry, J. W.; Bourhill, G.; Brédas, J.; Peirce, B. M. *Science* 1994, 265, 632-634.

5. Prasad, P. N.; Williams, D. J. *Introducation to Nonlinear Optical Effects in Molecules and Polymers* Wiley and Sons, New York, 1991, 79.

6. Aime, J. P.; Garrin, P.; Baker, G. L.; Ramakrishnan, S.; Timmins, P. *Synthetic Metals* 1991, 41(3), 859-67.

7. Blumstein, A.; Subramanyam, S. *Org. Supercond.[Proc. Int. Conf.]* 1990,335-40.

8. Adamson, A. W.; *Physical Chemistry of Surfaces, Fifth Edition*, 1990, John Wiley and Sons, New York, 119-120.

9. Roberts, G. *Langmuir-Blodgett Films*, 1990, Plenum Press, New York, 93-98.

10. Blodgett, K. B. *J. Am. Chem. Soc.* 1935, 57, 1007-1022.

11. Gaines, G. L. *Insoluble Monolayers at Liquid-Gas Interfaces*, Wiley-Interscience, New York, 1966, 20-21.

12. Moebius, D.; Moehwald, H. *Advanced Materials* 1991, 3(1), 19-24.

13. Lucassen, J.; Akamatsu, S.; Rondelez, F. *Journal of Colloid and Interface Science* 1991. *144*, 434.

14. Riegler, J. E.; LeGrange, J. D. *Physical Review Letters* 1988, 61(21), 2492-2495.

15. Berge, B.; Simon, A. J.; Libchaber A. *Physical Review A* 1990, *41*, 6893.

16. Riegler, J. E. *Review of Scientific Instruments* 1988, 59(10), 1988.

17. Moore, B.; Knobler, C. M.; Broseta, D.; Rondelez, F. *Journal of the Chemical Society, Faraday Transactions 2* 1986, *82*, 1753.

18. Hénon, S.; Meunier, J. *Review of Scientific Instruments* 1991, *62*, 936.

19. Hönig, D.; Möbius, D. *Journal of Physical Chemistry* 1991, *95*, 4590.

20. Mann, E. K.; Hénon, S.; Langevin, D.; Meunier, J. *Journal de Physique II France* 1992, *2*, 1683.

21. Adamson, A. W. *Physical Chemistry of Surfaces Fifth Edition* Wiley and Sons, New York, 1990, 123–124.

22. Tieke, B.; Lieser, G.; Weiss, K. *Thin Solid Films* 1983, 99, 95–103.

23. Laschewsky, A.; Ringsdorf, H.; Schmidt, G. *Polymer* 1988, 29, 448–453.

24. Wegmann, A.; Hunziker, M.; Tieke, B. *J. Chem. Soc. Chem. Commun.* 1989, 1179–1180.

25. Uekita, M.; Awaji, H.; Murata, M. *Thin Solid Films* 1988, 160, 21–24.

26. Thredgold, R. H. *Thin Solid Films* 1987, 152, 223–227.

27. Orthmann, E.; Wegner, G. *Angew. Chem. Int. Ed. Engl.* 1986, 25, 1105–1106.

28. Ulman, A. *An Introduction to Ultrathin Organic Films: From Langmuir–Blodgett to Self–Assembly* Academic Press, San Diego, 1991.

29. Tieke, B; *Advanced Materials* 1990, 2, 5, 222–231.

30. Penner, T. L.; Schildkraut, J. S.; Ringsdorf, H.; Schuster, A. *Macromolecules* 1991, 24, 1041–1049.

31. Peterson, I. R. *J. Physics D* 1989, 23, 379–395.

32. Agarwal, V. K. *Physics Today* 1988, 6, 40–46.

33. Embs, F.; Funhoff, D.; Laschewsky, A.; Licht, U.; Ohst, H.; Prass, W.; Ringsdorf, H.; Wegner, G.; Wehrmann, R.

Advanced Materials 1991, 3(1), 25–31.

34. Bamford, C. H.; Eastmond, G. C. *Quart. Rev. Chem. Soc.* 1969, 23, 271.

35. Lando, J. B.; Fort, T. in *Polymerization in Organized Systems* Elias, H. G., Ed.; Gordon Breach, New York, 1977, 63–78.

36. Morawetz, H. *Science* 1966, 152, 705.

37. Day, D.; Lando, J. B. *Macromolecules* 1980, 13, 1478–1483.

38. Day, D.; Lando, J. B. *Macromolecules* 1980, 13, 1483–1487.

39. Ogawa, K.; Mino, N.; Tamura, H.; Hatada, M. *Langmuir* 1990, 6, 1807–1809.

40. Foxman, B. M.; Jaufmann, J. D. *Journal of Polymer Science (C)* 1983, 70, 31–33.

41. Tieke, B. *Mol. Cryst. Liq. Cryst.* 1983, 93, 119–124.

42. Sandman, D. J.; Hamill, G. P.; Samuelson, L. A.; Foxman, B. M. *Mol. Cryst. Liq. Cryst.* 1984, 106, 199–202.

43. Kawaguchi, T.; Nakahara, H.; Fukuda, K. *Thin Solid Films* 1985, 133, 29–37.

44. Duda, G.; Wegner, G. *Makromol. Chem. Rapid Commun.* 1988, 9, 496–497.

45. Princen, H. M. *Journal of Colloid and Interface Science* 1983, 91(1), 160–175.

46. Wegner, G. *Thin Solid Films* 1992, 216, 105–116.

47. Le Moigne, J.; Francois, B.; Guillon, D.; Hilberer, A.; Skoulios, A.; Soldera, A.; Kajzar, F. *Inst. Phys. Conf. Ser. No. 103: Section 2.4* 1989, 209–214.

48. Aldissi, M. *Inherently Conducting Polymers*; Noyes Data Corporation, Park Ridge, NJ, 1989, 1–3.

49. Butcher, P. N.; Cotter, D. *The Elements of Nonlinear Optics*, Cambridge University Press, New York, NY, 1990, 13–14.

50. Le Moigne, J.; Soldera, A.; Guillon, D.; Skoulios, A. *Liquid Crystals* 1989, vol. 6, pp. 627–639.

51. Roberts, G. *Langmuir–Blodgett Films* 1990, Plenum Press, New York, 318.

52. Tieke, B. *Adv. Mater.* 1990, vol. 2, pp. 222–231.

53. Sakuhara, T.; Nakahara, H.; Fukuda, K. *Thin Solid Films* 1989, vol. 159, pp. 345–351.

54. Le Moigne, J.; Soldera, A.; Guillon, D.; Skoulios, A. *Liquid Crystals* 1989, vol. 6, 627–639.

55. Zhang, X.; Ozcayir, Y.; Feng, C.; Blumstein, A. *Polymer Preprints* 1990, vol. 31, 597–598.

56. Foxman, B. M.; Jaufmann, J. D. *J. Polym. Sci. (C)* 1983, 70, 31–37.

57. Tieke, B. *Mol. Cryst. Liq. Cryst.* 1983, 93, 119–126.

58. Sandman, D. J.; Hamill, G. P.; Samuelson, L. A.; Foxman, B. M. *Mol. Cryst. Liq. Cryst.* 1984, 106, 199–203.

59. Sandman, D. J. in *Crystallographically Ordered Polymers*, edited by D. J. Sandman, ACS Symposium Series 337, Washington, DC 1987, 1–10.

60. Roberts, M. J.; Advincula, R. C.; Zhang, X.; Blumstein, A.; Duran, R. S. *Polymer Preprints* 1991, vol. 32, no. 1, 252–254.

61. Advincula, R. C.; Roberts, M. J.; Zhang, X.; Blumstein, A.; Duran, R. S. *ACS Symposium Series on Macromolecular Assemblies in Polymeric Systems*, edited by P. Stroeve and A. C. Balazs, ACS Symposium Series 493, Washington, DC, 1992, 10–19.

62. Aldissi, M. *Inherently Conducting Polymers*; Noyes Data Corporation, Park Ridge, NJ, 1989.

63. Melissaris, A. P.; Litt, M. H. *Macromolecules* 1994, 27, 2675–2684.

64. Sandman, D. J. *ACS Symposium Series No. 337, Crystallographically Ordered Polymers* 1987, pp. 1–10.

65. Le Moigne, J.; Soldera, A.; Guillon, D.; Skoulios, A. *Liquid Crystals* 1989, vol. 6, pp. 627–639.

66. Zhang, X.; Ozcayir, Y.; Feng, C.; Blumstein, A. *Polymer Preprints* 1990, vol. 31, pp. 597–598.

67. Aime, J. P.; Garrin, P.; Baker, G. L.; Ramakrishnan, S.; Timmins, P. *Synthetic Metals* 1991, 41(3), 859–67.

68. Michel, R. H. *Journal of Polymer Science: Part A–1* 1967, 5, 920–926.

69. Müllen, K. *Angew. Chem.* 1987, 99, 192–201.

70. Zhou, H.; Elsebee, M.; Reuhe, J.; Wegner, G.; Duran, R. S. *Macromolecules*, submitted for publication.

71. Advincula, R. C. *Toward Two-dimensionally Ordered Substituted Polyacetylenes: Ordered Monomer and Preformed Polymer Approach* 1994, Ph. D. Thesis, University of Florida, 54.

72. Silverstein, R. M.; Bassler, G. C.; Morrill, T. C. *Spectrometric Identification of Organic Compounds, Fifth Edition* 1991, Wiley and Sons, New York, 130.

73. Tieke, B.; Lieser, G.; Wegner, G. Journal of Polymer Science: Polymer Chemistry Edition 1979, vol.17, pp. 1631–1644.

74. Ishii, T. *Thin Solid Films* 1989, vol. 178, pp. 47–52.

75. Vincett, P. S.; Barlow, W. A. *Thin Solid Films* 1980, 71, 305–326.

76. National Research Council, Committee on Polymer Science and Engineering, Board on Chemical Sciences and Technology, Commission on Physical Sciences, Mathematics and Applications; *Polymer Science and Engineering: The Shifting Research Frontiers* 1994, National Academy Press, Washington, D. C.

77. Butcher, P. N.; Cotter, D. *The Elements of Nonlinear Optics* Cambridge University Press, Avon, 1990.

78. Roberts, G. editor *Langmuir–Blodgett Films* Plenum Press, New York, 1990.

79. Hénon, S.; Meunier, J. *Review of Scientific Instruments* 1991, *62*, 936.

80. Hönig, D.; Möbius, D. *Journal of Physical Chemistry* 1991, *95*, 4590.

81. Berge, B.; Simon, A. J.; Libchaber A. *Physical Review A* 1990, *41*, 6893.

82. Mann, E. K.; Hénon, S.; Langevin, D.; Meunier, J. *Journal de Physique II France* 1992, *2*, 1683.

83. Eisenberg, A. presented at the Florida Advanced Materials Conference, Palm Coast, FL, March 1993.

84. Moore, B.; Knobler, C. M.; Broseta, D.; Rondelez, F. *Journal of the Chemical Society, Faraday Transactions 2* 1986, *82*, 1753.

85. Lucassen, J.; Akamatsu, S.; Rondelez, F. *Journal of Colloid and Interface Science* 1991. *144*, 434.

86. Moroni, M.; Le Moigne, J.; Luzzati, S. *Macromolecules* 1994, 27(2), 562.

87. de Gennes, P. G. *The Physics of Liquid Crystals*, Clarendon, Oxford, 1974.

88. Flory, P. J. *Proceedings of the Royal Society of London A* 1956, *234*, 73.

89. Chick, L. A.; Viney, C. *Molecular Crystals and Liquid Crystals* 1993, *226*, 63.

90. Frenkel, D.; Eppenga, R. *Physical Review A* 1985, *31(3)*, 1776.

91. Weire, D.; Rivier, N. *Contemporary Physics* 1984, *25*, 59.

92. Berge, B.; Simon, A. J.; Libchaber, A. *Physical Review A* 1990, *41*, 6893.

93. Moore, B.; Knobler,C. M.; Broseta,D.; Rondelez,F. *Journal of the Chemical Society, Faraday Transactions 2* 1986, *82*, 1753.

94. Stavans, J.; Domany, E.; Mukamel,D. *Europhysics Letters* 1991, *15*, 479.

95. Krichevsky, O.; Stavans J. *Physical Review B* 1992, *46*, 10579.

96. Glazier, J. A.; Gross, S. P.; Stavans J. *Physical Review A* 1987, *36*, 306.

97. Fradkov, V. E.; Glicksman, M. E.; Palmer, M.; Nordberg, J.; Rajan, K. *Physica D* 1993, *66*, 50–60.

98. Moore, B.; Knobler, C. M.; Broseta, D.; Rondelez, F. *J. Chem. Soc., Faraday Trans. 2* 1986, 82, 1753–1761.

99. Lucassen, J.; Akamatsu, S.; Rondelez, F. *Journal of Colloid and Interface Science* 1991, 144(2), 434–448.

100. Stine, K. J.; Bono, M. F.; Kretzer, J. S. *Journal of Colloid and Interface Science* 1994, 162, 320–322.

101. Mann, E. K.; Hénon, S.; Langevin, D.; Meunier, J. *J. Phys. II France* 1992, 2, 1683–1704.

102. Seul, M.; Morgan, N. Y.; Sire, C. *Physical Review Letters* 1994, 73(17), 2284–2287.

103. Goldstein, R. E.; Jackson, D. P. *J. P. Chem.* 1994, 98, 9626–9636.

104. McConnell, H. M. *Ann. Rev. Phys. Chem.* 1990, 42, 171–195.

105. McConnell, H. M. *J. P. Chem.* 1990, 94, 4728–4731.

106. McConnell, H. M.; Moy, V. T. *J. P. Chem.* 1988, 92, 4520–4525.

107. McConnell, H. M.; de Koker, R. *J. P. Chem.* 1992, 96, 7101–7103.

108. McConnell, H. M.; Rice, P. A.; Benvegnu, D. J. *J. P. Chem.* 1990, 94, 8965–8968.

109. Rice, P. A.; McConnell, H. M. *Proc. Natl. Acad. Sci. USA* 1989, 86, 6445–6448.

110. Keller, D. J.; McConnell, H. M.; Moy, V. T. *J. P. Chem.* 1986, 90, 2311–2315.

111. Keller, D. J.; Korb, J. P.; McConnell, H. M. *J. P. Chem.* 1987, 91, 6417–6422.

112. Aboav, D. A. *Metallography* 1970, *3*, 383.

113. Von Neumann, J.; in *Metal Interfaces*, Cleveland, Ohio, American Society for Metals, 1952, 108.

114. Stavans, J.; Domany, E.; Mukamel D. *Europhysics Letters* 1991, *15*, 479.

115. Herdtle, T.; Aref, H. *Journal of Fluid Mechanics* 1992, *241*, 233.

116. Moroni, M.; Le Moigne, J. *Macromolecules* 1994, 27, 562–571.

117. Stine, K. J.; Rauseo, S. A.; Moore, B. G.; Wise, J. A.; Knobler, C. M. *Physical Review A* 1990, *41*, 6885.

118. Roberts, G. editor *Langmuir–Blodgett Films* Plenum Press, New York, 1990, 255.

119. Adamson, A. W. *Physical Chemistry of Surfaces, Fifth Edition* 1990, Wiley and Sons, New York, 131–139.

120. Streitweiser, A.; Heathcock, C. *Introduction to Organic Chemistry* Macmillan, New York 1976.

121. Helm, C. A.; Möhwald, H.; Kjaer, K.; Als-Nielsen, J. *Biophysical Journal* 1987, *52*, 381.

122. Ballauff, M. *Macromolecules* 1986, 19, 1366.

123. Israelachvili, J. N. *Intermolecular and Surface Forces, Second Edition* Academic Press, London 1992.

124. Watanabe, J.; Ono, H.; Uematsu, I.; Abe, A. *Macromolecules* 1985, 18, 2141–2148.

125. Rodriguez-Parada, J. M.; Duran, R.; Wegner, G. *Macromolecules* 1989, 22, 2507–2516.

126. Tsujita, Y.; Ojika, R.; Takizawa, A.; Kinoshita, T. *Journal of Polymer Science: Part A: Polymer Chemistry* 1990, 28, 1341–1351.

127. Lakowicz, J. R. *Principles of Fluorescence Spectroscopy* Plenum Press, New York 1983.

128. Noever, D. A. *Langmuir* 1992, *8*, 1036.

129. Mann, E. K.; Henon, S.; Langevin, D.; Meunier, J. *Journal de Physique II France* 1992, 2, 1683.

130. Berge, B.; Simon, A. J.; Libchaber, A. *Phys. Rev. A* 1990, 41, 6893.

131. Vrij, A.; Overbeek, J. T. G. *Journal of the American Chemical Society* 1968, *90*, 3074.

132. Culick, F. E. C. *Journal of Applied Physics* 1960, *31*, 1128.

133. Muller, P.; Gallet, F. *Physical Review Letters* 1991, *67(9)*, 1106.

BIOGRAPHICAL SKETCH

The author graduated from Grisson High School in Huntsville, Alabama. He received his Bachelor of Science in Chemical Engineering from the University of Florida in 1987. After graduation, the author performed research work in the lab of Dr. Karl Söderholm of the Department of Dental Biomaterials at the University of Florida. In 1990, the author entered Graduate School in the Chemistry Department and chose Dr. Randy Duran as research advisor.

I certify that I have read this study and that in my opinion it conforms to acceptable standards of scholarly presentation and is fully adequate, in scope and quality, as a dissertation for the degree of Doctor of Philosophy.

Randolph S. Duran, Chair
Associate Professor of Chemistry

I certify that I have read this study and that in my opinion it conforms to acceptable standards of scholarly presentation and is fully adequate, in scope and quality, as a dissertation for the degree of Doctor of Philosophy.

John Eyler
Professor of Chemistry

I certify that I have read this study and that in my opinion it conforms to acceptable standards of scholarly presentation and is fully adequate, in scope and quality, as a dissertation for the degree of Doctor of Philosophy.

Robert Hanrahan
Professor of Chemistry

I certify that I have read this study and that in my opinion it conforms to acceptable standards of scholarly presentation and is fully adequate, in scope and quality, as a dissertation for the degree of Doctor of Philosophy.

David Tanner
Professor of Physics

I certify that I have read this study and that in my opinion it conforms to acceptable standards of scholarly presentation and is fully adequate, in scope and quality, as a dissertation for the degree of Doctor of Philosophy.

Daniel Talham
Assistant Professor of Chemistry

I certify that I have read this study and that in my opinion it conforms to acceptable standards of scholarly presentation and is fully adequate, in scope and quality, as a dissertation for the degree of Doctor of Philosophy.

Karl-Johan Söderholm

Karl-Johan Söderholm
Professor of Materials
Science and Engineering

This dissertation was submitted to the Graduate Faculty of the Department of Chemistry in the College of Liberal Arts and Sciences and to the Graduate School and was accepted as partial fulfillment of the requirements for the degree of Doctor of Philosophy.

May, 1995

Dean, Graduate School

LD
1780
1995
.R646